THESIS

APPLICATION OF AMBIENT DOSE EQUIVALENT ESTIMATION MODELS IN REMEDIATED CEDAR FORESTS OF KAWAUCHI VILLAGE JAPAN

Submitted by

Christian Robert Grabowski

Department of Environmental and Radiological Health Sciences

In partial fulfillment of the requirements

For the Degree of Master of Science

Colorado State University

Fort Collins, Colorado

Spring 2025

Master's Committee:

Advisor: Thomas Johnson

Alexander Brandl

Thomas Borch

ABSTRACT

APPLICATION OF AMBIENT DOSE EQUIVALENT ESTIMATION MODELS IN REMEDIATED CEDAR FORESTS OF KAWAUCHI VILLAGE JAPAN

Many regions contaminated by the release of radionuclides following the 2011 Fukushima Daiichi Nuclear Power Plant disaster are still being investigated today. The mountainous forest areas surrounding Fukushima prefecture were most affected by fallout radionuclides, primarily radiocesium (Cs134 and Cs137), and remain a focus area for remediation and scientific research. Several models have been developed to estimate ambient dose equivalent rates (H*(10)) using data on the depth distribution of fallout radiocesium in the forest soils.

Our hypothesis is that two different models will accurately predict radiation doses within 20% based on soil samples. The hypothesis was tested by applying the two models to a research plot in Kawauchi Village Japan, where forestry remediation such as clear-cutting and litter removal has been conducted. Using soil sampling data for radiocesium at the Kawauchi test site, these models were used to estimate H*(10) and compared to measurements taken using handheld instrumentation. The distribution of radiocesium in soil for each sampling location at the test site was determined using an exponential expression of vertical distribution. These

distribution values were then used in two different models, one estimating H*(10) using conversion coefficients from Bq/m^2 to $\mu Sv/hr$, and the other model estimating H*(10) using a "field of view" approach, estimating a surrounding area's contribution to total H*(10) measured at a central point within the test area. The results from this comparison provide a real-world test of computer model effectiveness. The conclusion was that both models could accurately predict radiation levels based on soil samples within 20% of measured values using field instrumentation but could improve if experimental conditions more closely matched those assumed in the model's design.

ACKNOWLEDGMENTS

I want to express my gratitude to my advisor, Dr. Tom Johnson, for his mentorship and guidance since our first phone call back in Summer of 2022. I also want to extend my gratitude to Dr. Alex Brandl and Dr. Ralf Sudowe of the CSU Department of Radiological Sciences. Thank you three for accepting me into this program and giving me an opportunity to advance my knowledge and career. This experience has quite literally changed my life, and I am honored to have studied under you.

Thank you to Dr. Thomas Borch for agreeing to be on my committee, even as an outside committee member whom I haven't taken a class with. I appreciate your feedback and advice during my thesis writing process.

I also want to express my gratitude to Dr. Yuichi Onda, staff, and students that the University of Tsukuba. Thank you for allowing me to participate in research with your lab and giving me a memorable experience while in Japan.

Thank you to my fellow classmates for the support, friendship, and memories made throughout the duration of my studies. Thank you to JoiLynn Drescher, who always answers dozens of phone calls and emails from me regarding anything HR related to the program.

Thank you to all my previous and current colleagues I have met in this field. You have helped solidify this is the career path I am meant to be in. And to all the CSU alumni, I am proud to join a group with such prestige and respect amongst the health physics community. I will do my best to continue the level of excellence you have achieved.

Thank you to my mom, brother, and in-laws for being supportive of this journey. Thank you to Milton for keeping me company during long writing days. Thank you to my father Mark, who ended his battle with brain cancer April 4th, 2024 – I know you are watching over me every step of the way, and I hope you are proud with what I have accomplished. I couldn't have asked for a better father to guide me to becoming the man I am today.

Finally, I want to give my greatest thank you to Sydney, for supporting this decision to move across the country, take a huge pay cut, and support us while I am in school, all to chase a brighter future for us and our future family.

"At the moment of commitment, the entire universe conspires to assist you."

-Johann Wolfgang von Goethe

DEDICATION

To my wife, Sydney, whose love and support has never wavered since the day we met. This is OUR master's degree. I am so incredibly grateful to you and all the chapters of life together.

TABLE OF CONTENTS

CHAPTER 1: INTRODUCTION

Fukushima Daiichi Nuclear Power Plant Disaster

On March 11, 2011 a 9.0 magnitude earthquake occurred off the eastern coast of Japan, creating a 15-meter tsunami. The tsunami swept over sea wall barriers and flooded the Fukushima Daiichi Nuclear Plant site. Over the course of a few days, the loss of electrical power and functionality of cooling systems led to a meltdown of three reactor cores. This resulted in a buildup of hydrogen gas within the containment structures and subsequent explosion, blowing off the roofs of the buildings and releasing radionuclides into the atmosphere (World Nuclear Association 2024).

The release of said radionuclides continues to pose a challenge for ecosystems surrounding Fukushima, as radionuclides such as cesium-134 (Cs134), with a 2-year half-life, and cesium-137 (Cs137), with a 30-year half-life, are mainly responsible for the contamination that remains today (National Nuclear Data Center 2024). Continued research in radioecology and decontamination efforts within Fukushima will continue for the foreseeable future due to the long half life of Cs-137.

Nuclear Accidents and Radioecology

Throughout the past 13 years since the accident, vast amounts of research into the extent of radioactive contamination and its effects on people and the environment of Japan has been conducted. Unfortunate events such as the 1979 Three Mile Island nuclear power plant partial core meltdown, the 1986 Chernobyl nuclear power plant explosion, and the 2011 Fukushima-Daiichi nuclear power plant accident have all resulted in growth of the scientific field of radioecology.

The unique physical and biological characteristics of ecosystems alter the ways radioactive contamination moves throughout the environment, and so, radionuclide movement dynamics is not a "one size fits all". The fundamental concepts are typically applicable, but the behavior observed may vary depending on the ecosystem. There is a significant amount of research on radiocesium movement dynamics in the environments surrounding the 1986 Chernobyl Nuclear Power Plant disaster. Any radiocesium movement mechanisms found to be supported in the literature for Chernobyl may not be *directly* applied to the situation in Fukushima. There are key differences in the ecosystem of Fukushima (soil type, forest coverage, landscape topography, weather, etc.) that researchers must consider, because these variables may contribute to different outcomes during scientific investigation (Yoschenko et al. 2018). This study acknowledges the unique characteristics of a nearby region to the Fukushima-Daiichi

nuclear plant, Kawauchi Village, and considers the current literature's findings on radiocesium's behavior in Japan's forest environments.

Radiocesium Generation

Cesium is the 55th element in the periodic table which, in its stable form, contains 55 protons and 78 neutrons. One of its radioactive isotopes, Cs137, can decay via beta minus (β-), ejecting a beta particle with an average energy of 174 keV in 94% of decays, decaying into barium-137 metastable (Ba137m). Ba137m exists with 662 keV of excess energy and will promptly de-excite via 662 keV gamma ray emission 85% of the time to form stable barium-137. Although alternative pathways with lower probabilities exist such as emitting a beta particle with 836 keV to directly reach its ground state of Ba137, or, as an alternative to gamma emission, its nucleus undergoes internal conversion of its excess energy and transfers it to a k-shell election where it is ejected with an energy of 622 keV minus its electron binding energy. However, the first pathway is most probable and is what is considered when dealing with Cs137 in practical settings. It is this moderately high energy gamma ray and its 30-year half-life that makes Cs137 a radioisotope of concern in the field of radioecology.

In similar fashion, Cs134 also undergoes beta minus decay into barium-134 metastable, where 70% of the time a beta particle with 210 keV average energy is emitted and leaves the

nucleus with an excess of 1400 keV. The nucleus then de-excites multiple times, predominantly emitting 795 keV (85%) and 605 keV (97%) gamma rays in succession before forming stable barium-134 (National Nuclear Data Center 2024). With its shorter half-life relative to Cs137, Cs134 decays more rapidly and is only considered a contributor to dose in the initial years after a nuclear accident.

In the context of light-water nuclear reactors, Cs134 and Cs137 are relevant because they are both produced during normal operations. When a U235 atom in a reactor fuel rod captures a thermal neutron, it very briefly exists as uranium-236 before it undergoes nuclear fission, resulting in two fission fragments, 2-3 neutrons, and gamma rays. The resulting fission fragments are radioactive themselves and thus undergo a chain of decays (now called fission products) before reaching a stable daughter. Cs137 is a high probability fission product, with a fission yield of roughly six atoms per 100 fission events of U235 (NCRP 2006) (IAEA n.d.). As for Cs134, it is a low yield fission fragment, and is also considered an activation product, which forms when the fission product Xe133 (fission yield of 6.7 atoms per 100 fission events of U235) beta decays (98.5%) into stable Cs133. With a thermal neutron capture cross section of 29 barns, Cs133 can capture a thermal neutron to become Cs134 (National Nuclear Data Center 2024).

With Cs134 being less persistent than Cs137 because it is lower yield and because of its shorter half-life, it is not as environmentally significant in the long term.

Radiocesium Dispersion

In a perfectly functioning light-water reactor, fission products such as Cs137 are contained and do not leak out of the reactor. However, in the Fukushima-Daiichi Nuclear Power Plant accident, this containment was compromised by the hydrogen gas explosions and overheating of fuel in three of the six reactor buildings. This caused a significant release of Cs137 into the surrounding atmosphere, with estimations in the range of 10-36 PBq spread throughout the greater Fukushima region (Onda et al, 2020) (Lopez-Vicente et al 2018). Of the estimated 10-36 PBq of Cs137 that was released, studies estimate around 2.7 PBq was deposited onto the terrestrial environment of Fukushima. Much of the fallout deposited onto the heavily forested regions to the west of the Fukushima Daiichi Nuclear Power Plant, with over 2,600 km^2 of forest receiving greater than 100 $kBqm^{-2}$ of Cs137 (Onda et al, 2020). In comparison to Chernobyl, more than 192,000 km^2 of Europe and former Soviet Union reached deposition levels greater than 37 $kBqm^{-2}$ (NCRP 2006).

Radiocesium Deposition

Much of the airborne radiocesium released from the accident was deposited onto the tree canopy due to the dense forest in Fukushima prefecture. The mechanism for radiocesium moving from the air to tree canopy and ultimately into the soil is a multi-step process with several variables affecting its progress. The basic pathway is removal of radiocesium particulates from the air by a process called *precipitation scavenging.* Precipitation scavenging is where micron sized particulates of radiocesium suspended in the air adhere to water droplets, either through condensation, *rainout,* or impingement, *washout*, and fall to earth due to gravity (Whicker et al, 1982). This rainfall can land directly onto the forest floor, a method known as *throughfall*. Alternatively, the raindrops can land on the tree foliage and remain there until the next rainfall event washes the radiocesium off the foliage or trickles down the tree trunks, known as *stemflow*, and falls onto the forest floor. If radiocesium remains on the tree foliage, it can also move to the forest floor through *litterfall*, when leaves, twigs, and branches fall off the canopy and onto the floor from either the changing seasons, wind, dying limbs, etc. The above-mentioned processes typically occur within the first year after fallout (Onda et al, 2020). Because of this, it is known that the litter layer on the soil surface of forests can be a large source of fallout radiocesium contamination.

The way in which radionuclides move about the environment is a complex mechanism governed by chemical, biological, and physical factors (Whicker et al, 1982). In the case of this study, those factors applicable to the unique characteristics of the forest soils of Fukushima Japan will be discussed in the context of vertical migration.

Vertical Migration in soils

Much of radiocesium's behavior in soils can be understood from its chemical properties and interactions with materials that make up soils. The chemical properties of a particular element do not typically change for each of its isotopes because they all have the same electron shell configuration. Cesium typically exists in the +1 oxidation state, meaning it only has one bound electron in its outermost electron shell or valence shell. In an attempt to gain chemical stability via a full valence electron shell (noble gas electron configuration), cesium tends to "give away" this single valence electron and exist as a Cs+ ion or creates ionic bonds with other molecules that have available negative charge (NCRP 2006). This classifies cesium as a Group I metal or "alkali metal", which all also have a single valence electron and follow the same process to gain a noble gas electron configuration. The behavior of these alkali metals in ecological processes are very similar and thus are referred to as "chemical analogs", who compete for binding sites on other molecules in nature.

The soils throughout the forested regions in Fukushima/Kawauchi are considered andosols. Andosols are described as rich in volcanic ash, organic matter, and clay materials. Additionally, they are generally slightly acidic, less dense, and highly fertile (IUSS, 2022). A high amount of organic matter is known to have a high cation exchange capacity (CEC), meaning it attracts positively charged ions like cesium and retains them (Manaka et al. 2019) (Manaka et al. 2022) (Park et al. 2019). As the material decomposes into smaller and smaller particles, the organic compounds binding radiocesium are carried closer to the clay materials of the soil. Clays are known to have frayed edge sites (FES) that are negatively charged and strongly bind the positively charged radiocesium cations (Whicker et al. 1982) (Manaka et al. 2019) (NCRP 2006) (Park et al. 2019). Once bound to clay, the radiocesium is generally considered "irreversibly bound", which is how it remains in the mineral soil for a long time without much further penetration. The binding rate process is generally governed by these previously mentioned soil characteristics and has been shown to be more rapid in Fukushima compared to Chernobyl. Studies have shown that less than 50% of the Cs137 inventory in forests of Fukushima remained in the litter by 2012 or 2013 and had already moved to the mineral soil layer (Hashimoto et al. 2013) (Takahashi et al. 2018). Takahashi et al. 2018 reported a change in the fraction of Cs137 in litter to mineral soil was observed to be 0.22-0.44y^{-1} in a six-year study monitoring vertical

distribution in several forests of nearby Fukushima. Also, over 80-95% of Cs137 had migrated to the mineral soil by 2017 (Takahashi et al. 2018).

Measuring Dose Rate

Regarding the potential health risks associated from radiation exposure due to fallout radiocesium, it is important to discuss the system of radiation protection quantities developed and recommended by the International Commission on Radiological Protection (ICRP). ICRP 60 was published in 1990 to provide a framework for how radiological protection should be quantified. The recommendations were based on the understanding of health risks from radiation exposure at the time and laid the groundwork for how radiation protection should be practiced worldwide. An updated version of these recommendations, ICRP 103, was published in 2007 to reflect the advances in radiation biology, dosimetry, and radiation risk assessment. ICRP 103 is the main reference for radiation dose guidelines today.

The basic concept in the ICRP's system of radiation protection is the three different types of radiation quantities. Since ionizing radiation is something humans cannot physically sense, instruments must be used to measure radiation fields and then be interpreted to represent relative biological risk. The first type of radiation quantities are physical quantities. Physical quantities are directly measurable by instrumentation to quantify how much energy is transferred

or absorbed in a mass of material. Kinetic Energy Released per unit Mass (KERMA) represents the total energy transferred to all charged particles liberated by uncharged radiation, such as gamma or x rays, divided by a unit mass of material. These liberated charged particles, such as electrons, then go on to directly ionize atoms in matter and deliver dose. Any energy that exits the mass of material, usually bremsstrahlung, is lost, and therefore not finally absorbed by the unit mass. This is what differentiates KERMA from absorbed dose. Absorbed dose is the final amount of energy absorbed from charged particles divided by a unit mass of material, and its unit is the Gray (J/kg).

The next set of radiation quantities is the protection quantities. Protection quantities begin to consider the biological risk associated with exposure to radiation. Typically, protection quantities are only measured with anthropomorphic phantoms in a laboratory setting to simulate the human body. The first protection quantity averages absorbed dose at a point over an entire organ and is called organ absorbed dose, also in units of Grays. Organ absorbed dose represents the total energy that was absorbed by an entire organ for the sake of estimating biological risk. However, different types of radiation produce different biological impacts. Radiation weighting factors characterize the biological effectiveness of a specific type of radiation incident on an organ. The radiation weighting factor is multiplied by organ absorbed dose measurements and

called equivalent dose, in units of the Sievert, and is the second protection quantity. Finally, to account for the specific tissue sensitivity of an organ, a tissue weighting factor is applied to create the final protection quantity. The result is what is called effective dose, also in units of sieverts, and represents the weighted sum of organ equivalent doses with respect to cancer induction and mortality (ICRP, 2007) (Johnson T.E. 2017) (Turner J.E. 2007).

In practical radiation exposure settings, these protection quantities for organ absorbed dose, equivalent dose, and effective dose cannot be *directly* measured for workers or the public. Because of this, a third set of quantities was introduced, called operational quantities. With the use of calibrated instrumentation, operational quantities are defined for use to estimate protection quantities from exposure to radiation in practical scenarios. Ambient dose equivalent, *H*(10),* is the operational quantity used for area monitoring. H*(10) represents the equivalent dose delivered by radiation, in most cases gamma rays, to a simple phantom known as the ICRU Sphere. The International Commission on Radiation Units and Measurements (ICRU) developed a spherical phantom that is 30 cm in diameter and 1 g cm^{-3} density of tissue-equivalent material composed of 76% oxygen, 11.1% carbon, 10.1% hydrogen, and 2.6% nitrogen. It is used to measure absorbed dose at 10 mm depth into the sphere, which represents theoretical dose delivered by gamma rays in an ambient area to human organs, hence it is written

as H*(10) for 10 mm. Using this ICRU sphere, field instruments can be calibrated to respond similarly and provide measurement readouts in dose equivalent that is produced by the radiation field in the ambient area (ICRP, 2007) (Johnson T.E. 2017) (Turner J.E. 2007).

The common instrument of choice to measure H*(10) in environmental settings is the sodium iodide scintillation counter. Scintillation detection is done using a crystal in which emits light once radiation interacts with it, where it is captured and then converted to an electronic signal that produces a measurement reading. Gamma ray photons interacting in a NaI scintillation crystal transfer all or part of their energy to the crystal's electrons. These electrons are now promoted to an excited state where they can de-excite back to their ground state by emitting visible or near-UV light photons in the eV range of energy. The number of light photons produced is proportional to the original energy of the primary interacting gamma ray. These light photons are collected by the photocathode, where new electrons are liberated. These photocathode electrons are accelerated by an applied high voltage and amplified through a series of dynodes in what is called the photomultiplier tube (PMT). The PMT will multiply the electrical signal by a factor close to a million. The detector output is an electronic pulse proportional to the energy absorbed by the crystal and provides the detector information to readout. (U.S. NRC 2010) (Knoll G.F. 2010)

The NaI instrument must be calibrated for the specific radionuclide of interest to determine H*(10). The NaI instrument can count the number of electrical signals due to gamma ray interactions, producing a count rate of radiation interactions. If the gamma rays are known to be from Cs137 and deposit 662 keV of energy during each interaction, the instrument can be calibrated to interpret a certain count rate of 662 keV gammas deposits X amount of energy and equates to X amount of equivalent dose. This conversion from count rate to equivalent dose is determined by the manufacturer and can be done so to represent the ICRU sphere and provide measurements of H*(10) within a given margin of error. Additionally, an energy response curve is provided with instrument calibration to show how it will response to gamma rays of different energies from different radionuclides. Proper corrections factors should be applied to convert these readings into the correct one, assuming the measured radionuclide is known (U.S. NRC 2010) (Knoll G.F. 2010).

Kawauchi Village Test Site

In a collaborative effort between the Japan Atomic Energy Agency, Japan Ministry of Forestry, Asia Air Survey Co., Ltd, The University of Tsukuba, and the Forestry and Forest Products Research Institute, scientific research efforts were initiated to address the extent of contamination in the forest ecosystems around Fukushima Prefecture. The Kawauchi Test site was established in 2012 in the forested mountains of Kawauchi, a village located in the

Fukushima Prefecture about 30 km southwest of the Fukushima Daiichi Nuclear Power Plant (37° 20' 07.8"N(37.3355)~ 37° 20' 10.3"N(37.3362), 140° 53' 17.5"E(140.8882)~ 140° 53' 20.8"E(140.8891)). The landscape is a 34-year-old Japanese ceder tree forest with a dense tree canopy shading the forest floor from sunlight. The forest floor is covered in a thick layer of dead debris, or litter, made of fallen twigs, pine needles, and dead tree limbs. The weather consists of average daily temperatures in the mid 20 degrees centigrade in the summers and 0 degrees centigrade in the winters. Average precipitation totals vary around 1100 – 1500 mm per year, with most of the precipitation falling during the summer rainy season (Japan Meteorological Agency 2024).

The test area named “Plot B” is a 60 m × 60 m area in the forest with an average slope of 34 degrees. As of November 2012, the average deposition of radioactive cesium (Cs134 + Cs137) was 1,120 kBq/m^2 and the measured air dose rate ranged from 2.2 – 4.5 μSv/hr (Noguchi,H et al. 2022). After these initial measurements were taken, a 40 m × 40 m area in the center of the test plot was clear cut (trees cut down and lumber removed) and had the litter removed (leaves and debris scraped off the forest floor), abbreviated as “CC+LR”. After the completion of the CC+LR, new cedar tree saplings were planted at a density of 3,000 per hectare and no follow up forestry clearing was conducted. Nearby, two sampling locations where the

forest was left untouched were used as a site for control sample/measurement collection. The forestry work was completed by the beginning of 2013.

Need for Further Data Analysis

The general motivation for conducting CC+LR at Plot B stems from the understanding that majority of fallout radiocesium tends to remain on vegetation surfaces or in the litter layer and will migrate into the soil over time. Removing the vegetation and litter should, in theory, reduce the amounts of radiocesium deposited on the forest floor and allow what is in the soil to move deeper in time, which also should reduce H*(10) measured within the CC+LR area. To gather data for analysis, a combination of soil sampling and H*(10) measurements were collected throughout 2013 (after completion of CC+LR) through 2019. Dr. Yuichi Onda and graduate researchers from the Center for Research in Radiation, Isotopes, and Earth System Sciences at the University of Tsukuba Japan currently retain the collected data and have been conducting a multitude of different studies in recent years. In early 2024, Dr. Onda expressed interest in collaborating with graduate researchers from the department of Environmental and Radiological Health Sciences at Colorado State University to further analyze the existing data. The details and goals of this study are presented in the next section.

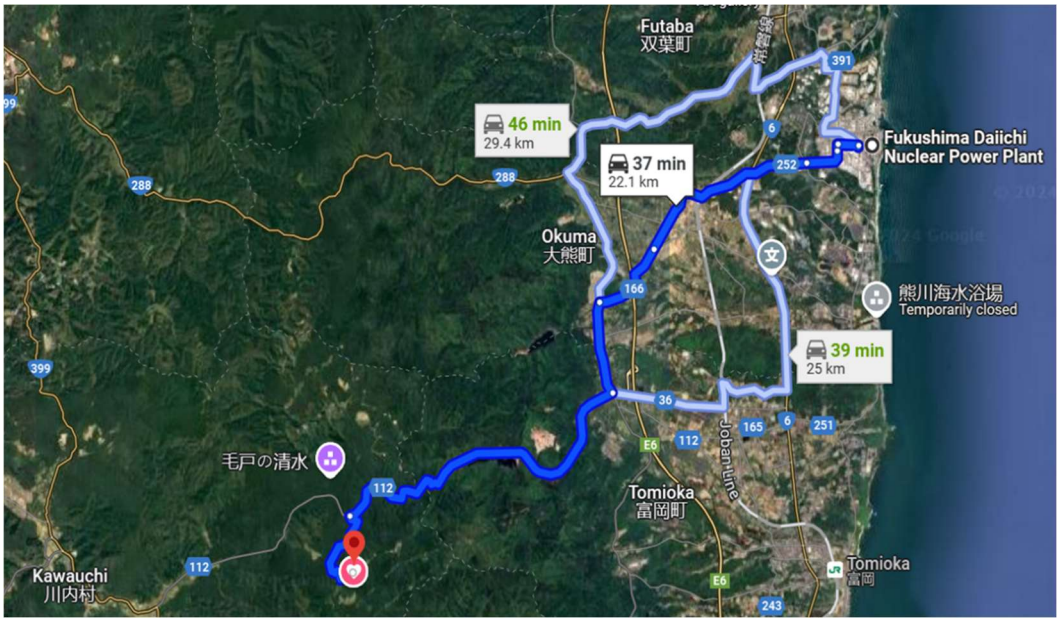

Figure 1: Screenshot of Google Maps route from Fukushima Daiichi Nuclear Power Plant to Kawauchi Test Site. Screenshot taken from Google (2025). Imagery ©2025 Airbus, Maxar Technologies, Map data ©2025.

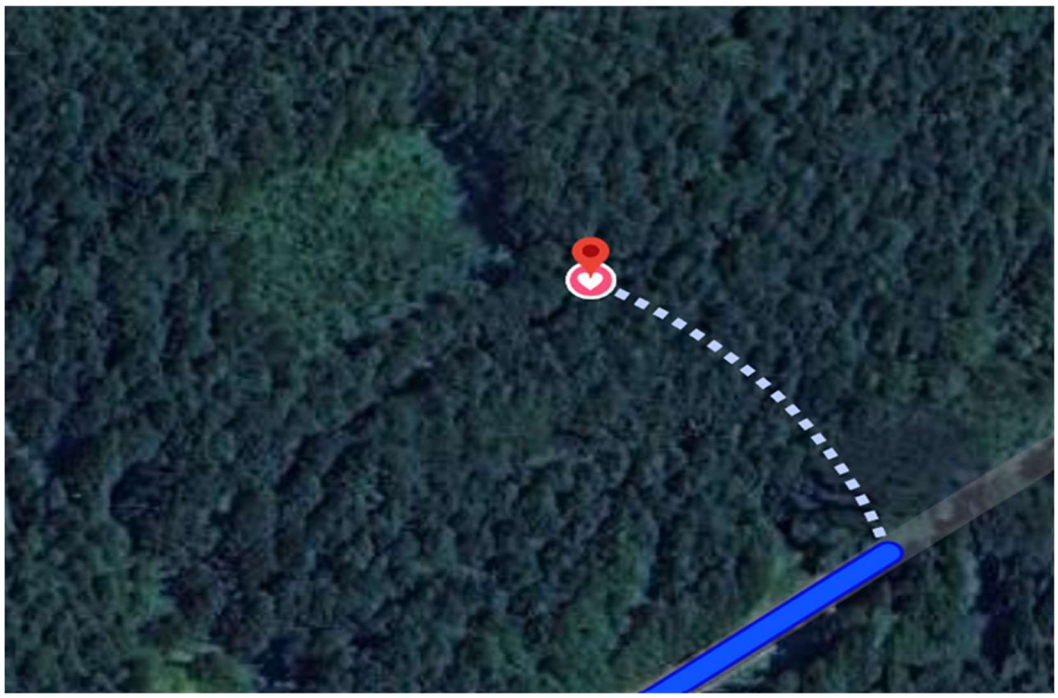

Figure 2: Screenshot of Google Maps arial view of the Plot B location at the Kawauchi Test Site. Screenshot taken from Google (2025). Imagery ©2025 Airbus, Maxar Technologies, Map data ©2025.

Figure 3: Picture of forest outside of Plot B boundary. Photo taken by Dr. Thomas Johnson, October 2024. (Johnson, 2024).

Figure 4: Picture emphasizing the slope of terrain at Kawauchi Test Site. Pictured left to right: Dr. Donovan Anderson of Hirosaki University, Dr. Junko Takahashi and Dr. Yuichi Onda, both from The University of Tsukuba. Photo taken by Dr. Thomas Johnson, October 2024. (Johnson, 2024).

Figure 5: Picture of Christian Grabowski from Colorado State University collecting H*(10) measurement at Plot B Kawauchi Test Site. Photo taken by Dr. Thomas Johnson, October 2024 (Johnson, 2024).

CHAPTER 2: LITERATURE REVIEW

Initial Findings from Kawauchi Test Site

The Japan Ministry of Forestry shared their initial data collection results in their 2020 report called *Verification project for prevention of diffusion of radioactive materials,* which is a yearly report available to the Japanese public on the past findings from the ongoing remediation research, the same reference as Noguchi, H et al. 2022. The University of Tsukuba has direct involvement with this work and also have access to the data published in the report. A summary of the results from Plot B within the report is written below. A diagram depicting the experimental setup at Plot B is shown in Figure 6. The grid format for H*(10) measurements across the CC+LR area are depicted in Figure 7. Note, coordinate G7 marks the center point of the CC+LR area.

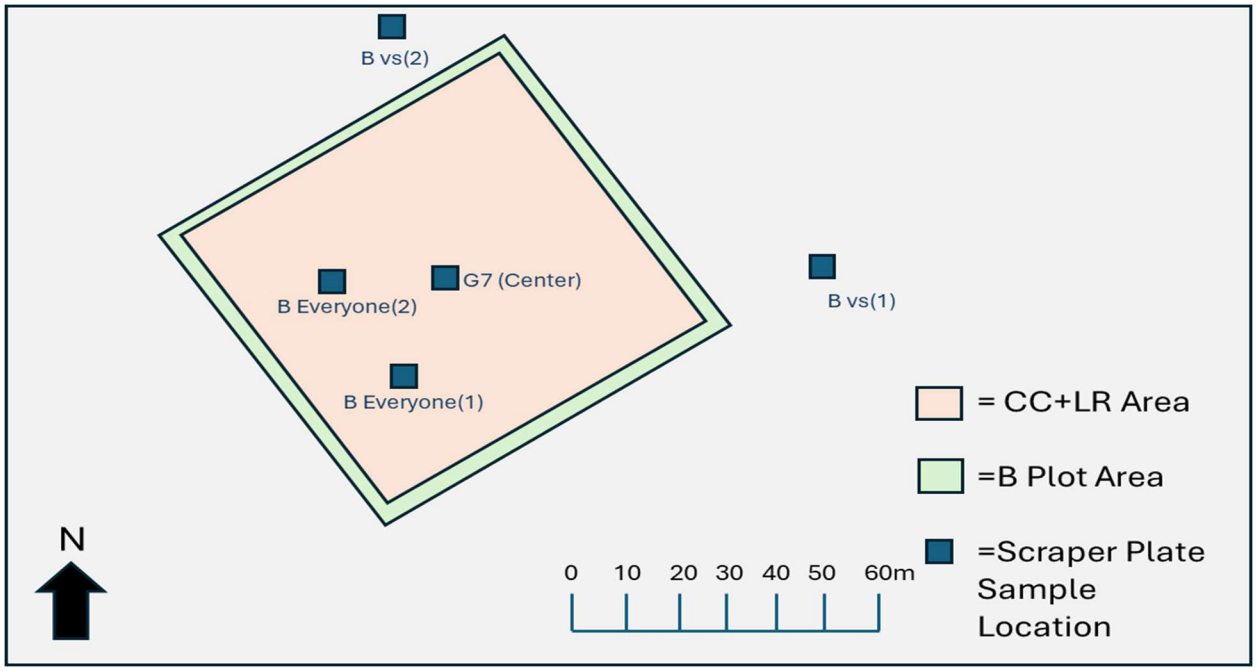

Figure 6: Diagram of Kawauchi Test Site Plot B showing forestry work areas and approximate scraper plate sampling locations. Recreated from Noguchi, H et al. 2022.

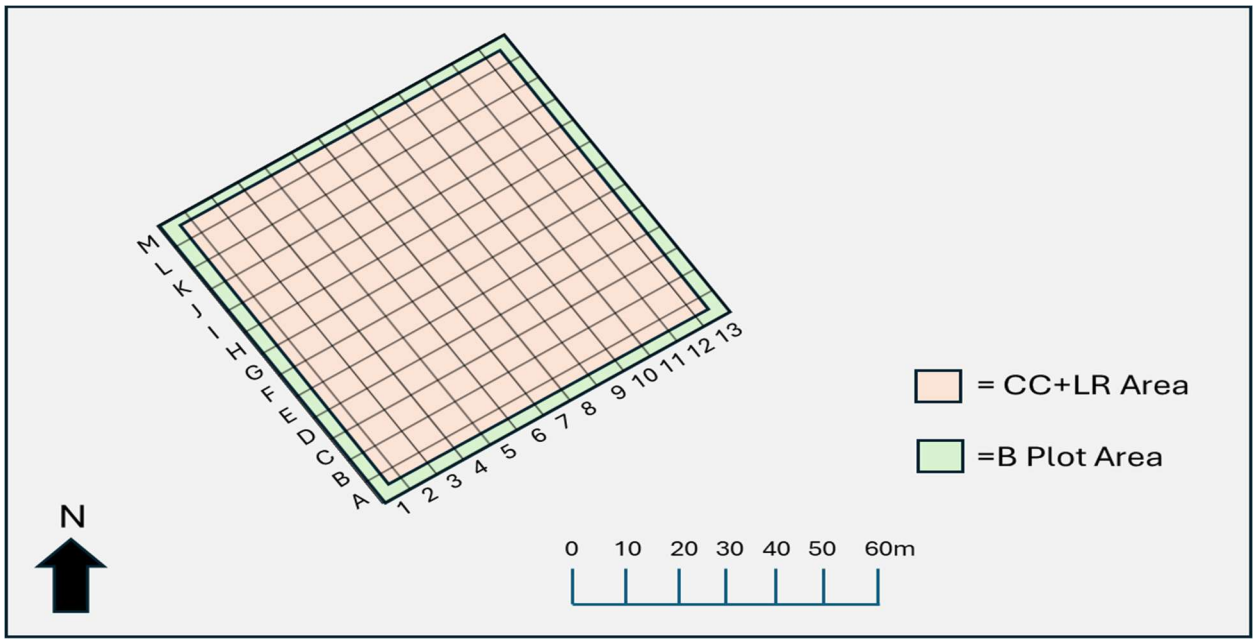

Figure 7: Diagram of Kawauchi Test Site Plot B showing grid coordinate overlay of Plot B area for approximate H*(10) measurement locations. G7 is the center. Recreated from Noguchi, H et al. 2022.

First were the reported results of H*(10) measurement at Plot B. Using a sodium iodide (NaI) scintillation detector, measurements were collected within the CC+LR area and compared to control sites outside the area boundary. The authors summarized that H*(10) at the center of the CC+LR plot decreased at a rate faster than the control plot as the CC+LR boundary was expanded from 20 m × 20 m to 40 m × 40 m. By 2017, the center of the CC+LR plot showed a 48% decline in H*(10) while the control plot H*(10) had declined by 20%. Note H*(10) measurements collected near the edge of the CC+LR boundary were moderately higher than those collected at the center (Noguchi, H et al. 2022).

These summarized results provide some information on the effectiveness of the CC+LR. First, CC+LR seemed to reduce H*(10) in the CC+LR boundary compared to control areas. Secondly, the contamination in untouched areas outside the CC+LR boundary seemed to have a larger effect on H*(10) measurements collected near the edge of the boundary compared to the centermost point. These findings suggest that CC+LR has the potential to significantly lower H*(10) compared to untouched forest, however, this conclusion can benefit from further analysis of the contamination basis for H*(10) values. Further investigation could be done to better

understand the amount of contamination that is producing H*(10) values and determine how much these measurements are influenced by contamination outside the test area boundary.

The second batch of reported results was from the soil sampling campaign each year from 2013 – 2019. Three locations within the CC+LR boundary and two locations in the control area of Plot B were sampled using a scraper plate to measure contamination levels at each layer of litter and soil. The authors summarized that the litter layers in the Control area had radiocesium concentrations five to seven times higher than the top 0-0.5 cm of soil in 2013. By 2016 this flipped, and the radiocesium concentration became higher in the 0-0.5 cm soil versus the litter layer, suggesting the radiocesium had begun to move downwards from litter to soil. As for the CC+LR area, concentrations of radiocesium increased in the deeper layers of soil below 0-0.5 cm from 2013-2017. A parameter known as *buffer depth*, which represents the depth in soil at which the concentration of radiocesium is 1/e or 36.8% of what is present at the surface layer, was shown to increase gradually over this course of time as well (more details in the Methodology section of this thesis). This suggests that the radiocesium is moving deeper with time. It was also noted that the control area from 2013-2017 did not show a significant increase in buffer depth. Finally, the authors commented that a new litter layer accumulated in the CC+LR area from fallen debris originating outside the boundary due to strong winds. The litter layers near the edge

of the boundary were thicker than the central part, which also increased the radiocesium concentration. Further analysis of the raw data from these soil samples may show a clearer relationship between how radiocesium is distributed and its role in the H*(10) measurements collected in Plot B. This is discussed further in the following section.

Relationship of Depth Distribution to H*(10)

In a situation like the Kawauchi Test Site, where fallout radiocesium has deposited and migrated to the litter layer and next into the soil, it is known that the quantity of radiocesium and its distribution within the upper layers of the forest floor are the highest contributors to H*(10) measurements (Takahashi et al. 2022) (Malins et al. 2021). Essentially, the more radiocesium deposited onto the floor, the higher the H*(10) due to a larger flux of gamma rays reaching the detector. Alternatively, the deeper the radiocesium has penetrated the soil, the greater the shielding effect from the soil above, reducing H*(10) measurements. This relationship is more complex in forests due to all its features, making it rather challenging for researchers to accurately evaluate through modelling.

Nevertheless, the relationship between fallout radiocesium deposition in forests and H*(10) values has been modelled using different methodologies over the years (Malins et al. 2021). One approach was performed by Saito et al. in 2014, using the Monte Carlo code YURI to

model H*(10) values based on radionuclide deposition densities and vertical distribution in soils. The Saito model produced a set of conversion coefficients, estimating H*(10) by applying the interpolated conversion coefficient (μ Sv/hr per Bq/m^2) at the corresponding relaxation depth (g/cm^2) (similar to buffer depth) to the radionuclide deposition (Bq/m^2) at the area of interest. Essentially, one could estimate H*(10) using data from soil sampling. The Saito method was used by Teramage and Sun in 2020 to predict H*(10) in radiocesium contaminated Japanese cypress forest in Tochigi Prefecture of central Japan. Their results highlight the practical use of the Saito method in a real-world situation and suggest it can be used to evaluate progress of decontamination measures (Saito et al. 2014) (Teramage and Sun, 2020).

In similar fashion, another approach to evaluate H*(10) from fallout radionuclides in the complex forest environment considers where the gamma rays contributing to H*(10) originate. High energy gamma rays like the 662 keV emissions from Cs137 can travel great distances in air between interactions. For reference, a 1 MeV photon in dry air can travel an average of 131 m between interactions. This average distance value is known as the mean free path. (Hubbell and Seltzer, 2004). Therefore, gamma rays can originate from a rather wide range of land and still retain enough energy to significantly contribute to H*(10). Malins et al. in 2015 describes modeling a “field of view” approach to determining photon contribution to H*(10) using the

Monte Carlo code PHITS. The Malins model provides a contribution fraction of total H*(10) for varying radii volumes of soil around a measurement point. Contribution fractions are governed by relaxation depths (g/cm^2) of fallout radionuclides, in this case Cs134 and Cs137. As the radius around the measurement point extends towards the limit of 1000 m, the contribution ratio of H*(10)(r) / H*(10)(1000) increases towards 1 at varying rates dependent on the relaxation depth. The Malins model can be used as a quick evaluation tool for the effectiveness of remediation work on lowering H*(10). Applying the contribution ratio that closely represents the radius of a remediation area and its relaxation depth of radiocesium in soil, one could estimate the maximum theoretical H*(10) achievable. Assuming all radiocesium was *perfectly* removed from the CC+LR area boundary, the only remaining contributor towards H*(10) at the center of the CC+LR area are gamma rays originating from outside the area (Malins et al. 2015). The Malins estimation can then be compared to H*(10) values measured by handheld instrumentation in the field.

The hypothesis for this thesis is that both models will effectively predict H*(10) within 20% using existing data at the Kawauchi Test Site Plot B. The hypothesis compares estimations of H*(10) derived from both models, incorporating soil sampling data, against H*(10) values measured by field instrumentation. This provides a contribution to two areas of radioecology

research: 1) Many models in radioecology exist, but few are tested with actual data. This study will test two models with actual data. 2) There remains a need for further analysis of data from the Kawauchi Test Site Plot B. The conclusions from the Noguchi, H et al. 2022 report lack deeper explanation into why the H*(10) values differ within the CC+LR boundary and in the Control area. The authors reported that CC+LR operations seem to reduce H*(10) more effectively compared to the untouched control areas, but deeper understanding of the underlying conditions could help to better explain these results. This could be achieved through further investigation of the distribution of radiocesium in soils and its relationship to H*(10) measured at Plot B.

CHAPTER 3: METHODOLOGY

Measured Ambient Dose Equivalent Rate Analysis

Data from field measurements of H*(10) was provided by the University of Tsukuba from their participation in the Kawauchi Test Site work efforts. Design and collection of measurements were conducted by Asia Air Survey Co., Ltd. (Noguchi, H. et al. 2022). Summary of design plan is described below.

H*(10) values in units of μSv/hr were measured using a Sodium Iodide (NaI(Tl)) scintillation detector held at 1 meter above the ground surface by a worker. The measurement points followed a grid coordinate pattern set across the Plot B area and at two locations in each of the two control areas, shown in Figure 7. For this experiment, the NaI measurements serve as the reference H*(10) values for models comparison. The Control area data points were the average (n=4) H*(10) from each year and the CC+LR data points were from the center coordinate at G7. These values are listed in Table 1.

Table 1: NaI H*(10) data points for the Control and center (G7) of CC+LR areas.

Year	G7 (μSv/hr)	Control (μSv/hr)
2013	1.02 ± 0.15	2.84 ± 0.47
2014	0.75 ± 0.11	2.26 ± 0.36
2015	0.54 ± 0.08	2.05 ± 0.34
2016	0.51 ± 0.08	1.77 ± 0.28
2017	0.43 ± 0.06	1.43 ± 0.23
2018	0.39 ± 0.06	1.36 ± 0.23
2019	0.36 ± 0.05	1.28 ± 0.21

Scraper Plate Data Analysis

Soil sampling data was also shared by the University of Tsukuba from their participation in the Kawauchi Test Site work efforts. Survey design and collection methodology are also listed in the same document as above and summarized below (Noguchi, H. et al. 2022).

Upon completion of the forestry clearing work, soil samples were collected once a year from 2013 - 2019 via scraper plate at three CC+LR sites and two control sites. The three CC+LR soil sampling locations were named *G7* at the center of the test plot, *B Everyone(1)* located downslope of *G7,* and *B Everyone(2)* located upslope of *G7.* The two control sampling locations were *B vs(1)* located outside the eastern corner of the CC+LR area and *B vs(2)* located upslope of the northern corner. See Figure 6 for approximate map locations. Samples were collected as close as possible to the previous year's location. Since no additional forestry clearing was done after 2013, any litter layer present was considered to be from nearby fallen debris from trees outside the CC+LR area and were taken into account when using the scraper plate. The scraper plate was 450 cm^2 in area and placed normal to the sloped surface. A single litter layer was collected at 1 cm thickness, while a few samples in later years considered 2 litter layers at 0.5 cm thickness each. The remaining soil layer segments were 0-0.5, 0.5-1.0, 1.0-1.5, 1.5-2.0, 2.0-3.0, 3.0-5.0, 5.0-7.0, and 7.0-10.0 cm deep from the soil surface. The soil samples were dried at 105 $^\circ$C and then dry weight was measured. Next, they were crushed to 4mm or less sized particles to

homogenize the material, filled into a U-8 container, and activity was measured via gamma ray spectrometry using a high purity germanium semiconductor. The resulting data per sample consisted of dry weight per unit area (kg/m^2) and Cs134/Cs137 concentration (kBq/kg). Activity was decay corrected back to the date of the accident, March 11, 2011, using Equation 1:

$$A_o = \frac{A_f}{e^{-\lambda}}$$

(Equation 1)

where A_f (kBq) is the activity of Cs134/Cs137 at the time of measurement, A_o (kBq) is the activity at the time of the accident, λ (yrs^{-1}) is the decay constant of Cs134/Cs137 (0.336 and 0.023 respectively), and t (yrs) is time passed between the accident and time of measurement. Decay correction was done to eliminate the physical decay of Cs134/Cs137, which allows the soil sample analysis to focus solely on the ecological decay, or migration of the radioisotopes, which is necessary for determining the coefficient of distribution in soil (explained below).

As described by Takahashi et al. 2015, the vertical distribution of radiocesium in soil follows an exponential decline with depth. The radiocesium concentration at a specific depth can be approximated from Equation 2 proposed by Beck, 1966:

$$C(x) = C(0) \cdot e^{-x/\alpha}$$

(Equation 2)

where C(x) is the activity concentration (Bq/kg) at depth x (cm), $C(0)$ is the activity concentration (Bq/kg) at depth x=0 (cm), α (cm) is the coefficient representing distribution characteristic, and x (cm) is the depth in soil (Beck 1966). However, in the case where uniformed density soil does NOT exist, mass depth (g/cm^2) should be used according to Isaksson and Erlandsson, 1998, changing Equation 2 into Equation 3:

$$C(x') = C(0) \cdot e^{-x'/\alpha \cdot D} \rightarrow C(x') = C(0) \cdot e^{-x'/\beta}$$

(Equation 3)

where C(x') is the activity concentration (Bq/kg) at mass depth x' (g/cm^2), $C(0)$ is the activity concentration (Bq/kg) at mass depth x=0 (g/cm^2), β (g/cm^2) is the coefficient when using mass depth, x (g/cm^2) is the mass depth in soil, and D (g/cm^3) is the bulk density of soil (Isaksson and Erlandsson 1998).

Using the soil sampling data with Equation 3 above, the method of least squares was used to determine β for each sampling event, which corresponds to the relaxation mass depth, i.e. the mass depth in the soil where the concentration $C(x')$ decreases to 1/e or 0.367 of $C(0)$. The

analysis spreadsheet to conduct the least squares approximation was provided by the University of Tsukuba. An example of this analysis is shown in Table 2 and was performed for both Cs134 and Cs137 using each of their own activity concentration data. The resulting β values for Cs134 and Cs137 for each year at each sample location are listed in Table 3. Note: the spreadsheet calculates β in units of (kg/m^2) but is converted to units of (g/cm^2) when used with the Saito and Malins models. To simplify the application of the models from Saito et al. 2014 and Malins et al. 2015, any litter layer present during soil sampling was considered part of the vertical depth distribution to determine β. The CC+LR process is supposed to remove any litter, so it is likely any remains present are from the neighboring forest outside the CC+LR boundary. Teramage and Sun were able to apply a conversion coefficient to the litter layer separate from the soil in their study. However, it is unclear how they were able to accurately achieve this. Attempts to contact the authors Teramage and Sun for clarification were unsuccessful. Saito, the primary model author, returned communication and confirmed this approach of combining the two layers is acceptable. Please see Appendix for proof of communication and soil data for β values.

Table 2: Example soil analysis table using Equation 3 and Method of Least Squares to approximate relaxation mass depth or β (kg/m^2). Values were converted to units of (g/cm^2) when applied to the H*(10) models. This was performed for both Cs134 and Cs137 at the three CC+LR and two Control soil samples from 2013 – 2019. Excel spreadsheet was shared by Dr. Junko Takahashi from the University of Tsukuba.

G7 11/11/2013										
Sampling layer/depth										
	χ			χ'	C	C(χ)	Residuals			
	Central Depth	dry weight of samples/ sampling area (450 cm^2)	dry weight /unit area (m^2)	dry mass depth	Cs-137 Conc.	Cs-137 conc. estimated by exponential equation	Difference between actual and predicted values	Squares of the residuals		
	cm	g	kg/m2	kg/m2	kBq/kg	kBq/kg				
Litter Layer (1.0-0)		157.2	3.493333333	3.493333333	8.9	8.180900789	0.719099211006668	0.517103675	β	7.73
0-0.5		56	1.244444444	4.737777778	6	6.964778071	-0.964778071394742	0.930796727	C(0)	12.85
0.5-1.0		111.4	2.475555556	7.213333333	5.2	5.056714777	0.143285222772547	0.020530655		
1.0-1.5		115.1	2.557777778	9.771111111	3.6	3.632550391	-0.0325503909403722	0.001059528		
1.5-2.0		143.5	3.188888889	12.96	2.3	2.40496452	-0.104964519501912	0.01101755		
2.0-3.0		334.5	7.433333333	20.39333333	1.4	0.919639823	0.480360177123046	0.2307459		
3.0-5.0		632.1	14.04666667	34.44	0.4	0.14951715	0.250482849858531	0.062741658		
5.0-7.0		701.6	15.59111111	50.03111111	0.2	0.019907696	0.180092304015011	0.032433238		
7.0-10.0		1073	23.84444444	73.87555556	0.1	0.000911602	0.0990883984933718	0.009818511		
							the sum of the squares of the residuals =	1.816247442		

Table 3: Resulting β (kg/m^2) values for Cs134 and Cs137 at each sample location from 2013 – 2019.

Cs134	Year	G7	B Everyone(1)	B Everyone(2)	B vs(1)	B vs(2)
	2013	7.12	5.82	2.53	1.18	0.89
	2014	6.17	12.00	6.87	5.79	2.01
	2015	10.55	12.14	12.25	3.89	6.23
	2016	19.30	30.37	15.79	32.36	13.73
	2017	12.19	39.39	100.99	41.90	22.24
	2018	22.68	67.88	49.75	30.93	17.65
	2019	30.59	35.27	40.13	1.54	45.88
Cs137	Year	G7	B Everyone(1)	B Everyone(2)	B vs(1)	B vs(2)
	2013	7.73	6.04	2.6	1.21	0.50
	2014	6.41	11.79	7.05	6.02	2.05
	2015	10.94	12.94	12.2	3.57	6.13
	2016	21.52	30.84	17.31	33.05	13.84
	2017	13.63	38.51	104.49	39.14	22.74
	2018	21.55	67.31	50.52	32.55	17.53
	2019	33.03	37.14	39.05	58.18	45.08

Saito et al 2014 Conversion Coefficient Analysis

The Saito et al. conversion coefficients [(μSv/hr)/(Bq/m^2)] for β of 0-10 g/cm^2 for both Cs134 and Cs137 are listed in Table 4. These values were plotted and an exponential trendline was fit for interpolation. The coefficients listed by Saito et al. were distinct numbers from 0.1-10 g/cm^2, so an equation was fit to determine an exact conversion coefficient for each β value at each sampling location from 2013 – 2019 (Note: Calculated β values were converted from units of kg/m^2 to g/cm^2 to match those used by Saito et al.).

The inventory (Bq/m^2) at each sampling location was determined using Equations 4 and 5. The inventory at each soil layer was summed to determine the total inventory of the soil sample for the year.

$$\text{Dry Weight}_{\text{layer}}\left({}^{\text{kg}}/_{\text{m}^2}\right) \times \text{Concentration}_{\text{layer}}\left({}^{\text{kBq}}/_{\text{kg}}\right) \times {}^{1000\ \text{Bq}}/_{\text{kBq}} = \text{Inventory}_{\text{layer}}\left({}^{\text{Bq}}/_{\text{m}^2}\right)$$

(Equation 4)

$$\sum_{\text{Litter Layer 1}}^{\text{7.0−10.0 Layer}} \text{Inventory}_{\text{layer}}(\text{Bq/m}^2)$$

(Equation 5)

Table 4: Saito et al. conversion coefficients [(μSv/hr)/(Bq/m²)] for β of 0-10 g/cm² for both Cs134 and Cs137 (Saito et al. 2014).

Cs137 Coeff.		Cs134 Coeff.	
Dose Conversion Coefficient [(μSv/h) / (Bq/m^2)]	β (g/cm^2)	Dose Conversion Coefficient [(μSv/h) / (Bq/m^2)]	β (g/cm^2)
3.15E-06	0	8.50E-06	0
2.83E-06	0.1	7.64E-06	0.1
2.65E-06	0.2	7.17E-06	0.2
2.52E-06	0.3	6.83E-06	0.3
2.32E-06	0.5	6.32E-06	0.5
2.04E-06	1	5.54E-06	1
1.71E-06	2	4.66E-06	2
1.51E-06	3	4.12E-06	3
1.25E-06	5	3.41E-06	5
9.09E-07	10	2.48E-06	10
6.03E-07	20	1.65E-06	20
4.50E-07	30	1.23E-06	30
3.04E-07	50	8.35E-07	50
1.69E-07	100	4.64E-07	100

Due to the natural randomness of fallout distribution on environmental surfaces, there exists an issue of spatial variability amongst soil samples from year to year. The average total inventory across 2013 -2019 at each sampling location was determined to account for spatial variability. The arithmetic mean was determined (n=7 years) using Equation 6. This was done to mitigate variability amongst each location's yearly soil samples.

$$\frac{\sum_{2013}^{2019} \text{Inventory}_{\text{Total}}(\frac{\text{Bq}}{\text{m}^2})}{7} = \text{Avg Inventory}_{\text{Sample Location}}$$

(Equation 6)

Next, the original decay correction needed to be reversed. Since the Saito et al. analysis evaluates H*(10) based on the actual amount and distribution of radiocesium present the year of measurement, both physical and ecological decay must be determined. This was done using Equation 7.

$$A_f = A_o e^{-\lambda t}$$

(Equation 7)

where A_f (Bq/m^2) is the representative inventory of Cs134/Cs137 at the time of sample collection, A_o (Bq/m^2) is the inventory that was averaged from Equation 6 above, λ (yrs^{-1}) is the decay constant of Cs134/Cs137 (0.336 and 0.023 respectively), and t (yrs) is time passed between the accident and time of sample collection. The resulting A_f values for each year were then multiplied by their corresponding conversion coefficients, to give an estimated H*(10) for that sample location. This was done each year, at each sample location, for both Cs134 and Cs137. Values are recorded in with their associated uncertainty values. The H*(10) from both Cs134 and Cs137 were then added together for a sum total H*(10) resulting from the radiocesium deposited on and in the soil. For comparison to the NaI measurement, 0.127 μSv/hr was added to each data point to account for background's contribution to H*(10). This value was generated from the Government of Japan's Ministry of the Environment's annual radiation

exposure estimates from terrestrial and cosmic sources (Ministry of the Environment, Japan. 2022). Complete data set from this section can be seen in Tables 5 and 6.

Table 5: Saito et al. Model data for Cs134 and Cs137 at each CC+LR and Control sampling location from 2013 – 2019.

Cs134	Year	Dose Conversion Coefficient [(μSv/h) / (Bq/m^2)]	"Af" Inventory Values (Bq/m^2)	Calculated Dose Rate (uSv/hr)	% Total Relative Uncertainty
G7	2013	5.50E-06	6291.53	0.03	32.83
	2014	5.66E-06	4434.42	0.03	32.83
	2015	5.07E-06	3171.86	0.02	32.83
	2016	4.39E-06	2270.86	0.01	32.83
	2017	4.91E-06	1585.89	0.01	32.83
	2018	4.22E-06	1156.50	0.00	32.83
	2019	3.88E-06	826.46	0.00	32.83
B Everyone(1)	2013	5.73E-06	16442.74	0.09	23.46
	2014	4.92E-06	11546.63	0.06	23.46
	2015	4.91E-06	8274.31	0.04	23.46
	2016	3.89E-06	5923.91	0.02	23.46
	2017	3.60E-06	4133.24	0.01	23.46
	2018	3.00E-06	3014.14	0.01	23.46
	2019	3.72E-06	2153.97	0.01	23.46
B Everyone(2)	2013	6.65E-06	11238.16	0.07	18.97
	2014	5.54E-06	7913.63	0.04	18.97
	2015	4.90E-06	5655.26	0.03	18.97
	2016	4.62E-06	4052.56	0.02	18.97
	2017	2.56E-06	2827.56	0.01	18.97
	2018	3.34E-06	2061.98	0.01	18.97
	2019	3.58E-06	1474.89	0.01	18.97
B vs(1)	2013	7.50E-06	42553.97	0.32	30.26
	2014	5.73E-06	29993.03	0.17	30.26
	2015	6.17E-06	21512.78	0.13	30.26
	2016	3.82E-06	15359.38	0.06	30.26
	2017	3.53E-06	10716.58	0.04	30.26
	2018	3.87E-06	7815.00	0.03	30.26
	2019	7.20E-06	5584.78	0.04	30.26
B vs(2)	2013	7.81E-06	81460.62	0.64	28.62
	2014	6.91E-06	57362.51	0.40	28.62
	2015	5.65E-06	41181.69	0.23	28.62
	2016	4.77E-06	29375.25	0.14	28.62
	2017	4.24E-06	20514.64	0.09	28.62
	2018	4.49E-06	14960.16	0.07	28.62
	2019	3.43E-06	10690.88	0.04	28.62

Cs137	Year	Dose Conversion Coefficient [(μSv/h) / (Bq/m^2)]	"Af" Inventory Values (Bq/m^2)	Calculated Dose Rate (uSv/hr)	% Total Relative Uncertainty
G7	2013	2.41E-06	78067.15	0.19	27.79
	2014	2.51E-06	76220.02	0.19	27.79
	2015	2.24E-06	74491.66	0.17	27.79
	2016	1.90E-06	72807.08	0.14	27.79
	2017	2.13E-06	71039.62	0.15	27.79
	2018	1.90E-06	69520.67	0.13	27.79
	2019	1.69E-06	67939.94	0.11	27.79
B Everyone(1)	2013	2.54E-06	233695.18	0.59	23.98
	2014	2.20E-06	228108.27	0.50	23.98
	2015	2.16E-06	222963.80	0.48	23.98
	2016	1.72E-06	217921.62	0.38	23.98
	2017	1.61E-06	212617.99	0.34	23.98
	2018	1.33E-06	208071.84	0.28	23.98
	2019	1.63E-06	203340.80	0.33	23.98
B Everyone(2)	2013	2.96E-06	188808.01	0.56	28.78
	2014	2.46E-06	184329.05	0.45	28.78
	2015	2.19E-06	180137.86	0.39	28.78
	2016	2.01E-06	176075.26	0.35	28.78
	2017	1.11E-06	171790.06	0.19	28.78
	2018	1.48E-06	168116.88	0.25	28.78
	2019	1.60E-06	164304.67	0.26	28.78
B vs(1)	2013	3.34E-06	512509.89	1.71	16.49
	2014	2.54E-06	500383.50	1.27	16.49
	2015	2.80E-06	489129.29	1.37	16.49
	2016	1.69E-06	477977.59	0.81	16.49
	2017	1.60E-06	466344.90	0.75	16.49
	2018	1.70E-06	456373.61	0.77	16.49
	2019	1.41E-06	445996.80	0.63	16.49
B vs(2)	2013	3.78E-06	1004182.66	3.80	18.03
	2014	3.08E-06	980361.12	3.02	18.03
	2015	2.53E-06	958372.05	2.42	18.03
	2016	2.12E-06	936463.02	1.99	18.03
	2017	1.87E-06	913729.61	1.71	18.03
	2018	2.50E-06	894192.42	2.23	18.03
	2019	1.53E-06	873860.71	1.34	18.03

Table 6: Final Data points of combined Cs134 and Cs137 at CC+LR and Control areas.

Cs134 + Cs137	Saito Soil All CC + LR Avg (uSv/hr)	Saito Soil All CC + LR Avg + 0.127 Avg Bkg (uSv/hr)	% Total Relative Uncertainty	Numerical Total Relative Uncertainty	Final Data Point
2013	0.51	0.64	37%	0.24	0.64 ± 0.24
2014	0.42	0.55		0.20	0.55 ± 0.20
2015	0.38	0.50		0.19	0.50 ± 0.19
2016	0.31	0.43		0.16	0.43 ± 0.16
2017	0.24	0.37		0.14	0.37 ± 0.14
2018	0.23	0.35		0.13	0.35 ± 0.13
2019	0.24	0.37		0.14	0.37 ± 0.14
Cs134 + Cs137	Saito Soil All Ctrl Avg (uSv/hr)	Saito Soil All Ctrl Avg + 0.127 Avg Bkg (uSv/hr)	% Total Relative Uncertainty	Numerical Total Relative Uncertainty	Final Data Point
2013	3.23	3.36	34.15%	1.15	3.36 ± 1.15
2014	2.43	2.56		0.87	2.56 ± 0.87
2015	2.08	2.21		0.75	2.21 ± 0.75
2016	1.50	1.62		0.55	1.62 ± 0.55
2017	1.29	1.42		0.48	1.42 ± 0.48
2018	1.55	1.68		0.57	1.68 ± 0.57
2019	1.02	1.15		0.39	1.15 ± 0.39

Malins et al. 2015 Field of View Analysis

The second method used to evaluate H*(10) in the CC+LR area was taken from Malins et al. 2015. The authors provided a figure showing the effect of radiocesium penetration into the soil on the field of view at the measurement point. As β changes, so do the impact ratios of each radii volume of ground underneath the measurement point. The data extraction tool from WebPlotDigitizer was utilized to collect data from each of the available β value graphs provided by Malins et al. 2015. The data was fitted with a trendline to better determine exact contribution ratios from the soil 30 m away from the measurement point, in this case coordinate G7 at the center of B Plot (Malins et al. 2015) (Anastasopoulos A 2024).

Next, β values from the two Control groups were averaged for each year and used with their closest matching contribution ratio from the WebPlotDigitizer extraction. The contribution ratio within 30m (size of the CC+LR area) was found for each year and represents the theoretical maximum reduction in dose rate if CC+LR was perfectly executed. Equation 8 shows how this was used to calculate the theoretical lowest remaining dose rate at G7.

$$\mathrm{H}^{*}_{\mathrm{Control}}(10) - \left[\mathrm{H}^{*}_{\mathrm{Control}}(10) \cdot \frac{\mathrm{H}^{*}(10)[30\mathrm{m}]}{\mathrm{H}^{*}(10)[1000\mathrm{m}]}\right] = \mathrm{H}^{*}_{\mathrm{Theoretical}}(10)\ \mu\mathrm{Sv/hr}$$

(Equation 8)

The resulting theoretical dose rates are shown in Table 7 using the middle, high uncertainty, and low uncertainty control NaI H*(10) values.

Table 7: Malins et al. Model data using Control site β and NaI H*(10) values.

Year	Avg Cs134 & Cs137 β Control (g/cm^2)	Closest β from Malins Model (WebPlotDigitizer) (g/cm^2)	<30m Impact Ratio	Control Dose Rate (uSv/hr)	Avg Malins Estimate (uSv/hr)	High Estimate (uSv/hr)	Low Estimate (uSv/hr)
2013	0.09	0.1	0.66	2.84 ± 0.47	0.97	1.13	0.81
2014	0.40	0.5	0.69	2.26 ± 0.36	0.70	0.81	0.59
2015	0.50	0.5	0.69	2.05 ± 0.34	0.63	0.74	0.53
2016	2.32	2	0.71	1.77 ± 0.28	0.51	0.59	0.43
2017	3.15	2	0.71	1.43 ± 0.23	0.41	0.48	0.35
2018	2.47	2	0.71	1.36 ± 0.23	0.39	0.46	0.33
2019	3.77	5	0.74	1.28 ± 0.21	0.33	0.39	0.28

CHAPTER 4: RESULTS

Measured Ambient Dose Equivalent Rate Analysis

The results from Table 1 show that the NaI measurements in the Control group were higher than G7 every year. A paired t-test confirms the two locations were significantly different ($t(6) = 9.93$, p value = 0.000058). Additionally, in 2013 the Control group H*(10) was 22x higher than the average background H*(10) of Japan (0.127 μSv/hr) while G7 was only 8x higher. By 2019, both groups reduced to 10x and 2.8x background respectfully.

Scraper Plate Data Analysis

The resulting β values for both Cs134 and Cs137 at each sample location from 2013-2019 are listed in Table 3. The general trend of change regardless of isotope or sampling location was that β values increased over time. The data was plotted in Figures 8 & 9 to visualize this trend. At least until 2015, the β values were lower in the Control locations compared to the CC+LR areas. From 2016 – 2019, it seems that this was no longer the case. This can be seen in Figures 8 & 9 as trends from year to year fluctuate more across all sampling locations in the latter portion of the study compared to earlier years.

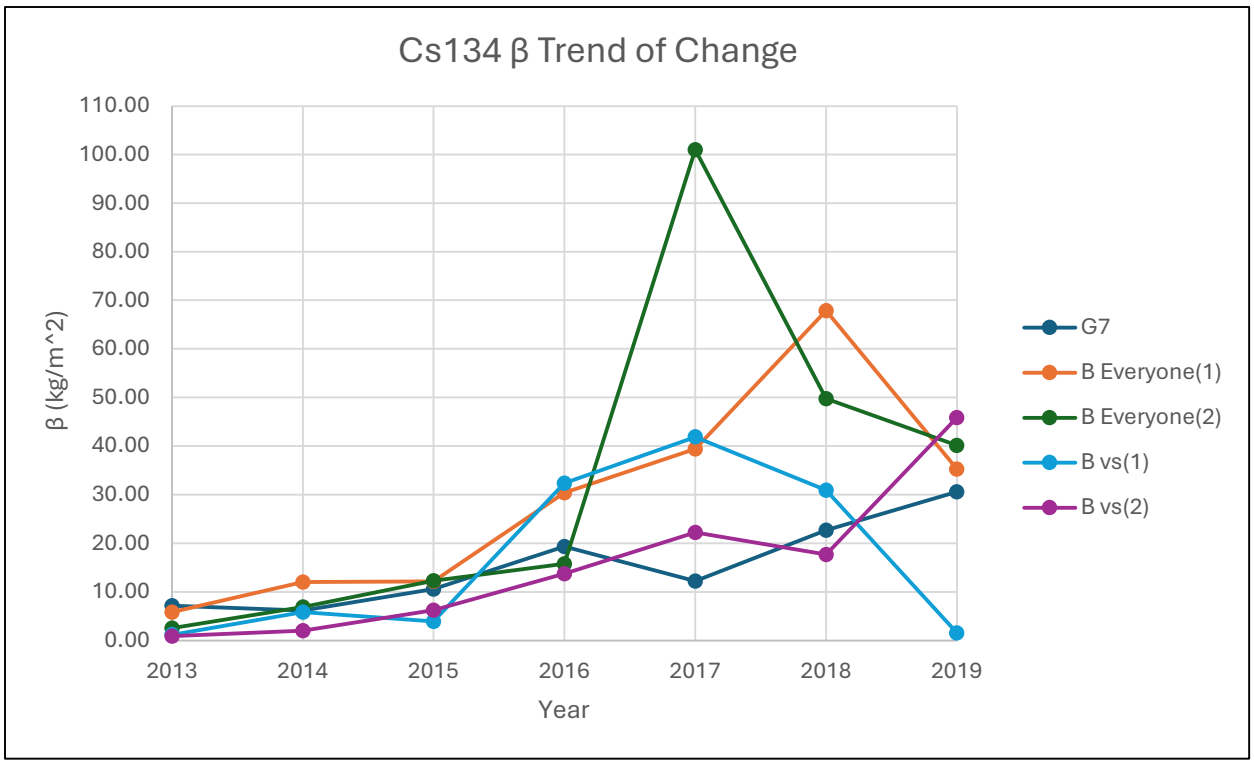

Figure 8: Cs134 β trend of change from 2013 - 2019

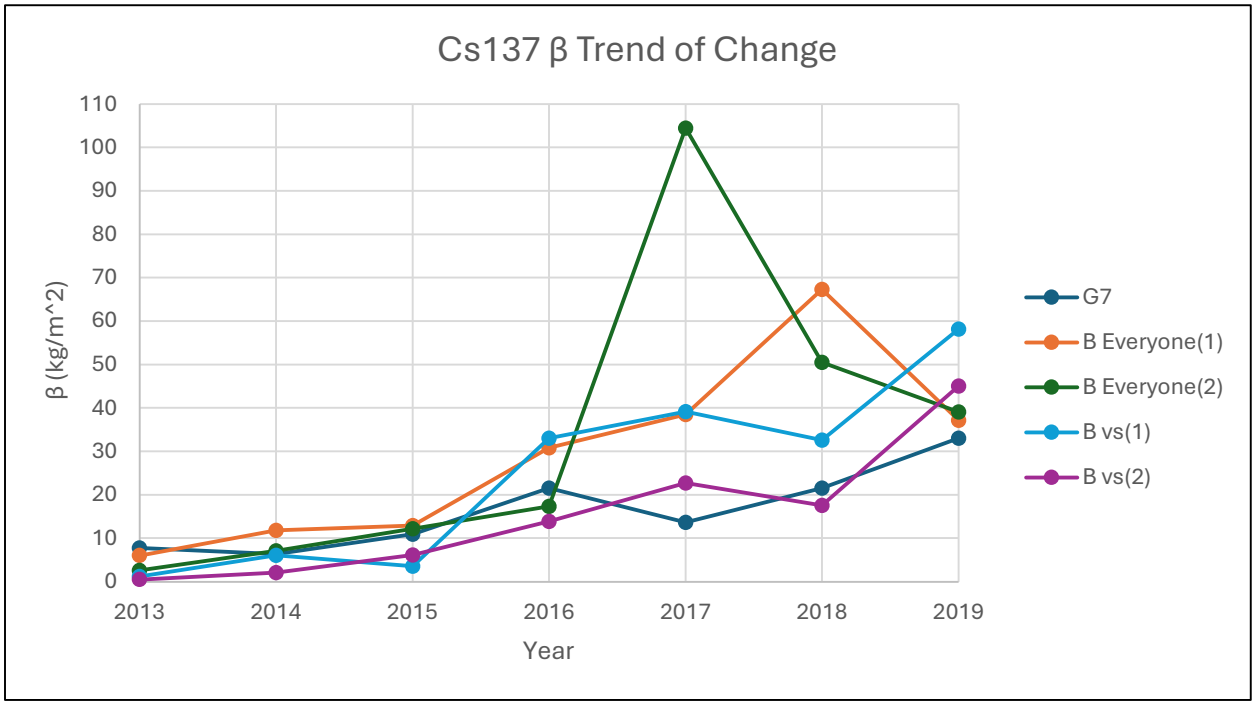

Figure 9: Cs137 β trend of change from 2013 - 2019

Saito et al 2014 Conversion Coefficient Data Analysis

The estimated H*(10) using the Saito et al. conversion coefficient method for both Cs134 and Cs137 at each sampling location from 2013-2019 are listed in Table 5 and the combined Control versus CC+LR comparison in Table 6. The final data points from Table 6 are plotted in Figure 10 for ease of comparison. A paired t-test shows the Saito Model Control and Saito Model CC+LR H*(10) estimates are significantly different ($t(6) = 6.17$, p value = 0.00083), with the Control being 5.25x higher in 2013 and decreasing to 3.1x higher in 2019. This indicates the CC+LR area was consistently a lower H*(10) compared to the Control area when using the Saito et al. model to estimate H*(10).

Next are comparisons of the model's H*(10) to the measured H*(10). Figure 11 compares Saito Model CC+LR values to the Measured NaI CC+LR value at G7. A paired t-test confirms the Saito et al. Model was able to predict H*(10) values statistically similar to those measured by the NaI from each year at the G7 (center) coordinate ($t(6) = 2.2$, p value = 0.069). Years 2013 and 2014 were the only two where the model did not predict H*(10) within 20%, which were 37% and 26% respectively. Figure 12 compares Saito Model Control values to the Measured NaI Control values. A paired t-test confirms the Saito et al. Model again was able to predict H*(10) values statistically similar to those measured by the NaI from each year in the

Control area ($t(6) = -1.51$, p value = 0.181). The only year where the model's estimate was outside of 20% was 2018, where it overestimated the NaI at 23% higher.

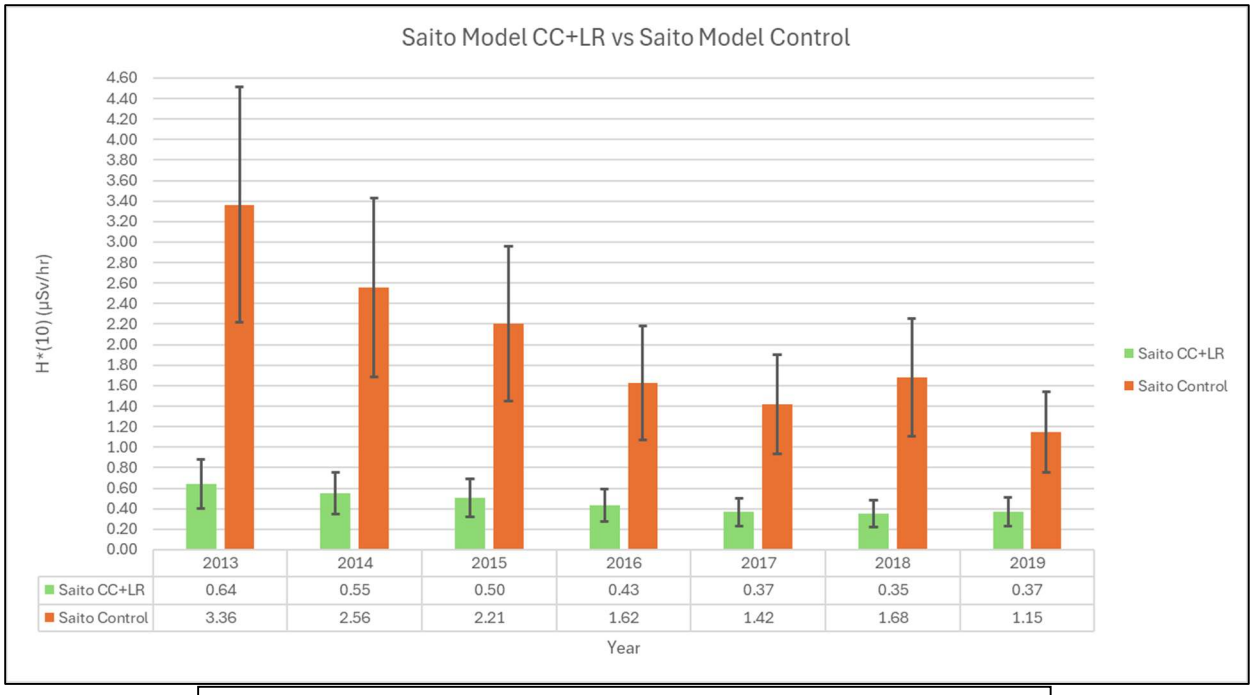

Figure 10: Comparison of Saito Model CC+LR to Saito Model Control H*(10) estimates.

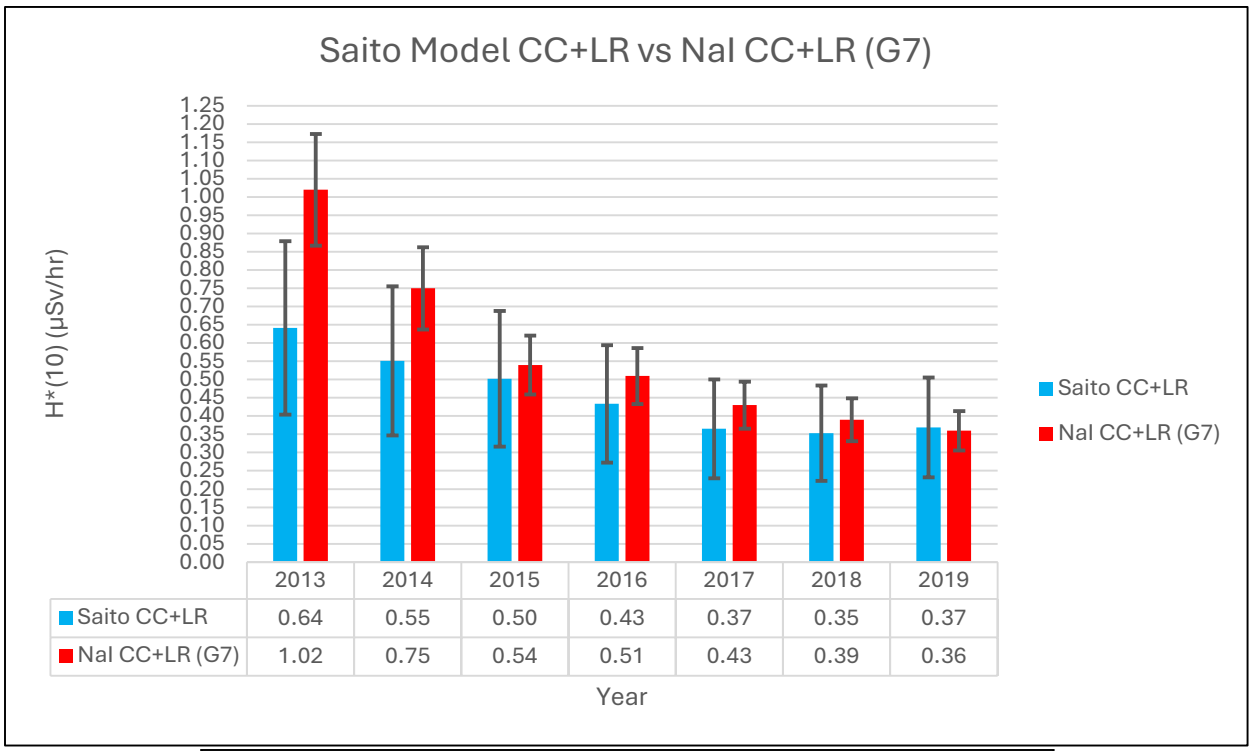

Figure 11: Comparison of H*(10) from Saito Model CC+LR to NaI CC+LR (G7). Model vs Field Measurement.

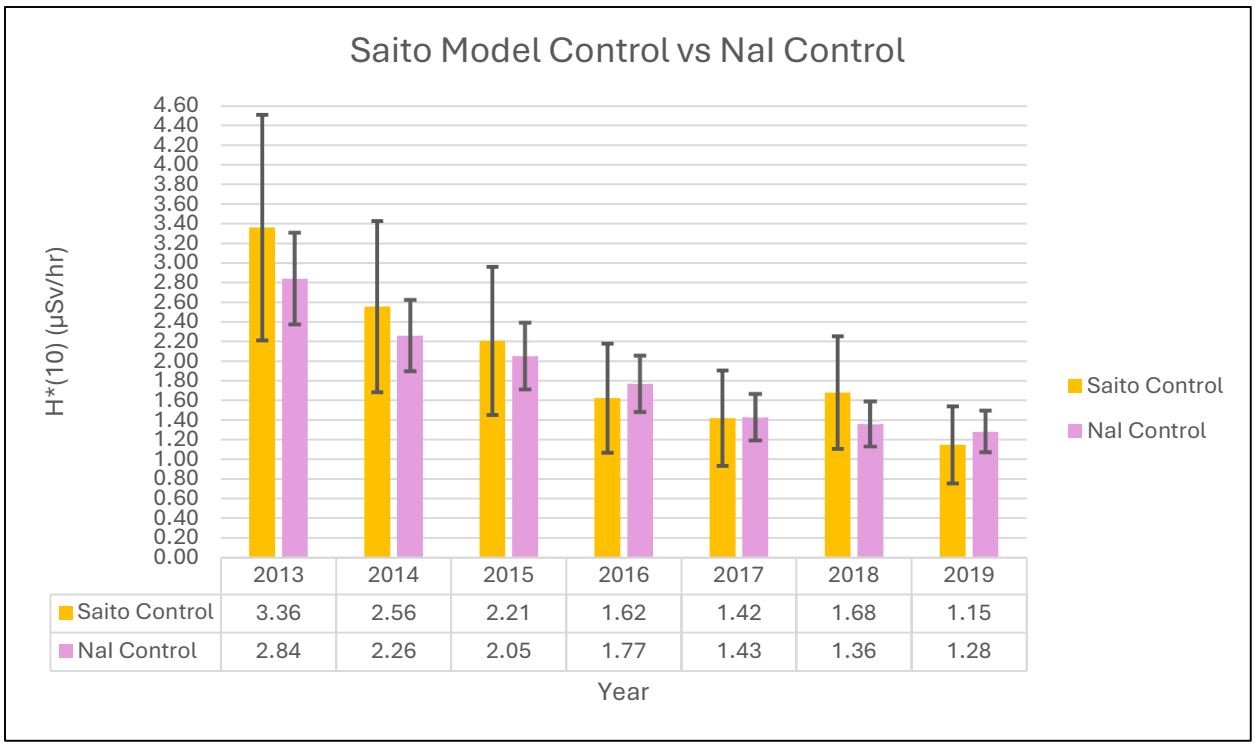

Figure 12: Comparison of H*(10) from Saito Model Control to NaI Control. Model vs Field Measurement.

Malins et al 2015 Field of View Analysis

Table 7 shows the resulting theoretical H*(10) using the Malins et al. 2015 method compared to the measured H*(10) via NaI at G7. These values are plotted in Figure 13 for visual comparison. A paired t-test ($t(6) = 0.34$, p value = 0.74) suggests the Malins Model was successful at estimating H*(10) at G7 when compared to the NaI measurements. Each year the model was within 20% of the NaI measurements. The uncertainty bars for the Malins Model values were from applying the impact ratio to both the high and low Control NaI values. Note that the Malins Model estimated H*(10) values either lower than or equal to the NaI values in every year expect 2015, where it was higher.

Figure 14 shows a final comparison of both the Malins Model and Saito Model to the NaI measurements at G7. While both models show that they can accurately estimate the H*(10) measured by the NaI detector, the Malins Model performed better statistically than the Saito Model.

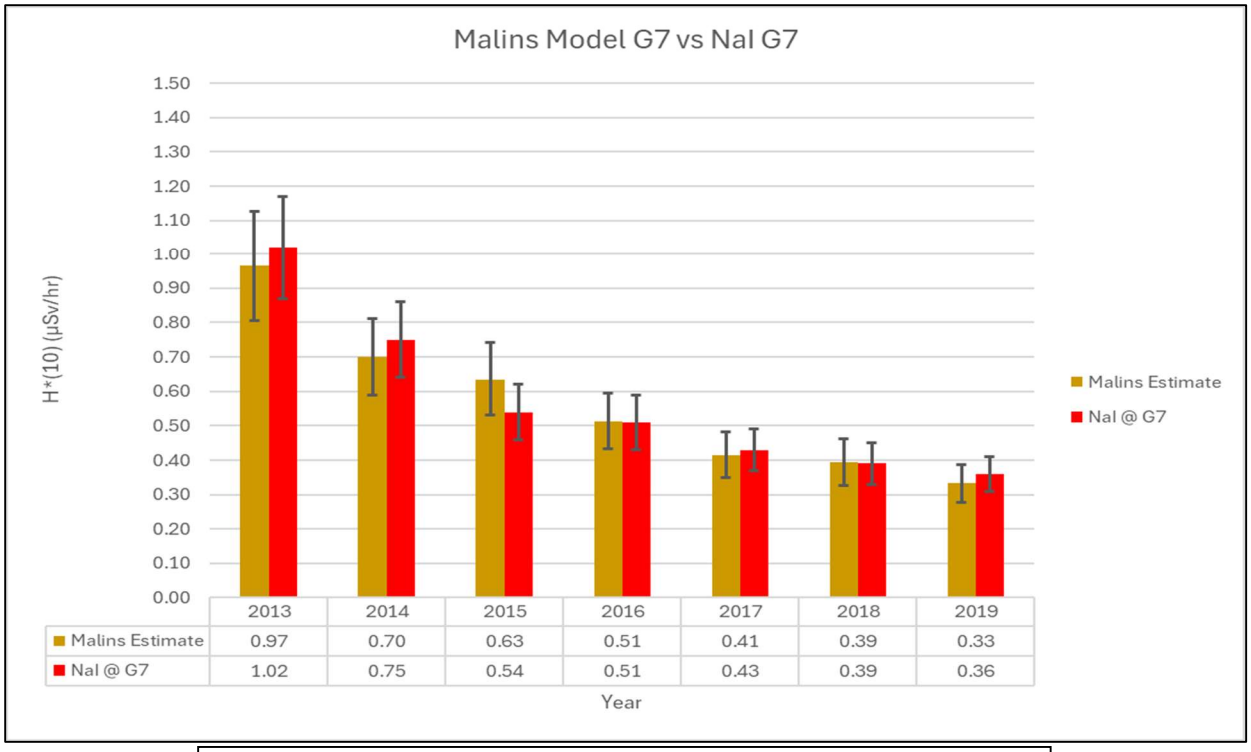

Figure 13: Comparison of H*(10) using Malins et al. Model at G7 versus NaI at G7.

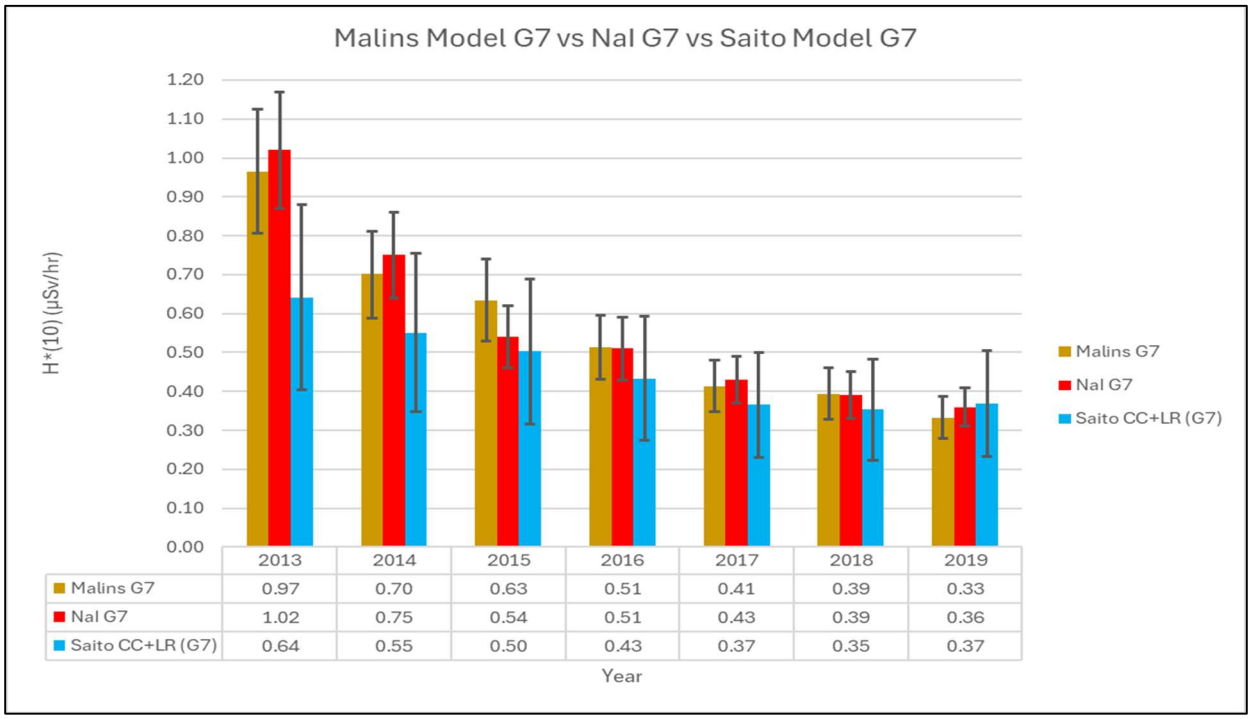

Figure 14: Comparison of Malins Model, Saito Model, and NaI Measurement of H*(10) at G7

CHAPTER 5: DISCUSSION

Measured H*(10)

The resulting trend in H*(10) values in both the CC+LR and Control areas decreased over time, which was to be expected following radiocesium's radiological decay and migration from the surface into deeper layers of soil. It is not surprising to see that H*(10) measurements within the CC+LR area are lower than the Control areas, as CC+LR removes the sources where radiocesium tends to concentrate the most. Removing this concentrated source would ideally remove the major contributor to dose rate and prevent additional radiocesium from migrating into the soils, which, would much more difficult to remediate in a dense mountainous forest.

A key observation provided by the authors from Noguchi, H. et al. was that the H*(10) measurements at coordinates near the edge of the CC+LR area were slightly higher compared to those towards the center. The edge of the CC+LR area is near the untouched forest which retained its vegetation and litter layer, and thus still contains most of its radiocesium contamination. Knowing that the range of radiocesium to contribute to H*(10) measurements can be upwards of 1000 m, the litter layer just outside the CC+LR boundary is very likely to be contributing to all measurement points within the CC+LR area (Malins, 2021). Conversely, this explains why the centermost point, G7, would be the least affected by outside H*(10), as it is the

furthest from any contaminated litter or soil. For simplicity, this is why we chose to use the G7 NaI measurement as the base reference H*(10) within the CC+LR area to compare the Saito et al. and Malins et al. models. At the G7 coordinate, the total H*(10) measured would be from contributions of remaining radiocesium in the CC+LR soil, the radiocesium in litter/soil outside the CC+LR area, and any natural background sources. This should be kept in mind when discussing the upcoming sections.

Scraper Plate Data

As discussed earlier, the literature suggests β will increase over time due to the downward migration of radiocesium from litter into the soil within the initial few years after deposition. A higher β value indicates that more of the total radiocesium present on the forest floor resides deeper below the surface. A higher β value results in reduced H*(10) measurements at 1 m above the surface because deeper soil penetration creates a greater shielding effect on the gamma rays from radiocesium; more soil exists between the measurement point and the radiocesium itself.

Collectively, β values increased over time for both Cs134 and Cs137 across all sampling areas. In the years 2013 – 2015, the Control area β values were lower than the CC+LR areas. This may suggest that the CC+LR work did promote the initial migration of radiocesium into

deeper layers of forest floor more rapidly than the Control area. However, after 2015 there seems to be no obvious difference amongst β values between CC+LR and Control areas. Each group's values generally increased, but it is difficult to determine any key differences because of the fluctuations. Several oddities/outliers should be noted: 1) At G7 both Cs134 & Cs137 saw β decrease from 2013-2014 and from 2016-2017. 2) At B Everyone(1) both isotopes showed a decrease from 2018-2019. 3) At B Everyone(2) there was a sharp increase from 2016-2017, followed by a sharp decrease from 2017-2019. 4) At B vs(1) Cs134 showed a decrease from 2014-2015 followed by a sharp increase from 2015-2017, ending with a sharp decrease from 2017-2019. Cs137 only showed decreasing from 2014-2015 and 2017-2019. 5) At B vs(2) both isotopes showed a decrease from 2017-2018. Fluctuations may be associated with the spatial variability of sampling from year to year.

Conducting CC+LR removal should remove the primary source of radiocesium continuing to enter the soil and promote larger β values since the upper layers of soil are not receiving new radioceisum to affect its distribution throughout the soil column. This may be the case from 2013 – 2015, but the results in later years seem to show that β values were unaffected by the completion of CC+LR in comparison to the Control, but does not account for additional litter accumulation (blowing in) from outside the test area. This would lead to the expectation

that total inventory (Bq/m^2) at a measurement area would likely be the cause for differences in H*(10) seem amongst the different sampling locations, rather than β in the case of this study.

Saito et al. Model vs Measured H*(10)

Similar to the comparison of NaI H*(10) CC+LR versus Control, the Saito et al. model also showed that there was a significant difference between H*(10) at G7 and in the Control area. The p-value in the Saito comparison was larger than the NaI comparison, 0.00083 and 0.000058 respectively, which may be due to the larger uncertainty values in the Saito et al. model data. The NaI data only considered the uncertainty range of the NaI detector, which was ±15% taken from the detector calibration form provided by the University of Tsukuba. Propagating the uncertainty of the detector and averaging the measurement points (G7 n=1 & Control n=4), the total uncertainty remained between 15% - 16% for each data point. Alternatively, the Saito et al. data required propagating uncertainty from the individual HPGe measurements from nine soil layers, combining Cs134 and Cs137 data, and averaging the three CC+LR or two Control sampling locations to produce one data point for the year. This created total uncertainties of 34% and 37% for CC+LR and Control data respectively. The larger uncertainty likely played a role in the Saito et al. model CC+LR versus Control comparison being more statistically different than the NaI CC+LR versus Control.

In comparing the H*(10) estimates from the Saito et al. model to the NaI measurements, the individual sources of radiation needed to be considered. As mentioned earlier, the NaI detector at G7 collects H*(10) originating from contamination remaining inside the CC+LR area, outside the area, and from natural background sources. The Saito et al. model provides an H*(10) value based on radiocesium in the soil alone. A rough estimate of natural background at 0.127 μSv/hr was added to each Saito et al. model data point to account for the background in addition to the radiocesium. The main caveat of the Saito model is that it cannot account for the added contribution of radiocesium contamination from outside the CC+LR boundary. The model assumes uniform soil conditions infinitely in all directions. The midpoint estimate provided by the model underestimated H*(10) compared to NaI in all years except 2019, which could be due to not accounting for this outside contribution.

As for comparing the model's Control estimate to the NaI's Control measurement, there is a key difference. The model's midpoint values overestimated H*(10) compared to NaI in years 2013, 2014, 2015, and 2018. In the control plot, all three of the H*(10) contribution sources still apply, although the outside contribution boundary now is "infinite", as in it exceeds the 1000 m range of gamma rays. This may explain why the model was able to better predict the Control

H*(10) than it can the CC+LR H*(10) as seen by the improved p-value statistic of p = 0.181 and p = 0.069 respectively.

These results inspire further discussion. Firstly, this study showed that the model can provide *representative* estimates of H*(10) using soil data. If predictions of future dose rates are desired, one could apply predicted changes in soil data, such as larger β to represent vertical migration, and model the expected H*(10). Secondly, does the model provide the *true* H*(10) that results from forestry clearing operations. Because the model cannot account for the additional outside contributions, perhaps in a situation such as Plot B where outside influence is likely, when using the model H*(10) may be higher at the point of interest inside the work area if outside boundary contamination levels are higher. If the contamination is contained in a smaller local area, the model should provide a conservatively high estimation of H*(10). If the contamination is consistent over a rather large range of land, relative to 1000 m, the model should be able to provide an acceptable estimation of the actual H*(10) to expect. Future users should be sure to understand the conditions of their experimental area to account for these impacts on their results.

Malins et al. Model vs Measured H*(10)

Understanding the implications of outside contamination's contribution to H*(10) measured within the CC+LR boundary helps in analyzing the results from the Malins et al. model. The results seen in Figure 13 show that the Malins et al. model was also able to estimate H*(10) within an acceptable range of uncertainty. Besides 2015, the model was able to predict H*(10) within 0.05 μSv/hr of the NaI measurements. The paired t-test results ($t(6) = 0.34$, p value = 0.74) were the best outcome of all comparisons in the study, showing the model is relatively accurate.

The authors of the Malins model explicitly mention one of its uses is for quick evaluations of land remediation effectiveness. The Malins model is designed to work in an experimental set up similar to Plot B. However, there are a few assumptions that the authors mention when using the Malins model. One issue is that the Malins model assumes remediation was perfect at removing all radionuclide contamination from the work area. This provides the user with a theoretical maximum effectiveness, or theoretical lowest H*(10) achievable at a survey point in the remediated area but still surrounded by outside contamination. A second issue is that the Malins model was also built to represent flat land without the shielding effects of trees, plants, and hilly topography. Thirdly, it assumes perfectly uniform distribution of fallout contamination

across the soil surface in all directions. Plot B does not meet all of those assumptions, as it is hilly, has dense vegetation, and spatial variation of radiocesium distribution exists.

Knowing that these conditions are not exact to the model's design there would likely be an unknown amount of error in the estimation. So, the fact that the model produced H*(10) values within 20% of the NaI measurements could be viewed as a success given the model allows "quick calculations on the order of magnitude reduction in air dose rate that can be achieved by remediation" (Malins et al. 2015).

Comparison of Saito et al. Model, Malins et al. Model, and Measured H*(10)

The H*(10) values from the NaI measurements, the Saito et al. model, and the Malins et al. model present some interesting comparisons regarding effectiveness. Figure 14 provides a combined visual comparison. Ultimately, the NaI detector provides the most useful measurement of H*(10) at the reference point. H*(10) measurement at G7 is what a person would witness from existing radiological conditions at the time, as it collects gamma rays from all sources; background, residual fallout in CC+LR area, and fallout outside the CC+LR area. The NaI measurement is not the *true* H*(10), but in the context of evaluating remediation effectiveness, it has its shortcomings. The NaI measurement represents current contamination, but it cannot accurately show the theoretical H*(10) that would occur at G7 if the CC+LR area boundary was

expanded or if there was negligible outside influence. The NaI measurement should mainly be used as a reference for real time radiological conditions.

The Saito et al. model also has a few shortcomings when used for evaluating remediation effectiveness. The model assumes uniform distribution of the modeled radionuclides in the soil. Since spatial variability exists in the Plot B area, variation in contamination becomes a source of error. Additionally, the Saito et al. model assumes a flat topography and uses generic soil composition, density, and moisture content. Soils in Fukushima Japan forests typically consist of more organic matter content, less density, and higher moisture levels than the Saito model assumptions. While the Saito et al. study used a 20% moisture level by weight, soils in Fukushima can be upwards of 37% moisture content (Nakanishi et al. 2023) (Saito et al. 2014). These differences would alter the amount of gamma ray shielding of Cs134 and Cs137. More density and more water would increase the shielding effect per physical distance in soil, which would lower H*(10) seen in the test area versus what the model estimates. Also, the model's H*(10) estimate is only based on the radionuclides the researcher has modeled. Therefore, contributions to H*(10) due to background radiation that come from primordial radionuclides like K40, Th232, U235, and U238 are not accounted for unless the researcher possesses appropriate soil

data for each. This is why the estimate of 0.127 μSv/hr from background was added to each of the Saito et al. model's data points, to closer match the NaI measurements.

The limitations of the Malins et al. model in the context of evaluating remediation effectiveness was primarily the assumption that the remediation is perfect at removing all contamination from the work area. The soil data from Chapter 4 showed that radiocesium remained in the CC+LR area soils, and this added contribution to H*(10) was not accounted for with the Malins model. Also, just like the Saito et al. model, the Malins et al. model assumed a flat topography and a chosen soil composition, density, and moisture level that was not verified to match the conditions during sampling at Kawauchi Plot B. Interestingly, the model was still able to very closely predict H*(10) measured with the NaI. Since the Malins model relied on β and H*(10) that was already established in the Control area, any deviation from the NaI measurements was likely due to the inherent uncertainty of the model. Even with this inherent uncertainty, the model still provided an accurate estimation. The authors of the Malins et al. model mention that there exists a more thorough estimation model created by Satoh et al. in 2014 to determine decontamination effects. This method accounts for topography, land type, and the remediation target to better account for outside influence of gamma rays (Satoh et al. 2014). This method was not used in our study because a quick and simple estimation model was

thought to be a better approach for a first-time analysis of the data at Plot B. To build off this study's findings, one may consider using this other model recommended by Malins et al in future research.

The two models and the NaI measurement produced similar H*(10) values from different combinations of sources of gamma rays. The NaI measured gamma rays from the CC+LR soil beneath it and the untouched Control area. The Saito et al. model assumed gamma rays were from the CC+LR soil and assumed these conditions extended infinitely in the horizontal plane. The Malins et al. model only assumed gamma rays were from the untouched Control area beyond a 30 m radius around the G7 coordinate. These three situations are depicted in Figure 15 below. If it is assumed each of the three methods provide accurate data, then these results suggest neither model is a perfect fit but can offer different perspectives. The NaI can discern the current H*(10). The Saito et al. model can offer a predicted H*(10) if the remediation area was extended to a large enough distance (roughly 1000 m radius) where outside contribution is negligible. The Malins et al. model can offer a theoretical minimum H*(10) value after remediation while accounting for outside contributions. Neither model is perfect, but they may provide a more credible estimation if the experimental setup more closely matches the assumptions mentioned

above. This conclusion could be verified through further testing of each model in experimental scenarios that match their assumptions.

For the sake of determining which model more accurately predicted H*(10) in this study, the Malins et al. model was better. The Malins et al. model statistical test results were better than those of the Saito et al. model. However, the Malins et al. model seemed to be a better fit for the conditions at Plot B, since the authors mention one of its main purposes is to evaluate remediation effectiveness while accounting for outside contribution, something the Saito et al. model cannot estimate.

Future Work

If this study were to be repeated, it would likely benefit from larger sample sizes of all measurements. More than one NaI measurement at G7 and control areas from each year could provide a stronger average data point to serve as reference. The same goes for soil sampling, with the addition of soil samples for CC+LR are only taken at the G7 coordinate, as G7 was less affected by post-CC+LR additions of new litter from outside debris that may contain radioceisum. Having additional soil data, specifically inventory (Bq/m^2) measurement averages, could help reduce the total uncertainty in the Saito et al. estimations. Finally, as mentioned

earlier, to better test these models, perhaps an experimental set up that more closely resembles the assumptions of each model would provide more credible results.

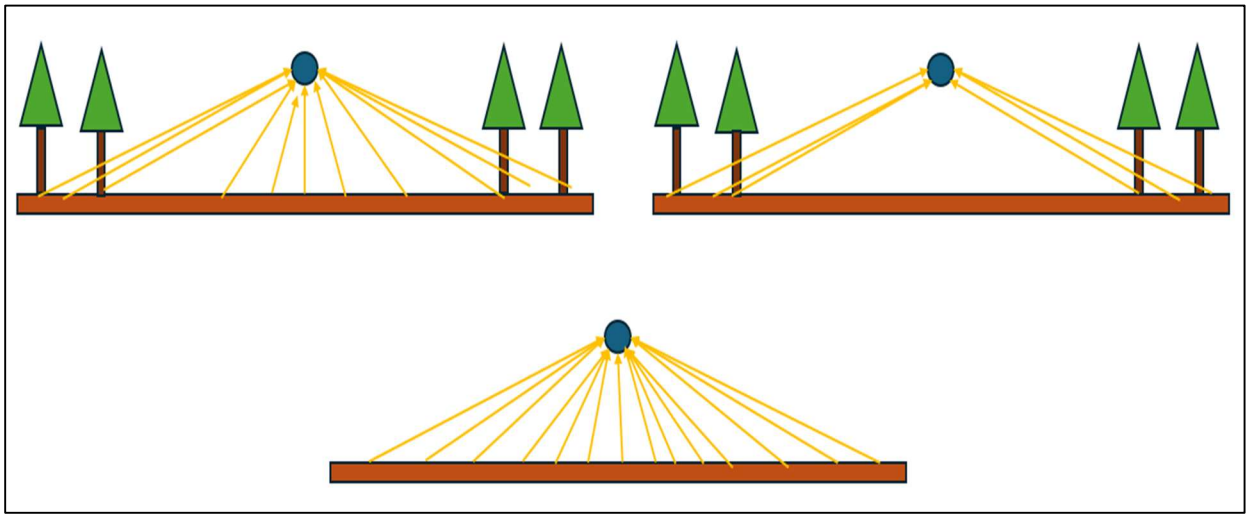

Figure 15: Depictions of all 3 H*(10) scenarios. Top left = NaI, Top Right = Malins et al., Bottom = Saito et al.

CHAPTER 6: CONCLUSION

Conclusion

The findings of this study show that CC+LR can help to reduce H*(10) in forests contaminated with fallout. Additionally, it showed the practicality of two models to aid in estimating H*(10) and evaluating the effectiveness of the CC+LR work. The Malins et al. field of view model was able to produce H*(10) estimates closest to the measured NaI H*(10) values at the center, G7, of the CC+LR plot. The Saito et al. conversion coefficient model was also able to produce H*(10) estimations that were within 20% of the NaI measurements. Although both models have their shortcomings in the contaminated forest setting, they both produced results that suggest they are useful for estimating H*(10) within a 20% range of measured H*(10). These methods are shown to be useful for researchers to gauge how well remediation practices work, albeit an experimental set up that closely matches the assumed conditions of the model would provide more credible results.

REFERENCES

Anastasopoulos, A. (n.d.). *WebPlotDigitizer*. Retrieved January 27, 2025, from https://automeris.io/

Beck, H.L., (1966). Environmental gamma radiation from deposited fission products, 1960e1964. Health Phys. 12, 313e322.

Google. (2025). Screenshot of the location of the Kawauchi Test Site in Kawauchi Village Japan [Screenshot]. Google Maps. https://www.google.com/maps

Google. (2025). Screenshot of the Plot B location of the Kawauchi Test Site. [Screenshot]. Google Map. https://www.google.com/maps

Hashimoto, S., Matsuura, T., Nanko, K., et al. (2013). Predicted spatio-temporal dynamics of radiocesium deposited onto forests following the Fukushima nuclear accident. *Scientific Reports, 3*, 2564. https://doi.org/10.1038/srep02564

Hubbell, J. H., & Seltzer, S. M. (2004). Tables of X-ray mass attenuation coefficients and mass energy absorption coefficients from 1 keV to 20 MeV for elements Z = 1 to 92 and 48 additional substances of dosimetric interest. *NISTIR 5632*. Retrieved from http://www.nist.gov/pml/data/xraycoef/ (accessed May 26, 2015)

International Atomic Energy Agency. (n.d.). *Weapons of mass destruction: Fission product yields*. International Atomic Energy Agency. https://www-nds.iaea.org/wimsd/fpyield.htm (Accessed November 20, 2024).

Isaksson, M., Erlandsson, B., (1998). Investigation of the distribution of 137Cs from fallout in the soils of the city of Lund and the province of Skåne in Sweden. J. Environ. Radioact. 38, 105e131.

IUSS Working Group WRB. (2022). *World Reference Base for Soil Resources. International Soil Classification System for Naming Soils and Creating Legends for Soil Maps* (4th ed.). Vienna, Austria.

Japan Meteorological Agency. (2024). *Annual precipitation data for Kawauchi (Fukushima Prefecture)*. Japan Meteorological Agency. https://www.data.jma.go.jp/stats/etrn/view/annually_a.php?prec_no=36&block_no=1129&year=&month=&day=&view=

Johnson, T. E. (2017). *Introduction to health physics* (5th ed.). McGraw-Hill Education.

Knoll GF. Radiation detection and measurement. 4th ed Hoboken, N.J: John Wiley; 2010.

López-Vicente, M., Onda, Y., Takahashi, J., Kato, H., Chayama, S., & Hisadome, K. (2018). Radiocesium concentrations in soil and leaf after decontamination practices in a forest plantation highly polluted by the Fukushima accident. *Environmental Pollution, 239*, 448-456. https://doi.org/10.1016/j.envpol.2018.04.045

Manaka, T., Komatsu, M., Sakashita, W., Imamura, N., Hashimoto, S., Hirai, K., Miura, S., Kaneko, S., Sakata, T., & Shinomiya, Y. (2022). Ten-year trends in vertical distribution of radiocesium in Fukushima forest soils, Japan. *Journal of Environmental Radioactivity, 251–252*, 106967. https://doi.org/10.1016/j.jenvrad.2022.106967

Manaka, T., Imamura, N., Kaneko, S., Miura, S., Furusawa, H., & Kanasashi, T. (2019). Six-year trends in exchangeable radiocesium in Fukushima forest soils. *Journal of Environmental Radioactivity, 203*, 84-92. https://doi.org/10.1016/j.jenvrad.2019.02.014

Malins, A., Imamura, N., Niizato, T., Takahashi, J., Kim, M., Sakuma, K., Shinomiya, Y., Miura, S., & Machida, M. (2021). Calculations for ambient dose equivalent rates in nine forests in eastern Japan from 134Cs and 137Cs radioactivity measurements. *Journal of Environmental Radioactivity, 226*, 106456. https://doi.org/10.1016/j.jenvrad.2020.106456

Malins, A., Okumura, M., Machida, M., Takemiya, H., & Saito, K. (2015). Fields of view for environmental radioactivity.

Ministry of the Environment, Japan. (2022). *Chemicals Management in Japan: Overview of the Basic Environment Law (BELS)*. Retrieved February 6, 2025, from https://www.env.go.jp/en/chemi/rhm/basic-info/1st/02-05-03.html

Nakanishi, M., Onda, Y., Takahashi, J., Kato, H., Iida, H., & Takada, M. (2023). Changes in air dose rates due to soil moisture content in the Fukushima prefecture forests. *Environmental Pollution, 334*, 122147. https://doi.org/10.1016/j.envpol.2023.122147

National Nuclear Data Center, information extracted from the NuDat database, https://www.nndc.bnl.gov/nudat/ (Accessed November 20, 2024).

NCRP. (2006). *NCRP Report No. 154: Cesium-137 in the environment: Radioecology and approaches to assessment and management: Recommendations of the National Council on Radiation Protection and Measurements*. National Council on Radiation Protection and Measurements.

Noguchi,H., Chayama,S., Onda, Y. and Miura, S. (2022) Verification of the Impact of Litter Removal and Logging on Air Dose Rates: Measurement data of radiocesium concentration in soil at the Kawauchi Testing Sites, Center for Research in Isotopes and Environmental Dynamics, University of Tsukuba. DOI: 10.34355/Forest.Agency.00052

Onda, Y., Taniguchi, K., Yoshimura, K., et al. (2020). Radionuclides from the Fukushima Daiichi Nuclear Power Plant in terrestrial systems. *Nature Reviews Earth & Environment, 1*, 644-660. https://doi.org/10.1038/s43017-020-0099-x

Park, S.-M., Alessi, D. S., & Baek, K. (2019). Selective adsorption and irreversible fixation behavior of cesium onto 2:1 layered clay mineral: A mini review. *Journal of Hazardous Materials, 369*, 569-576. https://doi.org/10.1016/j.jhazmat.2019.02.061

Saito, K., & Petoussi-Henss, N. (2014). Ambient dose equivalent conversion coefficients for radionuclides exponentially distributed in the ground. *Journal of Nuclear Science and Technology, 51*(10), 1274–1287. https://doi.org/10.1080/00223131.2014.919885

Satoh, D., Kojima, K., Oizumi, A., Matsuda, N., Iwamoto, H., Kugo, T., ... Okajima, S. (2014). Development of a calculation system for the estimation of decontamination effects. *Journal of Nuclear Science and Technology*, *51*(5), 656–670. https://doi.org/10.1080/00223131.2014.886534

Takahashi, J., Hihara, D., Sasaki, T., & Onda, Y. (2022). Evaluation of contribution rate of the infiltrated water collected using zero-tension lysimeter to the downward migration of 137Cs derived from the FDNPP accident in a cedar forest soil. *Science of the Total Environment, 816*, 151983. https://doi.org/10.1016/j.scitotenv.2021.151983

Takahashi, J., Onda, Y., Hihara, D., & Tamura, K. (2018). Six-year monitoring of the vertical distribution of radiocesium in three forest soils after the Fukushima Dai-ichi Nuclear Power

Plant accident. *Journal of Environmental Radioactivity, 192*, 172-180. https://doi.org/10.1016/j.jenvrad.2018.06.015

Takahashi, J., Onda, Y., Sasaki, T., Chayama, S., Kato, H., & Hisadome, K. (2018). Radiocesium concentrations in soil and leaf after decontamination practices in a forest plantation highly polluted by the Fukushima accident. *Environmental Pollution, 239*, 448-456. https://doi.org/10.1016/j.envpol.2018.04.045

Takahashi, J., Tamura, K., Suda, T., Matsumura, R., & Onda, Y. (2015). Vertical distribution and temporal changes of 137Cs in soil profiles under various land uses after the Fukushima Dai-ichi Nuclear Power Plant accident. *Journal of Environmental Radioactivity, 139*, 351-361. https://doi.org/10.1016/j.jenvrad.2014.07.004

Takahashi, J., Yuichi Onda, Daichi Hihara, Kenji Tamura. (2024). Downward migration of 137Cs promotes self-cleaning of forest ecosystem by reducing root uptake of Japanese cedar in Fukushima. *The Science of the Total Environment, 945*, 174010. https://doi.org/10.1016/j.scitotenv.2024.174010

Teramage, M. T., & Sun, X. (2020). Dosimetric depth distribution of Fukushima-derived 137Cs in coniferous forest soil. *Journal of Radioanalytical and Nuclear Chemistry, 323*, 233-239. https://doi.org/10.1007/s10967-019-724 06868-0

Turner, J. E. (2007). *Atoms, radiation, and radiation protection* (3rd completely rev. and enl. ed.). Wiley-VCH.

U.S. Nuclear Regulatory Commission. (2010, January 6). *ML11229A680 – Basic Health Physics – 07 – Solid Scintillators*. U.S. Nuclear Regulatory Commission. https://www.nrc.gov/docs/ML1122/ML11229A619.html

Whicker, F. W., & Schultz, V. (1982). *Radioecology: Nuclear energy and the environment, Volume I*. CRC Press.

World Nuclear Association. (2024). Fukushima Daiichi accident. *World Nuclear Association*. https://world-nuclear.org/information-library/safety-and-security/safety-of-plants/fukushima-daiichi-accident

Yoschenko, V., Ohkubo, T., & Kashparov, V. (2018). Radioactive contaminated forests in Fukushima and Chernobyl. *Journal of Forest Research, 23*(1), 3-14. https://doi.org/10.1080/13416979.2017.1356681

Data Tables for Scraper Plate Data Analysis

Cs134

G7 11/11/2013	x			x'		C		C(x)	Residuals			
Sampling layer/depth	Central D	dry weight of samples/ sampling area (450 cm^2)	dry weight /unit area (m^2)	dry mass depth		Cs-134 Conc.		Cs-134 conc. estimated by exponential equation	Difference between actual and predicted values	Squares of the residuals		
	cm	g	kg/m2	kg/m2		kBq/kg		kBq/kg				
Litter Layer (1.0-0)		157.2	3.493333	3.493333333		3.9		3.550239	0.349761267499112	0.122332944		
0-0.5		56	1.244444	4.737777778		2.5		2.980879	-0.480878591807376	0.23124422		
0.5-1.0		111.4	2.475556	7.213333333		2.2		2.105383	0.0946170335007914	0.008952383		
1.0-1.5		115.1	2.557778	9.771111111		1.4		1.469949	-0.0699488531963581	0.004892842	β	7.12
1.5-2.0		143.5	3.188889	12.96		0.94		0.939235	0.00076456291910198	5.84556E-07	C(0)	5.80
2.0-3.0		334.5	7.433333	20.39333333		0.6		0.330619	0.269380669075829	0.072565945		
3.0-5.0		632.1	14.04667	34.44		0.16		0.045968	0.114031830466816	0.013003258		
5.0-7.0		701.6	15.59111	50.03111111		0.062		0.005145	0.0568551539017988	0.003232509		
7.0-10.0		1073	23.84444	73.87555556		0.04		0.000181	0.039819357508038	0.001585581		
			3.493			3.900	13.624					
			1.244			2.500	3.111111					
			2.476			2.200	5.446222					
			2.558			1.400	3.580889					
			3.189			0.940	2.997556					
			7.433			0.600	4.46					
			14.047			0.160	2.247467					
			15.591			0.062	0.966649					
			23.844			0.040	0.953778					
							37.38767		the sum of the squares of the residuals =	0.45781027		

G7 11/28/2014												
Sampling layer/depth												
	x			x'		C		C(x)	Residuals			
	Central D	dry weight of samples/ sampling area (450 cm^2)	dry weight /unit area (m^2)	dry mass depth		Cs-134 Conc.		Cs-134 conc. estimated by exponential equation	Difference between actual and predicted values	Squares of the residuals		
	cm	g	kg/m2	kg/m2		kBq/kg		kBq/kg				
Litter Layer (1.0-0)		83.52	1.856	1.856		1.9		1.906046	-0.00604583576652007	3.65521E-05	β	6.17
0-0.5		131.8	2.928889	4.784888889		1.2		1.185387	0.0146127596462577	0.000213533	C(0)	2.58
0.5-1.0		148.5	3.3	8.084888889		0.73		0.694146	0.035853905992517	0.001285503		
1.0-1.5		124.5	2.766667	10.85155556		0.37		0.443203	-0.0732029369058763	0.00535867		
1.5-2.0		156.5	3.477778	14.32933333		0.23		0.252158	-0.0221580840172242	0.000490981		
2.0-3.0		253.6	5.635556	19.96488889		0.16		0.101106	0.0588939429397835	0.003468497		
3.0-5.0		673	14.95556	34.92044444		0.15		0.008943	0.141056632710927	0.019896974		
5.0-7.0		671	14.91111	49.83155556		0.16		0.000797	0.159203189493198	0.025345656		
7.0-10.0		1069	23.75556	73.58711111		0.13		1.69E-05	0.129983083105493	0.016895602		
									the sum of the squares of the residuals =	0.07299197		

G7 11/24/2015												
Sampling layer/depth												
	x			x'		C		C(x)	Residuals			
	Central D	dry weight of samples/ sampling area (450 cm^2)	dry weight /unit area (m^2)	dry mass depth		Cs-134 Conc.		Cs-134 conc. estimated by exponential equation	Difference between actual and predicted values	Squares of the residuals		
	cm	g	kg/m2	kg/m2		kBq/kg		kBq/kg				
Litter Layer (1.0-0)		39.8	0.884444	0.884444444		1.9		2.474388	-0.574388275919171	0.329921892	β	10.55
0-0.5		107.4	2.386667	3.271111111		2.6		1.973283	0.626717234513522	0.392774492	C(0)	2.69
0.5-1.0		138.5	3.077778	6.348888889		1.9		1.473846	0.426153966646607	0.181607203		
1.0-1.5		137.5	3.055556	9.404444444		1.1		1.103138	-0.0031383456156524	9.84921E-06		
1.5-2.0		163.4	3.631111	13.03555556		0.42		0.781821	-0.361821357777971	0.130914695		
2.0-3.0		270.5	6.011111	19.04666667		0.1		0.442162	-0.342161651880871	0.117074596		
3.0-5.0		620.5	13.78889	32.83555556		0.061		0.119613	-0.0586134702345739	0.003435539		
5.0-7.0		651.2	14.47111	47.30666667		0.064		0.030331	0.0336690191242437	0.001133603		
7.0-10.0		1077	23.93333	71.24		0.037		0.003136	0.0338641449444829	0.00114678		
									the sum of the squares of the residuals =	1.15801865		

G7 11/29/2016

Sampling layer/depth	x			x'	C	C(x)	Residuals			
	Central D	dry weight of samples/ sampling area (450 cm^2)	dry weight /unit area (m^2)	dry mass depth	Cs-134 Conc.	Cs-134 conc. estimated by exponential equation	Difference between actual and predicted values	Squares of the residuals		
	cm	g	kg/m2	kg/m2	kBq/kg	kBq/kg				
Litter Layer 1		14.54	0.323111	0.323111111	0.14	0.842403	-0.70240338154189	0.49337051		
Litter Layer 2		7.01	0.155778	0.478888889	1.2	0.835631	0.364369316229865	0.132764999	β	19.30
0-0.5		180.4	4.008889	4.487777778	0.97	0.678884	0.291115685510783	0.084748342	C(0)	0.86
0.5-1.0		126.3	2.806667	7.294444444	0.85	0.586993	0.263007233397574	0.069172805		
1.0-1.5		128.3	2.851111	10.14555556	0.67	0.506372	0.163628192215411	0.026774185		
1.5-2.0		149.9	3.331111	13.47666667	0.27	0.426093	-0.156092666534285	0.024364921		
2.0-3.0		258.1	5.735556	19.21222222	0.15	0.316539	-0.1665391578392	0.027735291		
3.0-5.0		462.8	10.28444	29.49666667	0.054	0.185772	-0.13177176847096	0.017363799		
5.0-7.0		666.6	14.81333	44.31	0.042	0.086221	-0.0442205861550874	0.00195546		
7.0-10.0		910.9	20.24222	64.55222222	0.026	0.030204	-0.0042041788114238 7	1.76751E-05		
*2 litter layers???							the sum of the squares of the residuals =	0.87826799		

G7 12/13/2017

Sampling layer/depth	x			x'	C	C(x)	Residuals			
	Central D	dry weight of samples/ sampling area (450 cm^2)	dry weight /unit area (m^2)	dry mass depth	Cs-134 Conc.	Cs-134 conc. estimated by exponential equation	Difference between actual and predicted values	Squares of the residuals		
	cm	g	kg/m2	kg/m2	kBq/kg	kBq/kg				
Litter Layer 1		4.98	0.110667	0.110666667	0.17	0.376242	-0.206242320188689	0.042535895		
Litter Layer 2		8.5	0.188889	0.299555556	0.48	0.370455	0.109544774261629	0.012000058	β	12.19
0-0.5		190.53	4.234	4.533555556	0.47	0.261721	0.20827946921218	0.043380337	C(0)	0.38
0.5-1.0		122.28	2.717333	7.250888889	0.24	0.209408	0.0305920308810301	0.000935872		
1.0-1.5		144.4	3.208889	10.45977778	0.094	0.160927	-0.0669273239824063	0.004479267		
1.5-2.0		141.51	3.144667	13.60444444	0.031	0.124324	-0.0933240720908999	0.008709382		
2.0-3.0		312.68	6.948444	20.55288889	0.046	0.070294	-0.0242935804183284	0.000590178		
3.0-5.0		620.3	13.78444	34.33733333	0.025	0.02268	0.00231994973369848	5.38217E-06		
5.0-7.0		644.88	14.33067	48.668	0.022	0.006997	0.0150031069365615	0.000225093		
7.0-10.0		1025.34	22.78533	71.45333333	0.021	0.001079	0.0199214363280648	0.000396864		
							the sum of the squares of the residuals =	0.11325833		

G7 11/13/2018

Sampling layer/depth	x			x'	C	C(x)	Residuals			
	Central D	dry weight of samples/ sampling area (450 cm^2)	dry weight /unit area (m^2)	dry mass depth	Cs-134 Conc.	Cs-134 conc. estimated by exponential equation	Difference between actual and predicted values	Squares of the residuals		
	cm	g	kg/m2	kg/m2	kBq/kg	kBq/kg				
Litter Layer 1		8.52	0.189333	0.189333333	0.062	0.093923	-0.0319230281523482	0.00101908		
Litter Layer 2		11.28	0.250667	0.44	0.087	0.092891	-0.00589063013489771	3.46995E-05	β	22.67899
0-0.5		107.69	2.393111	2.833111111	0.12	0.083588	0.0364118553021038	0.001325823	C(0)	0.09471
0.5-1.0		103.42	2.298222	5.131333333	0.1	0.075533	0.0244673797021642	0.000598653		
1.0-1.5		193.04	4.289778	9.421111111	0.053	0.062515	-0.00951537470405956	9.05424E-05		
1.5-2.0		186.81	4.151333	13.57244444	0.044	0.052058	-0.00805833667897393	6.49368E-05		
2.0-3.0		419.63	9.325111	22.89755556	0.024	0.034508	-0.0105078371844954	0.000110415		
3.0-5.0		924.1	20.53556	43.43311111	0.014	0.013953	0.000046948886141427	2.2042E-09		
5.0-7.0		881.16	19.58133	63.01444444	0.0086	0.005884	0.00271571573669679	7.37511E-06		
7.0-10.0		1199.83	26.66289	89.67733333	0.0096	0.001816	0.00778402926828305	6.05911E-05		
							the sum of the squares of the residuals =	0.00331212		

G7 11/27/2019

Sampling layer/depth	x			x'	C	C(x)	Residuals			
	Central D	dry weight of samples/ sampling area (450 cm^2)	dry weight /unit area (m^2)	dry mass depth	Cs-134 Conc.	Cs-134 conc. estimated by exponential equation	Difference between actual and predicted values	Squares of the residuals		
	cm	g	kg/m2	kg/m2	kBq/kg	kBq/kg				
Litter Layer 1		25.99	0.577556	0.577555556	0.1	0.551413	-0.451413453919376	0.203774106		
Litter Layer 2		156.5	3.477778	4.055333333	0.78	0.492154	0.287846023392563	0.082855333	β	30.58913
0-0.5		96.2	2.137778	6.193111111	0.66	0.458933	0.201066749946288	0.040427838	C(0)	0.561924
0.5-1.0		120.11	2.669111	8.862222222	0.55	0.420586	0.129414446835913	0.016748099		
1.0-1.5		108.49	2.410889	11.27311111	0.42	0.38871	0.0312903403416514	0.000979085		
1.5-2.0		137.7	3.06	14.33311111	0.38	0.351707	0.0282934578335585	0.00080052		
2.0-3.0		244.53	5.434	19.76711111	0.18	0.294463	-0.11446269271538	0.013101708		
3.0-5.0		534.48	11.87733	31.64444444	0.13	0.19971	-0.0697099748592221	0.004859481		
5.0-7.0		539.16	11.98133	43.62577778	0.048	0.134987	-0.0869872272273261	0.007566778		
7.0-10.0		1008.08	22.40178	66.02755556	0.031	0.064899	-0.0338992248120427	0.001149157		
							the sum of the squares of the residuals =	0.37226211		

B Everyone(1) 11/14/2013

Sampling layer/depth	x			x'	C	C(x)	Residuals			
	Central D	dry weight of samples/ sampling area (450 cm^2)	dry weight /unit area (m^2)	dry mass depth	Cs-134 Conc.	Cs-134 conc. estimated by exponential equation	Difference between actual and predicted values	Squares of the residuals		
	cm	g	kg/m2	kg/m2	kBq/kg	kBq/kg				
Litter Layer		169.5	3.766667	3.766666667	5.9	6.162618	-0.262617828274656	0.068968124	β	5.82
0-0.5		32.83	0.729556	4.496222222	5.8	5.436858	0.363142101445613	0.131872186	C(0)	11.77
0.5-1.0		84.37	1.874889	6.371111111	3.9	3.940041	-0.0400413352974107	0.001603309		
1.0-1.5		133.1	2.957778	9.328888889	2.3	2.370726	-0.070725819834486	0.005002142		
1.5-2.0		151	3.355556	12.68444444	1.3	1.332269	-0.0322686168331459	0.001041264		
2.0-3.0		321	7.133333	19.81777778	0.41	0.391309	0.0186914394875782	0.00034937		
3.0-5.0		705.7	15.68222	35.5	0.21	0.026472	0.183527879267902	0.033682482		
5.0-7.0		695.1	15.44667	50.94666667	0.17	0.001865	0.168135217802568	0.028269451		
7.0-10.0		1159	25.75556	76.70222222	0.08	2.24E-05	0.0799776369188128	0.006396422		
							the sum of the squares of the residuals =	0.27718475		

B Everyone(1) 11/28/2014

Sampling layer/depth	x			x'	C	C(x)	Residuals			
	Central D	dry weight of samples/ sampling area (450 cm^2)	dry weight /unit area (m^2)	dry mass depth	Cs-134 Conc.	Cs-134 conc. estimated by exponential equation	Difference between actual and predicted values	Squares of the residuals		
	cm	g	kg/m2	kg/m2	kBq/kg	kBq/kg				
Litter Layer		208.8	4.64	4.64	3.2	3.336777	-0.136777260749806	0.018708019	β	12.00
0-0.5		268.7	5.971111	10.61111111	2.6	2.028435	0.571565024533466	0.326686577	C(0)	4.91
0.5-1.0		136.7	3.037778	13.64888889	1.4	1.574662	-0.174662475406833	0.03050698		
1.0-1.5		140.4	3.12	16.76888889	0.91	1.214052	-0.304051913677327	0.092447566		
1.5-2.0		168.7	3.748889	20.51777778	0.75	0.888219	-0.138218891329601	0.019104462		
2.0-3.0		335.9	7.464444	27.98222222	0.56	0.476752	0.083248316882796	0.006930282		
3.0-5.0		729.1	16.20222	44.18444444	0.27	0.123521	0.146479372914475	0.021456207		
5.0-7.0		652.5	14.5	58.68444444	0.13	0.036882	0.0931183298969996	0.008671023		
7.0-10.0		101.2	2.248889	60.93333333	0.12	0.030577	0.0894228983200787	0.007996455		
							the sum of the squares of the residuals =	0.53250757		

B Everyone(1) 11/25/2015

Sampling layer/depth	x			x'	C	C(x)	Residuals			
	Central D	dry weight of samples/ sampling area (450 cm^2)	dry weight /unit area (m^2)	dry mass depth	Cs-134 Conc.	Cs-134 conc. estimated by exponential equation	Difference between actual and predicted values	Squares of the residuals		
	cm	g	kg/m2	kg/m2	kBq/kg	kBq/kg				
Litter Layer		22.1	0.491111	0.491111111	2.4	3.35557	-0.955569710217982	0.913113471	β	12.14
0-0.5		105.6	2.346667	2.837777778	3.7	2.76591	0.934090056246716	0.872524233	C(0)	3.49
0.5-1.0		105.8	2.351111	5.188888889	3.1	2.279034	0.820965755744376	0.673984772		
1.0-1.5		118.5	2.633333	7.822222222	1.7	1.834721	-0.13472096990506	0.01814974		
1.5-2.0		131.1	2.913333	10.73555556	1	1.443361	-0.443361227667389	0.196569178		
2.0-3.0		300.6	6.68	17.41555556	0.43	0.832656	-0.402656159032012	0.162131982		
3.0-5.0		630.6	14.01333	31.42888889	0.17	0.262591	-0.0925914882143639	0.008573184		
5.0-7.0		684.72	15.216	46.64488889	0.05	0.075004	-0.0250036454921933	0.000625182		
7.0-10.0		888	19.73333	66.37822222	0.044	0.014768	0.029231980472873	0.000854509		
							the sum of the squares of the residuals =	2.84652625		

B Everyone(1) 11/29/2016

Sampling layer/depth	x			x'	C	C(x)	Residuals			
	Central D	dry weight of samples/ sampling area (450 cm^2)	dry weight /unit area (m^2)	dry mass depth	Cs-134 Conc.	Cs-134 conc. estimated by exponential equation	Difference between actual and predicted values	Squares of the residuals		
	cm	g	kg/m2	kg/m2	kBq/kg	kBq/kg				
Litter Layer 1		10.19	0.226444	0.226444444	0.32	3.328959	-3.00895939297167	9.053836629		
Litter Layer 2		7.17	0.159333	0.385777778	3	3.31154	-0.311539578927432	0.097056909	β	30.37
0-0.5		180.1	4.002222	4.388	5.8	2.90266	2.89734019150344	8.394580185	C(0)	3.35
0.5-1.0		88.25	1.961111	6.349111111	4.3	2.721142	1.57885769283548	2.492791614		
1.0-1.5		89.46	1.988	8.337111111	3.1	2.548718	0.551281654922104	0.303911463		
1.5-2.0		134.5	2.988889	11.326	2.2	2.309826	-0.109825735057982	0.012061692		
2.0-3.0		272.8	6.062222	17.38822222	1	1.891849	-0.891848517519186	0.795393778		
3.0-5.0		604.7	13.43778	30.826	0.58	1.2154	-0.635400223264258	0.403733444		
5.0-7.0		709.2	15.76	46.586	0.29	0.723341	-0.433341374963565	0.187784747		
7.0-10.0		1135	25.22222	71.80822222	0.2	0.315248	-0.115248275344068	0.013282165		
							the sum of the squares of the residuals =	21.7544326		

B Everyone(1) 12/13/2017

Sampling layer/depth	x			x'		C		$C(x)$	Residuals			
	Central D	dry weight of samples/ sampling area (450 cm^2)	dry weight /unit area (m^2)	dry mass depth		Cs-134 Conc.		Cs-134 conc. estimated by exponential equation	Difference between actual and predicted values	Squares of the residuals		
	cm	g	kg/m2	kg/m2		kBq/kg		kBq/kg				
Litter Layer 1		46.82	1.040444	1.040444444		0.98		1.441636	-0.46163553545864	0.213107368		
Litter Layer 2		91.01	2.022444	3.062888889		1.4		1.36948	0.0305200213206558	0.000931472	β	39.39
0-0.5		112.24	2.494222	5.557111111		1.4		1.285446	0.114553518865339	0.013122509	$C(0)$	1.48
0.5-1.0		74.77	1.661556	7.218666667		1.4		1.232348	0.167651825504829	0.028107135		
1.0-1.5		123.28	2.739556	9.958222222		1.3		1.149547	0.150453206440524	0.022636167		
1.5-2.0		123.36	2.741333	12.69955556		1.1		1.07226	0.0277395668369735	0.000769484		
2.0-3.0		233.25	5.183333	17.88288889		1.2		0.940044	0.259956329248386	0.067577293		
3.0-5.0		582.88	12.95289	30.83577778		0.62		0.676593	-0.0565928961264686	0.003202756		
5.0-7.0		622.87	13.84156	44.67733333		0.26		0.476111	-0.21611104737657	0.046703985		
7.0-10.0		1034.3	22.98444	67.66177778		0.13		0.265631	-0.135630627779494	0.018395667		
									the sum of the squares of the residuals =	0.41455383		

B Everyone(1) 11/14/2018

Sampling layer/depth	x			x'		C		$C(x)$	Residuals			
	Central D	dry weight of samples/ sampling area (450 cm^2)	dry weight /unit area (m^2)	dry mass depth		Cs-134 Conc.		Cs-134 conc. estimated by exponential equation	Difference between actual and predicted values	Squares of the residuals		
	cm	g	kg/m2	kg/m2		kBq/kg		kBq/kg				
Litter Layer 1		15.3	0.34	0.34		0.071		0.957278	-0.886277702237898	0.785488165		
Litter Layer 2		54.07	1.201556	1.541555556		0.95		0.940481	0.00951891383703984	9.06097E-05	β	67.87686
0-0.5		265.8	5.906667	7.448222222		1.1		0.8621	0.237900056406288	0.056596437	$C(0)$	0.962085
0.5-1.0		94.75	2.105556	9.553777778		0.99		0.835768	0.154232068270325	0.023787531		
1.0-1.5		98.93	2.198444	11.75222222		1.2		0.809132	0.390867842513393	0.15277767		
1.5-2.0		98.03	2.178444	13.93066667		1.2		0.783576	0.416423891749795	0.173408858		
2.0-3.0		207.17	4.603778	18.53444444		0.87		0.732192	0.137808013429189	0.018991049		
3.0-5.0		510.42	11.34267	29.87711111		0.68		0.619515	0.0604854290682876	0.003658487		
5.0-7.0		551.67	12.25933	42.13644444		0.22		0.517146	-0.297145795736314	0.088295624		
7.0-10.0		786.7	17.48222	59.61866667		0.095		0.399721	-0.304721047600324	0.092854917		
									the sum of the squares of the residuals =	1.39594935		

B Everyone(1) 11/29/2019

Sampling layer/depth	x			x'		C		$C(x)$	Residuals			
	Central D	dry weight of samples/ sampling area (450 cm^2)	dry weight /unit area (m^2)	dry mass depth		Cs-134 Conc.		Cs-134 conc. estimated by exponential equation	Difference between actual and predicted values	Squares of the residuals		
	cm	g	kg/m2	kg/m2		kBq/kg		kBq/kg				
Litter Layer 1		22.27	0.494889	0.494888889		0.35		0.384666	-0.0346658497889119	0.001201721		
Litter Layer 2		226.95	5.043333	5.538222222		0.36		0.333409	0.0265911512650558	0.000707089	β	35.2667
0-0.5		78.85	1.752222	7.290444444		0.32		0.317248	0.00275174003236928	7.57207E-06	$C(0)$	0.390102
0.5-1.0		87.7	1.948889	9.239333333		0.3		0.300192	-0.00019227289701384	3.69689E-08		
1.0-1.5		114.25	2.538889	11.77822222		0.26		0.279341	-0.0193406695477695	0.000374061		
1.5-2.0		122.71	2.726889	14.50511111		0.28		0.258555	0.0214445537669881	0.000459869		
2.0-3.0		261.45	5.81	20.31511111		0.24		0.219284	0.0207164741364229	0.000429172		
3.0-5.0		620.64	13.792	34.10711111		0.18		0.148308	0.0316924098629661	0.001004409		
5.0-7.0		690.77	15.35044	49.45755556		0.051		0.095969	-0.0449686020284764	0.002022175		
7.0-10.0		1089.44	24.20978	73.66733333		0.019		0.048305	-0.02930543843616	0.000858809		
									the sum of the squares of the residuals =	0.00706491		

B Everyone(2) 11/12/2013

Sampling layer/depth

	x			x'	C	C(x)	Residuals			
	Central D	dry weight of samples/ sampling area (450 cm^2)	dry weight /unit area (m^2)	dry mass depth	Cs-134 Conc.	Cs-134 conc. estimated by exponential equation	Difference between actual and predicted values	Squares of the residuals		
	cm	g	kg/m2	kg/m2	kBq/kg	kBq/kg				
Litter Layer 1		249.5	5.544444	5.544444444	4.1	4.047908	0.0520920859620873	0.002713585	β	2.53
0-0.5		106.2	2.36	7.904444444	1.4	1.593388	−0.193387560423085	0.037398749	C(0)	36.18
0.5-1.0		124.1	2.757778	10.66222222	0.61	0.536	0.0739999717320321	0.005475996		
1.0-1.5		138.7	3.082222	13.74444444	0.43	0.158614	0.271385561040868	0.073650123		
1.5-2.0		145.9	3.242222	16.98666667	0.36	0.044063	0.315937497915969	0.099816503		
2.0-3.0		301.1	6.691111	23.67777778	0.21	0.003134	0.206866253402708	0.042793647		
3.0-5.0		490	10.88889	34.56666667	0.17	4.24E−05	0.169957553807005	0.02888557		
5.0-7.0		492.3	10.94	45.50666667	0.094	5.63E−07	0.0939994365642579	0.008835894		
7.0-10.0		747.6	16.61333	62.12	0.039	7.95E−10	0.0389999992048179	0.001521		
							the sum of the squares of the residuals =	0.30109107		

B Everyone(2) 11/27/2014

Sampling layer/depth

	x			x'	C	C(x)	Residuals			
	Central D	dry weight of samples/ sampling area (450 cm^2)	dry weight /unit area (m^2)	dry mass depth	Cs-134 Conc.	Cs-134 conc. estimated by exponential equation	Difference between actual and predicted values	Squares of the residuals		
	cm	g	kg/m2	kg/m2	kBq/kg	kBq/kg				
Litter Layer 1		87.2	1.937778	1.937777778	2.6	2.624382	−0.0243818198188936	0.000594473	β	6.87
0-0.5		156.7	3.482222	5.42	1.7	1.580945	0.119054740795546	0.014174031	C(0)	3.48
0.5-1.0		131.8	2.928889	8.348888889	0.88	1.032245	−0.152244727387715	0.023178457		
1.0-1.5		127.7	2.837778	11.18666667	0.75	0.682979	0.0670205775971071	0.004491758		
1.5-2.0		154.4	3.431111	14.61777778	0.36	0.414503	−0.0545034489093803	0.002970626		
2.0-3.0		289.6	6.435556	21.05333333	0.21	0.162457	0.0475429078758042	0.002260328		
3.0-5.0		587.6	13.05778	34.11111111	0.1	0.024286	0.0757137429698845	0.005732571		
5.0-7.0		647.5	14.38889	48.5	0.06	0.002991	0.057008814288209	0.003250005		
7.0-10.0		891	19.8	68.3	0.043	0.000168	0.0428323932476	0.001834614		
							the sum of the squares of the residuals =	0.05848686		

B Everyone(2) 11/25/2015

Sampling layer/depth

	x			x'	C	C(x)	Residuals			
	Central D	dry weight of samples/ sampling area (450 cm^2)	dry weight /unit area (m^2)	dry mass depth	Cs-134 Conc.	Cs-134 conc. estimated by exponential equation	Difference between actual and predicted values	Squares of the residuals		
	cm	g	kg/m2	kg/m2	kBq/kg	kBq/kg				
Litter Layer 1		31.3	0.695556	0.695555556	2.8	3.277948	−0.477948091094654	0.228434378	β	12.25
0-0.5		74	1.644444	2.34	3.3	2.866017	0.433982841054317	0.188341106	C(0)	3.47
0.5-1.0		81.6	1.813333	4.153333333	2.7	2.471528	0.228471963057506	0.052199438		
1.0-1.5		94.8	2.106667	6.26	2.2	2.080888	0.119112106191761	0.014187694		
1.5-2.0		109.3	2.428889	8.688888889	1.6	1.706489	−0.106489475989972	0.011340008		
2.0-3.0		270	6	14.68888889	0.72	1.045448	−0.325448001628551	0.105916402		
3.0-5.0		538	11.95556	26.64444444	0.48	0.393801	0.0861993879277503	0.007430334		
5.0-7.0		508.1	11.29111	37.93555556	0.14	0.156609	−0.0166087765667191	0.000275851		
7.0-10.0		761.9	16.93111	54.86666667	0.064	0.039294	0.0247063203602669	0.000610402		
							the sum of the squares of the residuals =	0.60873561		

B Everyone(2) 11/29/2016

Sampling layer/depth

	x			x'	C	C(x)	Residuals			
	Central D	dry weight of samples/ sampling area (450 cm^2)	dry weight /unit area (m^2)	dry mass depth	Cs-134 Conc.	Cs-134 conc. estimated by exponential equation	Difference between actual and predicted values	Squares of the residuals		
	cm	g	kg/m2	kg/m2	kBq/kg	kBq/kg				
Litter Layer 1		19.67	0.437111	0.437111111	1.3	1.435303	−0.135302905911919	0.018306876		
Litter Layer 2		8.47	0.188222	0.625333333	1.8	1.418294	0.381705920572623	0.14569941	β	15.79
0-0.5		112.1	2.491111	3.116444444	0.96	1.211282	−0.251282217564026	0.063142753	C(0)	1.48
0.5-1.0		90.1	2.002222	5.118666667	0.97	1.067018	−0.0970182767874523	0.009412546		
1.0-1.5		106.6	2.368889	7.487555556	0.87	0.91836	−0.0483596129803464	0.002338652		
1.5-2.0		115.3	2.562222	10.04977778	0.8	0.780793	0.019207140514336	0.000368914		
2.0-3.0		283.1	6.291111	16.34088889	0.7	0.524193	0.175806774617194	0.030908022		
3.0-5.0		550.7	12.23778	28.57866667	0.25	0.241478	0.0085223747330592	7.26309E−05		
5.0-7.0		595.3	13.22889	41.80755556	0.06	0.104472	−0.0444721924587398	0.001977776		
7.0-10.0		973.2	21.62667	63.43422222	0.048	0.026554	0.0214457682133311	0.000459921		
							the sum of the squares of the residuals =	0.2726875		

B Everyone(2) 12/12/2017

Sampling layer/depth	χ			χ'	C	C(χ)	Residuals			
	Central D	dry weight of samples/ sampling area (450 cm^2)	dry weight /unit area (m^2)	dry mass depth	Cs-134 Conc.	Cs-134 conc. estimated by exponential equation	Difference between actual and predicted values	Squares of the residuals		
	cm	g	kg/m2	kg/m2	kBq/kg	kBq/kg				
Litter Layer 1		13.74	0.305333	0.305333333	0.2	0.831441	-0.631441371017427	0.398718205		
Litter Layer 2		123.03	2.734	3.039333333	0.8	0.809235	-0.00923465865500672	8.52789E-05	β	100.99
0-0.5		244.85	5.441111	8.480444444	0.91	0.766789	0.143211138912294	0.02050943	C(0)	0.83
0.5-1.0		138.01	3.066889	11.54733333	0.92	0.743853	0.176147030173432	0.031027776		
1.0-1.5		107.08	2.379556	13.92688889	1	0.726531	0.273468948176208	0.074785266		
1.5-2.0		121.77	2.706	16.63288889	0.93	0.707322	0.222677562390884	0.049585297		
2.0-3.0		220.34	4.896444	21.52933333	0.93	0.673847	0.256153444857369	0.065614587		
3.0-5.0		446.85	9.93	31.45933333	0.55	0.610743	-0.0607430616960649	0.00368972		
5.0-7.0		504.34	11.20756	42.66688889	0.36	0.546591	-0.186590571390349	0.034816041		
7.0-10.0		762.26	16.93911	59.606	0.25	0.462187	-0.212187331985767	0.045023464		
							the sum of the squares of the residuals =	0.72385506		

B Everyone(2) 11/12/2018

Sampling layer/depth	χ			χ'	C	C(χ)	Residuals			
	Central D	dry weight of samples/ sampling area (450 cm^2)	dry weight /unit area (m^2)	dry mass depth	Cs-134 Conc.	Cs-134 conc. estimated by exponential equation	Difference between actual and predicted values	Squares of the residuals		
	cm	g	kg/m2	kg/m2	kBq/kg	kBq/kg				
Litter Layer 1		13.29	0.295333	0.295333333	0.42	1.38288	-0.96288046378133	0.927138788		
Litter Layer 2		18.51	0.411333	0.706666667	1.2	1.371494	-0.171493628423885	0.029410065	β	49.74865
0-0.5		58.68	1.304	2.010666667	1.4	1.336011	0.0639885836385385	0.004094539	C(0)	1.391114
0.5-1.0		75.17	1.670444	3.681111111	1.5	1.291896	0.208103959915853	0.043307258		
1.0-1.5		106.06	2.356889	6.038	1.5	1.232118	0.267881552167516	0.071760526		
1.5-2.0		106.52	2.367111	8.405111111	1.7	1.174865	0.525134595985479	0.275766344		
2.0-3.0		206.29	4.584222	12.98933333	1.6	1.071443	0.528557443190898	0.279372971		
3.0-5.0		461.29	10.25089	23.24022222	1	0.871929	0.12807134494441	0.016402269		
5.0-7.0		570.58	12.67956	35.91977778	0.33	0.675758	-0.345758159253783	0.119548705		
7.0-10.0		732.14	16.26978	52.18955556	0.12	0.487259	-0.367258941868576	0.13487913		
							the sum of the squares of the residuals =	1.90168059		

B Everyone(2) 11/27/2019

Sampling layer/depth	χ			χ'	C	C(χ)	Residuals			
	Central D	dry weight of samples/ sampling area (450 cm^2)	dry weight /unit area (m^2)	dry mass depth	Cs-134 Conc.	Cs-134 conc. estimated by exponential equation	Difference between actual and predicted values	Squares of the residuals		
	cm	g	kg/m2	kg/m2	kBq/kg	kBq/kg				
Litter Layer 1		23.47	0.521556	0.521555556	0.085	0.699543	-0.61454260970707	0.377662619		
Litter Layer 2		53.46	1.188	1.709555556	0.87	0.679135	0.190865457128789	0.036429623	β	40.12504
0-0.5		182.22	4.049333	5.758888889	0.85	0.613943	0.236057434881271	0.055723113	C(0)	0.708695
0.5-1.0		91.01	2.022444	7.781333333	0.69	0.583765	0.106235395770812	0.011285959		
1.0-1.5		88.86	1.974667	9.756	0.71	0.555731	0.154268650016283	0.023798816		
1.5-2.0		91.17	2.026	11.782	0.65	0.528368	0.121632096971986	0.014794367		
2.0-3.0		197.93	4.398444	16.18044444	0.52	0.473511	0.0464893655856436	0.002161261		
3.0-5.0		492.44	10.94311	27.12355556	0.33	0.360485	-0.0304845518259444	0.000929308		
5.0-7.0		484.11	10.758	37.88155556	0.11	0.275707	-0.165706582363199	0.027458671		
7.0-10.0		822.37	18.27489	56.15644444	0.049	0.174843	-0.125843039437662	0.015836471		
							the sum of the squares of the residuals =	0.56608021		

B vs (1) 11/14/2013

Sampling layer/depth

	x			x'	C	C(x)	Residuals			
	Central D	dry weight of samples/ sampling area (450 cm^2)	dry weight /unit area (m^2)	dry mass depth	Cs-134 Conc.	Cs-134 conc. estimated by exponential equation	Difference between actual and predicted values	Squares of the residuals		
	cm	g	kg/m2	kg/m2	kBq/kg	kBq/kg				
Litter Layer		433.3	9.628889	9.628888889	19	18.86679	0.133213993526279	0.017745968	β	1.18
0-0.5		97.6	2.168889	11.79777778	2.4	3.023036	−0.623036176642689	0.388174077	C(0)	64013.23
0.5-1.0		107.2	2.382222	14.18	1.9	0.404545	1.49545484582004	2.236385196		
1.0-1.5		109.1	2.424444	16.60444444	1.6	0.052241	1.54775926579978	2.395558745		
1.5-2.0		159.8	3.551111	20.15555556	1.2	0.002606	1.19739418931472	1.433752845		
2.0-3.0		312.2	6.937778	27.09333333	0.86	7.45E-06	0.859992550862696	0.739587188		
3.0-5.0		468.9	10.42	37.51333333	1.1	1.13E-09	1.0999999988742	1.209999998		
5.0-7.0		611.3	13.58444	51.09777778	0.44	1.18E-14	0.439999999999988	0.1936		
7.0-10.0		103.5	2.3	53.39777778	0.16	1.69E-15	0.159999999999998	0.0256		
							the sum of the squares of the residuals =	8.64040402		

B vs (1) 11/25/2014

Sampling layer/depth

	x			x'	C	C(x)	Residuals			
	Central D	dry weight of samples/ sampling area (450 cm^2)	dry weight /unit area (m^2)	dry mass depth	Cs-134 Conc.	Cs-134 conc. estimated by exponential equation	Difference between actual and predicted values	Squares of the residuals		
	cm	g	kg/m2	kg/m2	kBq/kg	kBq/kg				
Litter Layer		370.6	8.235556	8.235555556	14	13.8883	0.111702686195406	0.01247749	β	5.79
0-0.5		232	5.155556	13.39111111	5.6	5.700905	−0.100904626512158	0.010181744	C(0)	57.59
0.5-1.0		128.8	2.862222	16.25333333	2.7	3.477408	−0.777408407407872	0.604363832		
1.0-1.5		131.4	2.92	19.17333333	2.4	2.10007	0.299929576484942	0.089957751		
1.5-2.0		100.9	2.242222	21.41555556	1.9	1.425773	0.47422688781179	0.224891141		
2.0-3.0		299.1	6.646667	28.06222222	1.3	0.452377	0.847622804229773	0.718464418		
3.0-5.0		558.7	12.41556	40.47777778	0.74	0.052996	0.687004234385777	0.471974818		
5.0-7.0		604.7	13.43778	53.91555556	0.27	0.005204	0.264796359029233	0.070117112		
7.0-10.0		1363	30.28889	84.20444444	0.19	2.78E-05	0.189972176350058	0.036089428		
							the sum of the squares of the residuals =	2.23851773		

B vs (1) 11/24/2015

Sampling layer/depth

	x			x'	C	C(x)	Residuals			
	Central D	dry weight of samples/ sampling area (450 cm^2)	dry weight /unit area (m^2)	dry mass depth	Cs-134 Conc.	Cs-134 conc. estimated by exponential equation	Difference between actual and predicted values	Squares of the residuals		
	cm	g	kg/m2	kg/m2	kBq/kg	kBq/kg				
Litter Layer		92.8	2.062222	2.062222222	14	12.91717	1.08283132262489	1.172523673	β	3.89
0-0.5		55.2	1.226667	3.288888889	7.7	9.426513	−1.72651288257692	2.980846734	C(0)	2.19E+01
0.5-1.0		76.9	1.708889	4.997777778	6	6.077852	−0.0778523416382404	0.006060987		
1.0-1.5		98.2	2.182222	7.18	3.8	3.470212	0.329788125193387	0.108760208		
1.5-2.0		121.6	2.702222	9.882222222	2.4	1.733659	0.666341158568886	0.44401054		
2.0-3.0		270.5	6.011111	15.89333333	1.6	0.370266	1.22973354581304	1.512244594		
3.0-5.0		582.3	12.94	28.83333333	0.46	0.013343	0.446657061621273	0.199502531		
5.0-7.0		630.1	14.00222	42.83555556	0.34	0.000366	0.339633972564484	0.115351235		
7.0-10.0		1008	22.4	65.23555556	0.16	1.16E-06	0.159998838204575	0.025599628		
							the sum of the squares of the residuals =	6.56490013		

B vs (1) 11/29/2016

Sampling layer/depth

	x			x'	C	C(x)	Residuals			
	Central D	dry weight of samples/ sampling area (450 cm^2)	dry weight /unit area (m^2)	dry mass depth	Cs-134 Conc.	Cs-134 conc. estimated by exponential equation	Difference between actual and predicted values	Squares of the residuals		
	cm	g	kg/m2	kg/m2	kBq/kg	kBq/kg				
Litter Layer 1		5.79	0.128667	0.128666667	0.68	4.94101	−4.26100960379552	18.15620284		
Litter Layer 2		58.82	1.307111	1.435777778	4.4	4.745408	−0.345408363245339	0.119306937	β	32.36
0-0.5		189.6	4.213333	5.649111111	7.3	4.166088	3.13391160667059	9.821401958	C(0)	4.96E+00
0.5-1.0		59.12	1.313778	6.962888889	7	4.00034	2.99966001217625	8.997960189		
1.0-1.5		92.04	2.045333	9.008222222	4.6	3.755325	0.84467547961091	0.713476666		
1.5-2.0		105.5	2.344444	11.35266667	3.7	3.492881	0.207118782774308	0.04289819		
2.0-3.0		265.3	5.895556	17.24822222	2.1	2.911135	−0.811135458011	0.657940731		
3.0-5.0		624.3	13.87333	31.12155556	0.59	1.896161	−1.30616056488765	1.706055421		
5.0-7.0		656.4	14.58667	45.70822222	0.25	1.208132	−0.958132324142688	0.918017551		
7.0-10.0		1078	23.95556	69.66377778	0.12	0.57626	−0.456260122233942	0.208173299		
							the sum of the squares of the residuals =	41.3414338		

B vs (1) 12/11/2017

Sampling layer/depth	x			x'		C		$C(x)$	Residuals			
	Central D	dry weight of samples/ sampling area (450 cm^2)	dry weight /unit area (m^2)	dry mass depth		Cs-134 Conc.		Cs-134 conc. estimated by exponential equation	Difference between actual and predicted values	Squares of the residuals		
	cm	g	kg/m2	kg/m2		kBq/kg		kBq/kg				
Litter Layer 1		57.71	1.282444	1.282444444		0.6		2.215705	-1.61570479070418	2.610501971		
Litter Layer 2		449.32	9.984889	11.26733333		3.6		1.745852	1.85414782326352	3.437864151	β	41.90
0-0.5		72.05	1.601111	12.86844444		2.3		1.68039	0.619609647823874	0.383916116	$C(0)$	2.28
0.5-1.0		86.71	1.926889	14.79533333		1.8		1.604855	0.195144840733583	0.038081509		
1.0-1.5		109.95	2.443333	17.23866667		1.8		1.513938	0.286062356685061	0.081831672		
1.5-2.0		114.81	2.551333	19.79		1.3		1.424494	-0.124493897114721	0.01549873		
2.0-3.0		271.84	6.040889	25.83088889		0.94		1.233219	-0.293218671494644	0.085977189		
3.0-5.0		635.39	14.11978	39.95066667		0.25		0.880386	-0.630385664651586	0.397386086		
5.0-7.0		792.73	17.61622	57.56688889		0.11		0.578178	-0.4681776710103	0.219190332		
7.0-10.0		1221.71	27.14911	84.716		0.038		0.302434	-0.264434074792447	0.06992538		
									the sum of the squares of the residuals =	7.34017314		

B vs (1) 11/12/2018

Sampling layer/depth	x			x'		C		$C(x)$	Residuals			
	Central D	dry weight of samples/ sampling area (450 cm^2)	dry weight /unit area (m^2)	dry mass depth		Cs-134 Conc.		Cs-134 conc. estimated by exponential equation	Difference between actual and predicted values	Squares of the residuals		
	cm	g	kg/m2	kg/m2		kBq/kg		kBq/kg				
Litter Layer 1		24.06	0.534667	0.534666667		0.28		2.248657	-1.96865736017481	3.875611802		
Litter Layer 2		93.78	2.084	2.618666667		2.4		2.102158	0.297841753550238	0.08870971	β	30.93422
0-0.5		85.88	1.908444	4.527111111		2.5		1.976388	0.52361202847854	0.274169556	$C(0)$	2.287861
0.5-1.0		62.28	1.384	5.911111111		2.8		1.889913	0.910086942263572	0.828258242		
1.0-1.5		78.56	1.745778	7.656888889		2.4		1.786209	0.613790699515443	0.376739023		
1.5-2.0		67.64	1.503111	9.16		2.3		1.701491	0.598508693179193	0.358212656		
2.0-3.0		20.09	0.446444	9.606444444		1.7		1.677112	0.0228883651558607	0.000523877		
3.0-5.0		409.28	9.095111	18.70155556		0.9		1.249894	-0.349893689919455	0.122425594		
5.0-7.0		542.9	12.06444	30.766		0.33		0.846246	-0.516246429796022	0.266510376		
7.0-10.0		661.92	14.70933	45.47533333		0.083		0.526003	-0.443003050808527	0.196251703		
									the sum of the squares of the residuals =	6.38741254		

B vs (1) 11/28/2019

Sampling layer/depth	x			x'		C		$C(x)$	Residuals			
	Central D	dry weight of samples/ sampling area (450 cm^2)	dry weight /unit area (m^2)	dry mass depth		Cs-134 Conc.		Cs-134 conc. estimated by exponential equation	Difference between actual and predicted values	Squares of the residuals		
	cm	g	kg/m2	kg/m2		kBq/kg		kBq/kg				
Litter Layer 1		38.22	0.849333	0.849333333		0.26		0.259349	0.000651475077653063	4.2442E-07		
Litter Layer 2		919.34	20.42978	21.27911111		1.8		4.68E-07	1.79999953188825	3.239998315	β	1.544787
0-0.5		73.06	1.623556	22.90266667		0.87		1.64E-07	0.869999836352051	0.756899715	$C(0)$	0.449429
0.5-1.0		89.04	1.978667	24.88133333		0.54		4.55E-08	0.539999954539179	0.291599951		
1.0-1.5		95.5	2.122222	27.00355556		0.52		1.15E-08	0.519999988491852	0.270399988		
1.5-2.0		120.38	2.675111	29.67866667		0.33		2.04E-09	0.329999997963254	0.108899999		
2.0-3.0		245.52	5.456	35.13466667		0.24		5.96E-11	0.239999999940425	0.0576		
3.0-5.0		526.59	11.702	46.83666667		0.066		3.06E-14	0.0659999999999694	0.004356		
5.0-7.0		556.51	12.36689	59.20355556		0.053		1.02E-17	0.053	0.002809		
7.0-10.0		932.81	20.72911	79.93266667		0.042		1.52E-23	0.042	0.001764		
									the sum of the squares of the residuals =	4.73432739		

B vs (2) 11/12/2013

Sampling layer/depth

	x			x'	C	C(x)	Residuals			
	Central D	dry weight of samples/ sampling area (450 cm^2)	dry weight /unit area (m^2)	dry mass depth	Cs-134 Conc.	Cs-134 conc. estimated by exponential equation	Difference between actual and predicted values	Squares of the residuals		
	cm	g	kg/m2	kg/m2	kBq/kg	kBq/kg				
Litter Layer		695.9	15.46444	15.46444444	27	24.37793	2.62206773575699	6.875239211	β	0.89
0-0.5		31.78	0.706222	16.17066667	5.5	11.02776	-5.52775609052638	30.5560874	C(0)	8.53E+08
0.5-1.0		56.3	1.251111	17.42177778	2.4	2.705014	-0.305013515723955	0.093033245		
1.0-1.5		82.94	1.843111	19.26488889	2	0.341242	1.65875840729329	2.751479454		
1.5-2.0		117.1	2.602222	21.86711111	1.8	0.01835	1.7816496445873	3.174275456		
2.0-3.0		225.2	5.004444	26.87155556	0.95	6.64E-05	0.949933568565556	0.902373785		
3.0-5.0		463.5	10.3	37.17155556	0.44	6.28E-10	0.439999999372199	0.193599999		
5.0-7.0		437.8	9.728889	46.90044444	0.35	1.13E-14	0.349999999999989	0.1225		
7.0-10.0		723.4	16.07556	62.976	0.25	1.62E-22	0.25	0.0625		
							the sum of the squares of the residuals =	44.7310885		

B vs (2) 11/27/2014

Sampling layer/depth

	x			x'	C	C(x)	Residuals			
	Central D	dry weight of samples/ sampling area (450 cm^2)	dry weight /unit area (m^2)	dry mass depth	Cs-134 Conc.	Cs-134 conc. estimated by exponential equation	Difference between actual and predicted values	Squares of the residuals		
	cm	g	kg/m2	kg/m2	kBq/kg	kBq/kg				
Litter Layer		183.2	4.071111	4.071111111	50	49.95481	0.0451858776879277	0.002041764	β	2.01
0-0.5		142.7	3.171111	7.242222222	10	10.28873	-0.288726217164729	0.083362828	C(0)	3.80E+02
0.5-1.0		73.6	1.635556	8.877777778	4.2	4.554429	-0.354429070904072	0.125619966		
1.0-1.5		79.83	1.774	10.65177778	2.7	1.881687	0.818312707409133	0.669635687		
1.5-2.0		73.91	1.642444	12.29422222	1.6	0.830097	0.769902594998644	0.592750006		
2.0-3.0		157.6	3.502222	15.79644444	1.1	0.144965	0.955035319694155	0.912092462		
3.0-5.0		207.9	4.62	20.41644444	0.72	0.014505	0.705495167555969	0.497723431		
5.0-7.0		607	13.48889	33.90533333	0.59	1.75E-05	0.589982518801022	0.348079372		
7.0-10.0		674.2	14.98222	48.88755556	0.38	1E-08	0.379999989988979	0.144399992		
							the sum of the squares of the residuals =	3.37570551		

B vs (2) 11/25/2015

Sampling layer/depth

	x			x'	C	C(x)	Residuals			
	Central D	dry weight of samples/ sampling area (450 cm^2)	dry weight /unit area (m^2)	dry mass depth	Cs-134 Conc.	Cs-134 conc. estimated by exponential equation	Difference between actual and predicted values	Squares of the residuals		
	cm	g	kg/m2	kg/m2	kBq/kg	kBq/kg				
Litter Layer		161.9	3.597778	3.597777778	22	34.72894	-12.7289353271512	162.0257946	β	6.23
0-0.5		20.93	0.465111	4.062888889	43	32.23038	10.7696182528818	115.9846773	C(0)	6.19E+01
0.5-1.0		25.97	0.577111	4.64	30	29.3786	0.621395883072886	0.386132843		
1.0-1.5		28.68	0.637333	5.277333333	33	26.52152	6.47848254883369	41.97073614		
1.5-2.0		45.81	1.018	6.295333333	21	22.52303	-1.52302663182972	2.319610121		
2.0-3.0		120.9	2.686667	8.982	11	14.63259	-3.63258881427446	13.19570149		
3.0-5.0		298.8	6.64	15.622	3.5	5.039671	-1.5396707391915	2.370585985		
5.0-7.0		384.8	8.551111	24.17311111	1.3	1.277164	0.0228357190879291	0.00052147		
7.0-10.0		692.1	15.38	39.55311111	0.72	0.108144	0.611855697059232	0.374367394		
							the sum of the squares of the residuals =	338.628127		

B vs (2) 11/29/2016

Sampling layer/depth

	x			x'	C	C(x)	Residuals			
	Central D	dry weight of samples/ sampling area (450 cm^2)	dry weight /unit area (m^2)	dry mass depth	Cs-134 Conc.	Cs-134 conc. estimated by exponential equation	Difference between actual and predicted values	Squares of the residuals		
	cm	g	kg/m2	kg/m2	kBq/kg	kBq/kg				
Litter Layer 1		18.62	0.413778	0.413777778	1.7	20.20335	-18.5033467621534	342.3738414		
Litter Layer 2		33.52	0.744889	1.158666667	16	19.13681	-3.13681495021786	9.839608032	β	13.73
0-0.5		75.52	1.678222	2.836888889	41	16.93572	24.0642804439577	579.0895933	C(0)	2.08E+01
0.5-1.0		27.67	0.614889	3.451777778	28	16.19424	11.8057574132574	139.3759081		
1.0-1.5		66.43	1.476222	4.928	13	14.54394	-1.54393587472722	2.383737985		
1.5-2.0		86.27	1.917111	6.845111111	8.1	12.64917	-4.54917475535552	20.69499095		
2.0-3.0		133.4	2.964444	9.809555556	3.9	10.19355	-6.29354792356316	39.60874547		
3.0-5.0		493.3	10.96222	20.77177778	0.55	4.588766	-4.03876556539546	16.31162729		
5.0-7.0		567	12.6	33.37177778	0.64	1.833493	-1.19349291724805	1.424425344		
7.0-10.0		1006	22.35556	55.72733333	0.36	0.360071	-0.00007116844236143	5.06495E-09		
							the sum of the squares of the residuals =	1151.10248		

B vs (2) 12/11/2017

Sampling layer/depth

	χ			χ'	C	C(χ)	Residuals			
	Central D	dry weight of samples/ sampling area (450 cm^2)	dry weight /unit area (m^2)	dry mass depth	Cs-134 Conc.	Cs-134 conc. estimated by exponential equation	Difference between actual and predicted values	Squares of the residuals		
	cm	g	kg/m2	kg/m2	kBq/kg	kBq/kg				
Litter Layer 1		28.76	0.639111	0.639111111	1.6	6.806266	-5.20626568118551	27.10520234		
Litter Layer 2		162.38	3.608444	4.247555556	9.7	5.78703	3.91296978267008	15.31133252	β	22.24
0-0.5		108.48	2.410667	6.658222222	8	5.192645	2.8073549212567	7.881241654	C(0)	7.00
0.5-1.0		54.57	1.212667	7.870888889	6.8	4.917132	1.88286758131273	3.545190329		
1.0-1.5		68.3	1.517778	9.388666667	4.9	4.592805	0.307194852041187	0.094368677		
1.5-2.0		87.03	1.934	11.32266667	3.7	4.210344	-0.510344167441046	0.260451169		
2.0-3.0		191.36	4.252444	15.57511111	2.2	3.477688	-1.27768833895865	1.632487492		
3.0-5.0		366.05	8.134444	23.70955556	0.86	2.412512	-1.55251227417932	2.410294361		
5.0-7.0		413.76	9.194667	32.90422222	0.42	1.595688	-1.17568834715513	1.38224309		
7.0-10.0		866.84	19.26311	52.16733333	0.31	0.671189	-0.36118936309595	0.130457756		
							the sum of the squares of the residuals =	59.7532694		

B vs (2) 11/13/2018

Sampling layer/depth

	χ			χ'	C	C(χ)	Residuals			
	Central D	dry weight of samples/ sampling area (450 cm^2)	dry weight /unit area (m^2)	dry mass depth	Cs-134 Conc.	Cs-134 conc. estimated by exponential equation	Difference between actual and predicted values	Squares of the residuals		
	cm	g	kg/m2	kg/m2	kBq/kg	kBq/kg				
Litter Layer 1		10.5	0.233333	0.233333333	0.46	8.352843	-7.89284266462387	62.29696533		
Litter Layer 2		102.45	2.276667	2.51	9.1	7.341956	1.75804432080598	3.090719834	β	17.64903
0-0.5		30.71	0.682444	3.192444444	13	7.063479	5.93652086819836	35.24228002	C(0)	8.464007
0.5-1.0		40.12	0.891556	4.084	9.9	6.715524	3.18447575139755	10.14088581		
1.0-1.5		54.57	1.212667	5.296666667	7.4	6.269595	1.13040467083801	1.27781472		
1.5-2.0		71.7	1.593333	6.89	5.4	5.728381	-0.328381491335891	0.107834404		
2.0-3.0		169.96	3.776889	10.66688889	3	4.624801	-1.62480070758809	2.639977339		
3.0-5.0		375.39	8.342	19.00888889	0.97	2.882831	-1.91283116754362	3.658923076		
5.0-7.0		452.09	10.04644	29.05533333	0.35	1.631562	-1.2815623563666	1.642402073		
7.0-10.0		691.98	15.37733	44.43266667	0.12	0.682668	-0.562667995512199	0.316595273		
							the sum of the squares of the residuals =	120.414398		

B vs (2) 11/28/2019

Sampling layer/depth

	χ			χ'	C	C(χ)	Residuals			
	Central D	dry weight of samples/ sampling area (450 cm^2)	dry weight /unit area (m^2)	dry mass depth	Cs-134 Conc.	Cs-134 conc. estimated by exponential equation	Difference between actual and predicted values	Squares of the residuals		
	cm	g	kg/m2	kg/m2	kBq/kg	kBq/kg				
Litter Layer 1		17.77	0.394889	0.394888889	0.19	2.42456	-2.23456022043356	4.993259379		
Litter Layer 2		633.43	14.07622	14.47111111	6	1.783934	4.21606550609843	17.77520835	β	45.87646
0-0.5		85.31	1.895778	16.36688889	2.9	1.711718	1.18828160164206	1.412013165	C(0)	2.44552
0.5-1.0		75.07	1.668222	18.03511111	1.8	1.650593	0.149407324831712	0.022322549		
1.0-1.5		85.86	1.908	19.94311111	1.3	1.583353	-0.283352551284274	0.080288668		
1.5-2.0		104.66	2.325778	22.26888889	0.77	1.505083	-0.7350828273582	0.540346763		
2.0-3.0		245	5.444444	27.71333333	0.51	1.336657	-0.826657013107288	0.683361817		
3.0-5.0		497.6	11.05778	38.77111111	0.24	1.050365	-0.810365232732947	0.65669181		
5.0-7.0		444.25	9.872222	48.64333333	0.17	0.847001	-0.677000923942873	0.458330251		
7.0-10.0		717.37	15.94156	64.58488889	0.098	0.598372	-0.500372233973426	0.250372373		
							the sum of the squares of the residuals =	26.8721951		

Cs137

G7 11/11/2013

Sampling layer/depth	x			x'	C	C(x)	Residuals			
	Central Depth	dry weight of samples/ sampling area (450 cm^2)	dry weight /unit area (m^2)	dry mass depth	Cs-137 Conc.	Cs-137 conc. estimated by exponential equation	Difference between actual and predicted values	Squares of the residuals		
	cm	g	kg/m2	kg/m2	kBq/kg	kBq/kg				
Litter Layer (1.0-0)		157.2	3.493333333	3.493333333	8.9	8.180900789	0.719099211006668	0.517103675	β	7.73
0-0.5		56	1.244444444	4.737777778	6	6.964778071	-0.964778071394742	0.930796727	C(0)	12.85
0.5-1.0		111.4	2.475555556	7.213333333	5.2	5.056714777	0.143285222772547	0.020530655		
1.0-1.5		115.1	2.557777778	9.771111111	3.6	3.632550391	-0.0325503909403722	0.001059528		
1.5-2.0		143.5	3.188888889	12.96	2.3	2.40496452	-0.104964519501912	0.01101755		
2.0-3.0		334.5	7.433333333	20.39333333	1.4	0.919639823	0.480360177123046	0.2307459		
3.0-5.0		632.1	14.04666667	34.44	0.4	0.14951715	0.250482849858531	0.062741658		
5.0-7.0		701.6	15.59111111	50.03111111	0.2	0.019907696	0.180092304015011	0.032433238		
7.0-10.0		1073	23.84444444	73.87555556	0.1	0.000911602	0.0990883984933718	0.009818511		
							the sum of the squares of the residuals =	1.816247442		

G7 11/28/2014

Sampling layer/depth	x			x'	C	C(x)	Residuals			
	Central Depth	dry weight of samples/ sampling area (450 cm^2)	dry weight /unit area (m^2)	dry mass depth	Cs-137 Conc.	Cs-137 conc. estimated by exponential equation	Difference between actual and predicted values	Squares of the residuals		
	cm	g	kg/m2	kg/m2	kBq/kg	kBq/kg				
Litter Layer (1.0-0)		83.52	1.856	1.856	6.3	6.389927155	-0.0899271554131893	0.008086893	β	6.41
0-0.5		131.8	2.928888889	4.784888889	4.3	4.044972455	0.255027544803235	0.065039049	C(0)	8.54
0.5-1.0		148.5	3.3	8.084888889	2.4	2.416427028	-0.0164270277912881	0.000269847		
1.0-1.5		124.5	2.766666667	10.85155556	1.3	1.568888593	-0.268888592583475	0.072301075		
1.5-2.0		156.5	3.477777778	14.32933333	0.8	0.911584194	-0.11158419445898	0.012451032		
2.0-3.0		253.6	5.635555556	19.96488889	0.6	0.378183784	0.221816216251988	0.049202434		
3.0-5.0		673	14.95555556	34.92044444	0.6	0.036619103	0.563380897307036	0.317398035		
5.0-7.0		671	14.91111111	49.83155556	0.5	0.003570474	0.496429526184256	0.246442274		
7.0-10.0		1069	23.75555556	73.58711111	0.5	8.75156E-05	0.499912484369827	0.249912492		
							the sum of the squares of the residuals =	1.021103133		

G7 11/24/2015

Sampling layer/depth	x			x'	C	C(x)	Residuals			
	Central Depth	dry weight of samples/ sampling area (450 cm^2)	dry weight /unit area (m^2)	dry mass depth	Cs-137 Conc.	Cs-137 conc. estimated by exponential equation	Difference between actual and predicted values	Squares of the residuals		
	cm	g	kg/m2	kg/m2	kBq/kg	kBq/kg				
Litter Layer (1.0-0)		39.8	0.884444444	0.884444444	8.3	11.06928464	-2.76928463988233	7.668937417	β	10.94
0-0.5		107.4	2.386666667	3.271111111	12	8.900478494	3.09952150586674	9.607033565	C(0)	12.00
0.5-1.0		138.5	3.077777778	6.348888889	8.4	6.718663964	1.68133603583165	2.826890865		
1.0-1.5		137.5	3.055555556	9.404444444	5.4	5.081995704	0.318004296058027	0.101126732		
1.5-2.0		163.4	3.631111111	13.03555556	1.9	3.647092973	-1.74709297317728	3.052333857		
2.0-3.0		270.5	6.011111111	19.04666667	0.5	2.105802894	-1.60580289379914	2.578602934		
3.0-5.0		620.5	13.78888889	32.83555556	0.4	0.597386954	-0.197386953526897	0.038961609		
5.0-7.0		651.2	14.47111111	47.30666667	0.3	0.159229026	0.14077097430646	0.019816467		
7.0-10.0		1077	23.93333333	71.24	0.2	0.01787783	0.182122169613554	0.033168485		
							the sum of the squares of the residuals =	25.92687193		

G7 11/29/2016

Sampling layer/depth	x			x'	C	C(x)	Residuals			
	Central Depth	dry weight of samples/ sampling area (450 cm^2)	dry weight /unit area (m^2)	dry mass depth	Cs-137 Conc.	Cs-137 conc. estimated by exponential equation	Difference between actual and predicted values	Squares of the residuals		
	cm	g	kg/m2	kg/m2	kBq/kg	kBq/kg				
Litter Layer 1		14.54	0.323111111	0.323111111	0.8	4.732163272	-3.93216327184576	15.461908		
Litter Layer 2		7.01	0.155777778	0.478888889	6.4	4.698028182	1.70197181813427	2.89670807	β	21.52
0-0.5		180.4	4.008888889	4.487777778	5.6	3.89944846	1.70055154019165	2.891875541	C(0)	4.80
0.5-1.0		126.3	2.806666667	7.294444444	5.3	3.422594996	1.8774050044848	3.524649551		
1.0-1.5		128.3	2.851111111	10.14555556	3.9	2.997856248	0.902143752349001	0.81386335		
1.5-2.0		149.9	3.331111111	13.47666667	1.8	2.567900155	-0.767900155171531	0.589670648		
2.0-3.0		258.1	5.735555556	19.21222222	0.9	1.967052467	-1.06705246722464	1.138600968		
3.0-5.0		462.8	10.28444444	29.49666667	0.5	1.219670059	-0.71967005935346	0.517924994		
5.0-7.0		666.6	14.81333333	44.31	0.3	0.612718587	-0.312718587124976	0.097792915		
7.0-10.0		910.9	20.24222222	64.55222222	0.2	0.239170213	-0.0391702127415209	0.001534306		
							the sum of the squares of the residuals =	27.93452834		

G7 12/13/2017

Sampling layer/depth	x			x'	C	C(x)	Residuals			
	Central Depth	dry weight of samples/ sampling area (450 cm^2)	dry weight /unit area (m^2)	dry mass depth	Cs-137 Conc.	Cs-137 conc. estimated by exponential equation	Difference between actual and predicted values	Squares of the residuals		
	cm	g	kg/m2	kg/m2	kBq/kg	kBq/kg				
Litter Layer 1		4.98	0.110666667	0.110666667	1.3	3.065172382	-1.76517238246129	3.11583354		
Litter Layer 2		8.5	0.188888889	0.299555556	3.9	3.022995151	0.877004848701906	0.769137505	β	13.63
0-0.5		190.53	4.234	4.533555556	4	2.215921982	1.78407801751091	3.182934373	C(0)	3.09
0.5-1.0		122.28	2.717333333	7.250888889	2.1	1.81546588	0.284534120351909	0.080959666		
1.0-1.5		144.4	3.208888889	10.45977778	0.93	1.434703571	-0.504703570550136	0.254725694		
1.5-2.0		141.51	3.144666667	13.60444444	0.43	1.139153375	-0.709153375300352	0.50289851		
2.0-3.0		312.68	6.948444444	20.55288889	0.41	0.684265862	-0.274265861727817	0.075221763		
3.0-5.0		620.3	13.78444444	34.33733333	0.23	0.248938674	-0.0189386741724847	0.000358673		
5.0-7.0		644.88	14.33066667	48.668	0.22	0.087007925	0.132992074909244	0.017686892		
7.0-10.0		1025.34	22.78533333	71.45333333	0.15	0.016356261	0.133643738563322	0.017860649		
							the sum of the squares of the residuals =	8.017617264		

G7 11/13/2018

Sampling layer/depth	x			x'	C	C(x)	Residuals			
	Central Depth	dry weight of samples/ sampling area (450 cm^2)	dry weight /unit area (m^2)	dry mass depth	Cs-137 Conc.	Cs-137 conc. estimated by exponential equation	Difference between actual and predicted values	Squares of the residuals		
	cm	g	kg/m2	kg/m2	kBq/kg	kBq/kg				
Litter Layer 1		8.52	0.189333333	0.189333333	0.8	1.211158007	-0.411158006697883	0.169050906		
Litter Layer 2		11.28	0.250666667	0.44	1.2	1.197149406	0.00285059387546016	8.12589E-06	β	21.54661
0-0.5		107.69	2.393111111	2.833111111	1.5	1.071303897	0.428696102943472	0.183780349	C(0)	1.221848
0.5-1.0		103.42	2.298222222	5.131333333	1.2	0.962918655	0.237081345450455	0.056207564		
1.0-1.5		193.04	4.289777778	9.421111111	0.71	0.789086513	-0.079086513301821	0.006254677		
1.5-2.0		186.81	4.151333333	13.57244444	0.5	0.650803881	-0.150803880800141	0.02274181		
2.0-3.0		419.63	9.325111111	22.89755556	0.33	0.422175201	-0.0921752007473604	0.008496268		
3.0-5.0		924.1	20.53555556	43.43311111	0.17	0.162770993	0.00722900705904039	5.22585E-05		
5.0-7.0		881.16	19.58133333	63.01444444	0.12	0.065598613	0.0544013867040092	0.002959511		
7.0-10.0		1199.83	26.66288889	89.67733333	0.11	0.019031635	0.0909683645734706	0.008275243		
							the sum of the squares of the residuals =	0.457826713		

G7 11/27/2019

Sampling layer/depth	x			x'	C	C(x)	Residuals			
	Central Depth	dry weight of samples/ sampling area (450 cm^2)	dry weight /unit area (m^2)	dry mass depth	Cs-137 Conc.	Cs-137 conc. estimated by exponential equation	Difference between actual and predicted values	Squares of the residuals		
	cm	g	kg/m2	kg/m2	kBq/kg	kBq/kg				
Litter Layer 1		25.99	0.577555556	0.577555556	1.4	8.302634305	-6.90263430488437	47.64636035		
Litter Layer 2		156.5	3.477777778	4.055333333	11	7.472925944	3.52707405598386	12.4402514	β	33.03165
0-0.5		96.2	2.137777778	6.193111111	10	7.004603223	2.99539677741219	8.972401854	C(0)	8.449082
0.5-1.0		120.11	2.669111111	8.862222222	9.3	6.460862826	2.83913717411028	8.060699893		
1.0-1.5		108.49	2.410888889	11.27311111	6.8	6.006100059	0.793899941111373	0.630277116		
1.5-2.0		137.7	3.06	14.33311111	5.8	5.474698453	0.325301546892618	0.105821096		
2.0-3.0		244.53	5.434	19.76711111	3.1	4.644242568	-1.54424256845599	2.38468511		
3.0-5.0		534.48	11.87733333	31.64444444	1.9	3.24155754	-1.34155753960691	1.799776632		
5.0-7.0		539.16	11.98133333	43.62577778	1.1	2.255408438	-1.15540843772558	1.334968658		
7.0-10.0		1008.08	22.40177778	66.02755556	0.45	1.144696709	-0.694696709289565	0.482603518		
							the sum of the squares of the residuals =	83.85784562		

B Everyone(1) 11/14/2013

Sampling layer/depth

	x			x'	C	C(x)	Residuals			
	Central Depth	dry weight of samples/ sampling area (450 cm^2)	dry weight /unit area (m^2)	dry mass depth	Cs-137 Conc.	Cs-137 conc. estimated by exponential equation	Difference between actual and predicted values	Squares of the residuals		
	cm	g	kg/m2	kg/m2	kBq/kg	kBq/kg				
Litter Layer		169.5	3.766666667	3.766666667	14	14.38141464	-0.381414638494471	0.145477126	β	6.04
0-0.5		32.83	0.729555556	4.496222222	13	12.74577841	0.254221588894623	0.064628616	C(0)	26.82
0.5-1.0		84.37	1.874888889	6.371111111	9.8	9.345719415	0.454280585128252	0.20637085		
1.0-1.5		133.1	2.957777778	9.328888889	5.5	5.728340055	-0.228340055173199	0.052139181		
1.5-2.0		151	3.355555556	12.68444444	3.1	3.287421705	-0.187421705277103	0.035126896		
2.0-3.0		321	7.133333333	19.81777778	0.9	1.009630249	-0.109630248597529	0.012018791		
3.0-5.0		705.7	15.68222222	35.5	0.5	0.075341836	0.424658164114456	0.180334556		
5.0-7.0		695.1	15.44666667	50.94666667	0.4	0.005845748	0.394154251928971	0.155357574		
7.0-10.0		1159	25.75555556	76.70222222	0.2	8.23597E-05	0.199917640316622	0.039967063		
							the sum of the squares of the residuals =	0.891420654		

B Everyone(1) 11/28/2014

Sampling layer/depth

	x			x'	C	C(x)	Residuals			
	Central Depth	dry weight of samples/ sampling area (450 cm^2)	dry weight /unit area (m^2)	dry mass depth	Cs-137 Conc.	Cs-137 conc. estimated by exponential equation	Difference between actual and predicted values	Squares of the residuals		
	cm	g	kg/m2	kg/m2	kBq/kg	kBq/kg				
Litter Layer		208.8	4.64	4.64	11	11.43096683	-0.43096682799723	0.185732407	β	11.79
0-0.5		268.7	5.971111111	10.61111111	8.7	6.888170626	1.81182937351319	3.282725679	C(0)	16.94
0.5-1.0		136.7	3.037777778	13.64888889	4.8	5.323416748	-0.523416748444571	0.273965093		
1.0-1.5		140.4	3.12	16.76888889	3.1	4.085525488	-0.985525487874067	0.971260487		
1.5-2.0		168.7	3.748888889	20.51777778	2.5	2.972601988	-0.472601988210455	0.223352639		
2.0-3.0		335.9	7.464444444	27.98222222	1.8	1.57812886	0.221871140330625	0.049226803		
3.0-5.0		729.1	16.20222222	44.18444444	1	0.399248733	0.600751266704713	0.360902084		
5.0-7.0		652.5	14.5	58.68444444	0.5	0.11669586	0.383304139934159	0.146922064		
7.0-10.0		101.2	2.248888889	60.93333333	0.4	0.096428437	0.303571563178032	0.092155694		
							the sum of the squares of the residuals =	5.58624295		

B Everyone(1) 11/25/2015

Sampling layer/depth

	x			x'	C	C(x)	Residuals			
	Central Depth	dry weight of samples/ sampling area (450 cm^2)	dry weight /unit area (m^2)	dry mass depth	Cs-137 Conc.	Cs-137 conc. estimated by exponential equation	Difference between actual and predicted values	Squares of the residuals		
	cm	g	kg/m2	kg/m2	kBq/kg	kBq/kg				
Litter Layer		22.1	0.491111111	0.491111111	10	14.82080083	-4.82080082599553	23.2401206	β	12.94
0-0.5		105.6	2.346666667	2.837777778	17	12.36352617	4.63647382595901	21.49688954	C(0)	15.39
0.5-1.0		105.8	2.351111111	5.188888889	14	10.31012488	3.68987511845929	13.61517839		
1.0-1.5		118.5	2.633333333	7.822222222	8.2	8.412345584	-0.212345583836816	0.045090647		
1.5-2.0		131.1	2.913333333	10.73555556	4.8	6.717016978	-1.91701697832014	3.674954095		
2.0-3.0		300.6	6.68	17.41555556	1.9	4.009279046	-2.10927904619455	4.449058095		
3.0-5.0		630.6	14.01333333	31.42888889	0.8	1.358085157	-0.558085156995583	0.311459042		
5.0-7.0		684.72	15.216	46.64488889	0.3	0.419217058	-0.119217057655261	0.014212707		
7.0-10.0		888	19.73333333	66.37822222	0.2	0.091284481	0.108715519041145	0.011819064		
							the sum of the squares of the residuals =	66.85878218		

B Everyone(1) 11/29/2016

Sampling layer/depth

	x			x'	C	C(x)	Residuals			
	Central Depth	dry weight of samples/ sampling area (450 cm^2)	dry weight /unit area (m^2)	dry mass depth	Cs-137 Conc.	Cs-137 conc. estimated by exponential equation	Difference between actual and predicted values	Squares of the residuals		
	cm	g	kg/m2	kg/m2	kBq/kg	kBq/kg				
Litter Layer 1		10.19	0.226444444	0.226444444	2.5	20.16867154	-17.668671535507	312.1819538		
Litter Layer 2		7.17	0.159333333	0.385777778	17	20.06472703	-3.06472702769567	9.392551754	β	30.84
0-0.5		180.1	4.002222222	4.388	36	17.62245012	18.3775498847767	337.7343398	C(0)	20.32
0.5-1.0		88.25	1.961111111	6.349111111	26	16.5365978	9.46340220312448	89.55598126		
1.0-1.5		89.46	1.988	8.337111111	19	15.50412769	3.49587231072788	12.22112321		
1.5-2.0		134.5	2.988888889	11.326	13	14.07187839	-1.07187839003718	1.148923283		
2.0-3.0		272.8	6.062222222	17.38822222	6.5	11.56038342	-5.0603834151305	25.60748031		
3.0-5.0		604.7	13.43777778	30.826	3.5	7.47679874	-3.97679874031038	15.81492822		
5.0-7.0		709.2	15.76	46.586	1.8	4.484904064	-2.68490406432087	7.208709835		
7.0-10.0		1135	25.22222222	71.80822222	1.3	1.979363109	-0.679363108582239	0.461534233		
							the sum of the squares of the residuals =	811.3275257		

B Everyone(1) 12/13/2017

Sampling layer/depth

	x			x'	C	C(x)	Residuals			
	Central Depth	dry weight of samples/ sampling area (450 cm^2)	dry weight /unit area (m^2)	dry mass depth	Cs-137 Conc.	Cs-137 conc. estimated by exponential equation	Difference between actual and predicted values	Squares of the residuals		
	cm	g	kg/m2	kg/m2	kBq/kg	kBq/kg				
Litter Layer 1		46.82	1.040444444	1.040444444	8.9	13.58094234	-4.68094234289488	21.91122122		
Litter Layer 2		91.01	2.022444444	3.062888889	13	12.88605234	0.113947660249243	0.012984069	β	38.51
0-0.5		112.24	2.494222222	5.557111111	13	12.07783133	0.922168674899384	0.850395065	C(0)	13.95
0.5-1.0		74.77	1.661555556	7.218666667	13	11.56775838	1.43224162338952	2.051316068		
1.0-1.5		123.28	2.739555556	9.958222222	13	10.77336319	2.2266368105177	4.957911486		
1.5-2.0		123.36	2.741333333	12.69955556	11	10.03305846	0.966941542236016	0.934975946		
2.0-3.0		233.25	5.183333333	17.88288889	11	8.769471855	2.23052814457411	4.975255804		
3.0-5.0		582.88	12.95288889	30.83577778	5.2	6.264480811	-1.06448081120881	1.133119397		
5.0-7.0		622.87	13.84155556	44.67733333	2.4	4.372944405	-1.97294440457859	3.892509624		
7.0-10.0		1034.3	22.98444444	67.66177778	0.93	2.407383738	-1.47738373755038	2.182662708		
							the sum of the squares of the residuals =	42.90235138		

B Everyone(1) 11/14/2018

Sampling layer/depth

	x			x'	C	C(x)	Residuals			
	Central Depth	dry weight of samples/ sampling area (450 cm^2)	dry weight /unit area (m^2)	dry mass depth	Cs-137 Conc.	Cs-137 conc. estimated by exponential equation	Difference between actual and predicted values	Squares of the residuals		
	cm	g	kg/m2	kg/m2	kBq/kg	kBq/kg				
Litter Layer 1		15.3	0.34	0.34	0.77	11.40246012	-10.6324601192376	113.0492082		
Litter Layer 2		54.07	1.201555556	1.541555556	11	11.20070918	-0.200709175178032	0.040284173	β	67.30636
0-0.5		265.8	5.906666667	7.448222222	14	10.2596545	3.74034549905405	13.99018445	C(0)	11.46021
0.5-1.0		94.75	2.105555556	9.553777778	12	9.943668379	2.05633162118415	4.228499736		
1.0-1.5		98.93	2.198444444	11.75222222	14	9.62412295	4.37587705044837	19.14829996		
1.5-2.0		98.03	2.178444444	13.93066667	14	9.3176146	4.68238539970095	21.92473303		
2.0-3.0		207.17	4.603777778	18.53444444	10	8.701594731	1.29840526908129	1.685856243		
3.0-5.0		510.42	11.34266667	29.87711111	8.2	7.352080618	0.847919382105902	0.718967279		
5.0-7.0		551.67	12.25933333	42.13644444	2.7	6.127832337	-3.42783233694765	11.75003453		
7.0-10.0		786.7	17.48222222	59.61866667	1	4.72609863	-3.72609863025279	13.883811		
							the sum of the squares of the residuals =	200.4198786		

B Everyone(1) 11/29/2019

Sampling layer/depth

	x			x'	C	C(x)	Residuals			
	Central Depth	dry weight of samples/ sampling area (450 cm^2)	dry weight /unit area (m^2)	dry mass depth	Cs-137 Conc.	Cs-137 conc. estimated by exponential equation	Difference between actual and predicted values	Squares of the residuals		
	cm	g	kg/m2	kg/m2	kBq/kg	kBq/kg				
Litter Layer 1		22.27	0.494888889	0.494888889	4.9	5.893499729	-0.993499729319812	0.987041712		
Litter Layer 2		226.95	5.043333333	5.538222222	5.8	5.145230416	0.654769584098645	0.428723208	β	37.14346
0-0.5		78.85	1.752222222	7.290444444	5.1	4.908143203	0.19185679731424	0.036809031	C(0)	5.972548
0.5-1.0		87.7	1.948888889	9.239333333	4.8	4.657256165	0.142743834777756	0.020375802		
1.0-1.5		114.25	2.538888889	11.77822222	4.3	4.349552109	-0.0495521086025867	0.002455411		
1.5-2.0		122.71	2.726888889	14.50511111	4.5	4.041669411	0.458330589116867	0.210066929		
2.0-3.0		261.45	5.81	20.31511111	3.4	3.456433531	-0.0564335310208985	0.003184743		
3.0-5.0		620.64	13.792	34.10711111	2.7	2.384334927	0.315665072907307	0.099644438		
5.0-7.0		690.77	15.35044444	49.45755556	1	1.577191498	-0.577191497692494	0.333150025		
7.0-10.0		1089.44	24.20977778	73.66733333	0.33	0.821892714	-0.491892714222176	0.241958442		
							the sum of the squares of the residuals =	2.363409743		

B Everyone(2) 11/12/2013

Sampling layer/depth	x			x'	C	C(x)	Residuals			
	Central Depth	dry weight of samples/ sampling area (450 cm^2)	dry weight /unit area (m^2)	dry mass depth	Cs-137 Conc.	Cs-137 conc. estimated by exponential equation	Difference between actual and predicted values	Squares of the residuals		
	cm	g	kg/m2	kg/m2	kBq/kg	kBq/kg				
Litter Layer 1		249.5	5.544444444	5.544444444	9.6	9.478658541	0.121341459192037	0.01472375	β	2.60
0-0.5		106.2	2.36	7.904444444	3.4	3.822935733	-0.422935733283316	0.178874634	C(0)	80.02
0.5-1.0		124.1	2.757777778	10.66222222	1.4	1.32305982	0.076940179922142 3	0.005919791		
1.0-1.5		138.7	3.082222222	13.74444444	1.1	0.40415517	0.69584483026257	0.484200028		
1.5-2.0		145.9	3.242222222	16.98666667	0.8	0.116086365	0.683913635340303	0.467737861		
2.0-3.0		301.1	6.691111111	23.67777778	0.5	0.008845327	0.491154673010726	0.241232913		
3.0-5.0		490	10.88888889	34.56666667	0.4	0.000134032	0.399865967909824	0.159892792		
5.0-7.0		492.3	10.94	45.50666667	0.2	1.99142E-06	0.199998008578672	0.039999203		
7.0-10.0		747.6	16.61333333	62.12	0.1	3.33517E-09	0.099999966648281	0.009999999		
							the sum of the squares of the residuals =	1.602580972		

B Everyone(2) 11/27/2014

Sampling layer/depth	x			x'	C	C(x)	Residuals			
	Central Depth	dry weight of samples/ sampling area (450 cm^2)	dry weight /unit area (m^2)	dry mass depth	Cs-137 Conc.	Cs-137 conc. estimated by exponential equation	Difference between actual and predicted values	Squares of the residuals		
	cm	g	kg/m2	kg/m2	kBq/kg	kBq/kg				
Litter Layer 1		87.2	1.937777778	1.937777778	8.4	8.531611863	-0.131611863228086	0.017321683	β	7.05
0-0.5		156.7	3.482222222	5.42	5.7	5.204773264	0.495226735594145	0.24524952	C(0)	11.23
0.5-1.0		131.8	2.928888889	8.348888889	3	3.434611654	-0.434611653991593	0.18888729		
1.0-1.5		127.7	2.837777778	11.18666667	2.4	2.295985612	0.104014387674243	0.010818993		
1.5-2.0		154.4	3.431111111	14.61777778	1.2	1.410880263	-0.210880262738612	0.044470485		
2.0-3.0		289.6	6.435555556	21.05333333	0.7	0.566017758	0.133982241929722	0.017951241		
3.0-5.0		587.6	13.05777778	34.11111111	0.3	0.088716525	0.211283475465941	0.044640707		
5.0-7.0		647.5	14.38888889	48.5	0.2	0.011511581	0.188488418534741	0.035527884		
7.0-10.0		891	19.8	68.3	0.1	0.000693023	0.099306976865611	0.009861876		
							the sum of the squares of the residuals =	0.614729678		

B Everyone(2) 11/25/2015

Sampling layer/depth	x			x'	C	C(x)	Residuals			
	Central Depth	dry weight of samples/ sampling area (450 cm^2)	dry weight /unit area (m^2)	dry mass depth	Cs-137 Conc.	Cs-137 conc. estimated by exponential equation	Difference between actual and predicted values	Squares of the residuals		
	cm	g	kg/m2	kg/m2	kBq/kg	kBq/kg				
Litter Layer 1		31.3	0.695555556	0.695555556	13	14.92666706	-1.92666706188025	3.712045967	β	12.20
0-0.5		74	1.644444444	2.34	15	13.0443379	1.95566209771409	3.82461424	C(0)	15.80
0.5-1.0		81.6	1.813333333	4.153333333	12	11.24265634	0.757343658695515	0.573569417		
1.0-1.5		94.8	2.106666667	6.26	9.7	9.459614034	0.240385965550111	0.057785412		
1.5-2.0		109.3	2.428888889	8.688888889	7.5	7.75188042	-0.251880420173785	0.063443746		
2.0-3.0		270	6	14.68888889	3.4	4.740369913	-1.34036991322953	1.796591504		
3.0-5.0		538	11.95555556	26.64444444	2.2	1.779118	0.420882000069797	0.177141658		
5.0-7.0		508.1	11.29111111	37.93555556	0.7	0.70510034	-0.0051003394402059	2.60135E-05		
7.0-10.0		761.9	16.93111111	54.86666667	0.3	0.176002142	0.123997858245781	0.015375469		
							the sum of the squares of the residuals =	10.22059343		

B Everyone(2) 11/29/2016

Sampling layer/depth	x			x'	C	C(x)	Residuals			
	Central Depth	dry weight of samples/ sampling area (450 cm^2)	dry weight /unit area (m^2)	dry mass depth	Cs-137 Conc.	Cs-137 conc. estimated by exponential equation	Difference between actual and predicted values	Squares of the residuals		
	cm	g	kg/m2	kg/m2	kBq/kg	kBq/kg				
Litter Layer 1		19.67	0.437111111	0.437111111	7.7	8.393697299	-0.693697299417216	0.481215943		
Litter Layer 2		8.47	0.188222222	0.625333333	10	8.302923667	1.6970763325071	2.880068078	β	17.31
0-0.5		112.1	2.491111111	3.116444444	5.9	7.190054987	-1.29005498665874	1.664241869	C(0)	8.61
0.5-1.0		90.1	2.002222222	5.118666667	6.1	6.404702822	-0.304702821952704	0.09284381		
1.0-1.5		106.6	2.368888889	7.487555556	5.6	5.585557809	0.014442190833752 2	0.000208577		
1.5-2.0		115.3	2.562222222	10.04977778	5	4.817077454	0.182922545907773	0.033460658		
2.0-3.0		283.1	6.291111111	16.34088889	4.1	3.349250201	0.750749799099296	0.563625261		
3.0-5.0		550.7	12.23777778	28.57866667	1.5	1.651646852	-0.151646851500794	0.022996768		
5.0-7.0		595.3	13.22888889	41.80755556	0.4	0.769167754	-0.369167753602865	0.13628483		
7.0-10.0		973.2	21.62666667	63.43422222	0.3	0.220513559	0.079486441043215	0.006318094		
							the sum of the squares of the residuals =	5.881263888		

B Everyone(2) 12/12/2017

Sampling layer/depth

	χ			χ'	C	C(χ)	Residuals			
	Central Depth	dry weight of samples/ sampling area (450 cm^2)	dry weight /unit area (m^2)	dry mass depth	Cs-137 Conc.	Cs-137 conc. estimated by exponential equation	Difference between actual and predicted values	Squares of the residuals		
	cm	g	kg/m2	kg/m2	kBq/kg	kBq/kg				
Litter Layer 1		13.74	0.305333333	0.305333333	1.7	7.286499332	-5.58649933249982	31.20897479		
Litter Layer 2		123.03	2.734	3.039333333	7	7.098311856	-0.0983118561139174	0.009665221	β	104.49
0-0.5		244.85	5.441111111	8.480444444	7.9	6.738126058	1.16187394225163	1.349951058	C(0)	7.31
0.5-1.0		138.01	3.066888889	11.54733333	8.3	6.543221575	1.75677842494642	3.086270434		
1.0-1.5		107.08	2.379555556	13.92688889	8.7	6.395890495	2.30410950530354	5.308920612		
1.5-2.0		121.77	2.706	16.63288889	8.1	6.23237458	1.86762542028487	3.48802471		
2.0-3.0		220.34	4.896444444	21.52933333	8.3	5.947048865	2.35295113463897	5.536379042		
3.0-5.0		446.85	9.93	31.45933333	4.9	5.407885957	-0.507885956670013	0.257948145		
5.0-7.0		504.34	11.20755556	42.66688889	3.3	4.857842055	-1.55784205533377	2.426871869		
7.0-10.0		762.26	16.93911111	59.606	2.2	4.130818198	-1.93081819783285	3.728058913		
							the sum of the squares of the residuals =	56.4010648		

B Everyone(2) 11/12/2018

Sampling layer/depth

	χ			χ'	C	C(χ)	Residuals			
	Central Depth	dry weight of samples/ sampling area (450 cm^2)	dry weight /unit area (m^2)	dry mass depth	Cs-137 Conc.	Cs-137 conc. estimated by exponential equation	Difference between actual and predicted values	Squares of the residuals		
	cm	g	kg/m2	kg/m2	kBq/kg	kBq/kg				
Litter Layer 1		13.29	0.295333333	0.295333333	4.6	15.72566399	-11.1256639925303	123.7803993		
Litter Layer 2		18.51	0.411333333	0.706666667	14	15.59813737	-1.59813737367189	2.554043065	β	50.51672
0-0.5		58.68	1.304	2.010666667	17	15.20065123	1.79934876720055	3.237655986	C(0)	15.81787
0.5-1.0		75.17	1.670444444	3.681111111	16	14.70622848	1.29377152038352	1.673844747		
1.0-1.5		106.06	2.356888889	6.038	17	14.03586007	2.96413993149829	8.786125534		
1.5-2.0		106.52	2.367111111	8.405111111	19	13.39333926	5.60666074299942	31.43464469		
2.0-3.0		206.29	4.584222222	12.98933333	18	12.23145456	5.76854543678006	33.27611646		
3.0-5.0		461.29	10.25088889	23.24022222	12	9.985061779	2.01493822136603	4.059976036		
5.0-7.0		570.58	12.67955556	35.91977778	3.9	7.76862307	-3.86862307011789	14.96624446		
7.0-10.0		732.14	16.26977778	52.18955556	1.4	5.629528773	-4.2295287729229	17.88891364		
							the sum of the squares of the residuals =	241.6579639		

B Everyone(2) 11/27/2019

Sampling layer/depth

	χ			χ'	C	C(χ)	Residuals			
	Central Depth	dry weight of samples/ sampling area (450 cm^2)	dry weight /unit area (m^2)	dry mass depth	Cs-137 Conc.	Cs-137 conc. estimated by exponential equation	Difference between actual and predicted values	Squares of the residuals		
	cm	g	kg/m2	kg/m2	kBq/kg	kBq/kg				
Litter Layer 1		23.47	0.521555556	0.521555556	1.4	11.24144564	-9.84144563865163	96.85405226		
Litter Layer 2		53.46	1.188	1.709555556	15	10.90460028	4.09539972254225	16.77229889	β	39.04978
0-0.5		182.22	4.049333333	5.758888889	14	9.830482721	4.16951727895512	17.38487434	C(0)	11.3926
0.5-1.0		91.01	2.022444444	7.781333333	11	9.334307539	1.66569246104603	2.774531375		
1.0-1.5		88.86	1.974666667	9.756	10	8.874026686	1.12597331402164	1.267815904		
1.5-2.0		91.17	2.026	11.782	9.8	8.425359649	1.37464035092408	1.889636094		
2.0-3.0		197.93	4.398444444	16.18044444	8	7.527848698	0.47215130180316	0.222926852		
3.0-5.0		492.44	10.94311111	27.12355556	5.5	5.688089318	-0.188089318198806	0.035377592		
5.0-7.0		484.11	10.758	37.88155556	2	4.318378028	-2.31837802807913	5.374876681		
7.0-10.0		822.37	18.27488889	56.15644444	1	2.704427677	-1.70442767654508	2.905073705		
							the sum of the squares of the residuals =	145.4814637		

B vs (1) 11/14/2013

Sampling layer/depth

	x			x'	C	C(x)	Residuals			
	Central Depth	dry weight of samples/ sampling area (450 cm^2)	dry weight /unit area (m^2)	dry mass depth	Cs-137 Conc.	Cs-137 conc. estimated by exponential equation	Difference between actual and predicted values	Squares of the residuals		
	cm	g	kg/m2	kg/m2	kBq/kg	kBq/kg				
Litter Layer		433.3	9.628888889	9.628888889	43	42.87548279	0.124517207136591	0.015504535	β	1.21
0-0.5		97.6	2.168888889	11.79777778	5.8	7.123134895	-1.323134894497499	1.75068595	C(0)	1.24E+05
0.5-1.0		107.2	2.382222222	14.18	4.5	0.991876178	3.50812382197637	12.30693275		
1.0-1.5		109.1	2.424444444	16.60444444	3.9	0.133373123	3.76662687674723	14.18747803		
1.5-2.0		159.8	3.551111111	20.15555556	2.7	0.007058864	2.69294113581492	7.251931961		
2.0-3.0		312.2	6.937777778	27.09333333	2	2.26554E-05	1.99997734457885	3.999909379		
3.0-5.0		468.9	10.42	37.51333333	2.5	4.07414E-09	2.49999999592586	6.24999998		
5.0-7.0		611.3	13.58444444	51.09777778	1	5.34E-14	0.999999999999947	1		
7.0-10.0		103.5	2.3	53.39777778	0.4	7.95939E-15	0.399999999999992	0.16		
							the sum of the squares of the residuals =	46.92244258		

B vs (1) 11/25/2014

Sampling layer/depth

	x			x'	C	C(x)	Residuals			
	Central Depth	dry weight of samples/ sampling area (450 cm^2)	dry weight /unit area (m^2)	dry mass depth	Cs-137 Conc.	Cs-137 conc. estimated by exponential equation	Difference between actual and predicted values	Squares of the residuals		
	cm	g	kg/m2	kg/m2	kBq/kg	kBq/kg				
Litter Layer		370.6	8.235555556	8.235555556	45	44.70180221	0.298197787139543	0.08892192	β	6.02
0-0.5		232	5.155555556	13.39111111	19	18.98702209	0.0129779119199718	0.000168426	C(0)	1.76E+02
0.5-1.0		128.8	2.862222222	16.25333333	9.3	11.80336677	-2.5033667660455	6.266845165		
1.0-1.5		131.4	2.92	19.17333333	8	7.267540498	0.732459502156889	0.536496922		
1.5-2.0		100.9	2.242222222	21.41555556	6.2	5.007913987	1.19208601253864	1.421069061		
2.0-3.0		299.1	6.646666667	28.06222222	4.2	1.660486814	2.53951318611086	6.449127222		
3.0-5.0		558.7	12.41555556	40.47777778	2.3	0.21120604	2.08879395984675	4.363060207		
5.0-7.0		604.7	13.43777778	53.91555556	0.9	0.022669647	0.877330353197665	0.769708549		
7.0-10.0		1363	30.28888889	84.20444444	0.6	0.000148156	0.599851844010376	0.359822235		
							the sum of the squares of the residuals =	20.25521971		

B vs (1) 11/24/2015

Sampling layer/depth

	x			x'	C	C(x)	Residuals			
	Central Depth	dry weight of samples/ sampling area (450 cm^2)	dry weight /unit area (m^2)	dry mass depth	Cs-137 Conc.	Cs-137 conc. estimated by exponential equation	Difference between actual and predicted values	Squares of the residuals		
	cm	g	kg/m2	kg/m2	kBq/kg	kBq/kg				
Litter Layer		92.8	2.062222222	2.062222222	65	59.93955297	5.06044703226041	25.60812417	β	3.57
0-0.5		55.2	1.226666667	3.288888889	34	42.51568718	-8.51568717727918	72.5169281	C(0)	1.07E+02
0.5-1.0		76.9	1.708888889	4.997777778	26	26.34790223	-0.347902229869767	0.121035962		
1.0-1.5		98.2	2.182222222	7.18	17	14.30160968	2.69839031647691	7.2813103		
1.5-2.0		121.6	2.702222222	9.882222222	10	6.711059792	3.28894020786413	10.81712769		
2.0-3.0		270.5	6.011111111	15.89333333	7	1.246901104	5.75309889640913	33.09814691		
3.0-5.0		582.3	12.94	28.83333333	1.9	0.033289772	1.86671022849468	3.484607077		
5.0-7.0		630.1	14.00222222	42.83555556	1.5	0.000660119	1.49933988137641	2.24802008		
7.0-10.0		1008	22.4	65.23555556	0.6	1.24667E-06	0.599998753327959	0.359998504		
							the sum of the squares of the residuals =	155.5352988		

B vs (1) 11/29/2016

Sampling layer/depth

	x			x'	C	C(x)	Residuals			
	Central Depth	dry weight of samples/ sampling area (450 cm^2)	dry weight /unit area (m^2)	dry mass depth	Cs-137 Conc.	Cs-137 conc. estimated by exponential equation	Difference between actual and predicted values	Squares of the residuals		
	cm	g	kg/m2	kg/m2	kBq/kg	kBq/kg				
Litter Layer 1		5.79	0.128666667	0.128666667	3.1	29.51380289	-26.4138028920712	697.6889832		
Litter Layer 2		58.82	1.307111111	1.435777778	26	28.36931572	-2.36931571553075	5.61365696	β	33.05
0-0.5		189.6	4.213333333	5.649111111	44	24.97369765	19.0263023464873	362.000181	C(0)	2.96E+01
0.5-1.0		59.12	1.313777778	6.962888889	43	24.00042505	18.9995749540744	360.9838484		
1.0-1.5		92.04	2.045333333	9.008222222	28	22.5601451	5.43985489981962	29.59202133		
1.5-2.0		105.5	2.344444444	11.35266667	22	21.01523857	0.984761434466645	0.969755083		
2.0-3.0		265.3	5.895555556	17.24822222	13	17.58177797	-4.58177797019321	20.99268937		
3.0-5.0		624.3	13.87333333	31.12155556	3.5	11.55468035	-8.0546803549241	64.87787562		
5.0-7.0		656.4	14.58666667	45.70822222	1.5	7.431550005	-5.93155000484024	35.18328546		
7.0-10.0		1078	23.95555556	69.66377778	0.8	3.599875014	-2.79987501444008	7.839300096		
							the sum of the squares of the residuals =	1585.741597		

B vs (1) 12/11/2017

Sampling layer/depth	x			x'	C	$C(x)$	Residuals			
	Central Depth	dry weight of samples/ sampling area (450 cm^2)	dry weight /unit area (m^2)	dry mass depth	Cs-137 Conc.	Cs-137 conc. estimated by exponential equation	Difference between actual and predicted values	Squares of the residuals		
	cm	g	kg/m2	kg/m2	kBq/kg	kBq/kg				
Litter Layer 1		57.71	1.282444444	1.282444444	4.9	16.73682986	-11.8368298609867	140.1105412		
Litter Layer 2		449.32	9.984888889	11.26733333	31	12.96849766	18.03150233363454	325.1350765	β	39.14
0-0.5		72.05	1.601111111	12.86844444	19	12.44873292	6.55126708397865	42.91910041	C(0)	17.29
0.5-1.0		86.71	1.926888889	14.79533333	15	11.85075685	3.14924315486681	9.917732448		
1.0-1.5		109.95	2.443333333	17.23866667	1	11.13363585	-10.1336358476531	102.6905755		
1.5-2.0		114.81	2.551333333	19.79	11	10.43108934	0.568910663501066	0.323659343		
2.0-3.0		271.84	6.040888889	25.83088889	8.1	8.93933643	-0.839336429770283	0.704485642		
3.0-5.0		635.39	14.11977778	39.95066667	2.2	6.232247091	-4.03224709097522	16.2590166		
5.0-7.0		792.73	17.61622222	57.56688889	1	3.97365883	-2.97365883035028	8.842646839		
7.0-10.0		1221.71	27.14911111	84.716	0.34	1.985948357	-1.64594835678201	2.709145993		
							the sum of the squares of the residuals =	649.6119804		

B vs (1) 11/12/2018

Sampling layer/depth	x			x'	C	$C(x)$	Residuals			
	Central Depth	dry weight of samples/ sampling area (450 cm^2)	dry weight /unit area (m^2)	dry mass depth	Cs-137 Conc.	Cs-137 conc. estimated by exponential equation	Difference between actual and predicted values	Squares of the residuals		
	cm	g	kg/m2	kg/m2	kBq/kg	kBq/kg				
Litter Layer 1		24.06	0.534666667	0.534666667	2.6	25.55410479	-22.9541047898867	526.8909267		
Litter Layer 2		93.78	2.084	2.618666667	26	23.9694469	2.03055310076306	4.123145895	β	32.55335
0-0.5		85.88	1.908444444	4.527111111	29	22.60463204	6.39536796110007	40.90073136	C(0)	25.97728
0.5-1.0		62.28	1.384	5.911111111	31	21.66374266	9.33625733718001	87.16570107		
1.0-1.5		78.56	1.745777778	7.656888889	29	20.53255782	8.46744217660486	71.69757701		
1.5-2.0		67.64	1.503111111	9.16	28	19.60604697	8.39395303467269	70.45844755		
2.0-3.0		20.09	0.446444444	9.606444444	20	19.3390003	0.660999699200694	0.436920602		
3.0-5.0		409.28	9.095111111	18.70155556	10	14.62500687	-4.62500687045135	21.39068855		
5.0-7.0		542.9	12.06444444	30.766	4.4	10.09588141	-5.69588140853688	32.44306502		
7.0-10.0		661.92	14.70933333	45.47533333	0.98	6.425499896	-5.44549989601843	29.65346912		
							the sum of the squares of the residuals =	885.1606729		

B vs (1) 11/28/2019

Sampling layer/depth	x			x'	C	$C(x)$	Residuals			
	Central Depth	dry weight of samples/ sampling area (450 cm^2)	dry weight /unit area (m^2)	dry mass depth	Cs-137 Conc.	Cs-137 conc. estimated by exponential equation	Difference between actual and predicted values	Squares of the residuals		
	cm	g	kg/m2	kg/m2	kBq/kg	kBq/kg				
Litter Layer 1		38.22	0.849333333	0.849333333	3.8	12.95514599	-9.15514598805922	83.81669806		
Litter Layer 2		919.34	20.42977778	21.27911111	28	9.119081043	18.8809189568714	356.4891007	β	58.18393
0-0.5		73.06	1.623555556	22.90266667	14	8.868140978	5.13185902177326	26.33597702	C(0)	13.14564
0.5-1.0		89.04	1.978666667	24.88133333	9.3	8.57163153	0.728368469593317	0.530520627		
1.0-1.5		95.5	2.122222222	27.00355556	8	8.264619745	-0.264619745196187	0.07002361		
1.5-2.0		120.38	2.675111111	29.67866667	5.4	7.893241767	-2.49324176711036	6.216254509		
2.0-3.0		245.52	5.456	35.13466667	3.3	7.186723232	-3.88672323224219	15.10661748		
3.0-5.0		526.59	11.702	46.83666667	1.2	5.877400142	-4.67740014227873	21.87807209		
5.0-7.0		556.51	12.36688889	59.20355556	0.77	4.752003564	-3.98200356434536	15.85635239		
7.0-10.0		932.81	20.72911111	79.93266667	0.59	3.327754262	-2.73775426234579	7.495298401		
							the sum of the squares of the residuals =	533.7949148		

B vs (2) 11/12/2013

Sampling layer/depth

	x			x'		C	C(x)	Residuals			
	Central Depth	dry weight of samples/ sampling area (450 cm^2)	dry weight /unit area (m^2)	dry mass depth		Cs-137 Conc.	Cs-137 conc. estimated by exponential equation	Difference between actual and predicted values	Squares of the residuals		
	cm	g	kg/m2	kg/m2		kBq/kg	kBq/kg				
Litter Layer		695.9	15.46444444	15.46444444		63	62.61500531	0.384994693233878	0.148220914	β	0.50
0-0.5		31.78	0.706222222	16.17066667		13	15.20352199	-2.20352199096095	4.855509165	C(0)	1.81E+15
0.5-1.0		56.3	1.251111111	17.42177778		5.7	1.238537272	4.46146272835597	19.90464968		
1.0-1.5		82.94	1.843111111	19.26488889		4.8	0.030801011	4.76919898906205	22.745259		
1.5-2.0		117.1	2.602222222	21.86711111		4.3	0.000167282	4.29983271797302	18.4885614		
2.0-3.0		225.2	5.004444444	26.87155556		2.3	7.36731E-09	2.29999999263269	5.289999966		
3.0-5.0		463.5	10.3	37.17155556		1	7.97313E-18	1	1		
5.0-7.0		437.8	9.728888889	46.90044444		0.9	2.71066E-26	0.9	0.81		
7.0-10.0		723.4	16.07555556	62.976		0.6	2.75447E-40	0.6	0.36		
								the sum of the squares of the residuals =	73.60220012		

B vs (2) 11/27/2014

Sampling layer/depth

	x			x'		C	C(x)	Residuals			
	Central Depth	dry weight of samples/ sampling area (450 cm^2)	dry weight /unit area (m^2)	dry mass depth		Cs-137 Conc.	Cs-137 conc. estimated by exponential equation	Difference between actual and predicted values	Squares of the residuals		
	cm	g	kg/m2	kg/m2		kBq/kg	kBq/kg				
Litter Layer		183.2	4.071111111	4.071111111		160	159.8396799	0.160320092750993	0.025702532	β	2.05
0-0.5		142.7	3.171111111	7.242222222		33	33.96671545	-0.966715446310843	0.934538754	C(0)	1.17E+03
0.5-1.0		73.6	1.635555556	8.877777778		14	15.2803191	-1.28031909894102	1.639216995		
1.0-1.5		79.83	1.774	10.65177778		9.1	6.424591993	2.67540800703038	7.157808004		
1.5-2.0		73.91	1.642444444	12.29422222		5.6	2.880469003	2.71953099686521	7.395848843		
2.0-3.0		157.6	3.502222222	15.79644444		3.6	0.520714275	3.07928572504845	9.482000576		
3.0-5.0		207.9	4.62	20.41644444		2.3	0.054530762	2.24546923811792	5.042132099		
5.0-7.0		607	13.48888889	33.90533333		1.8	7.50732E-05	1.79992492679284	3.239729742		
7.0-10.0		674.2	14.98222222	48.88755556		1.2	4.98396E-08	1.19999995016043	1.43999988		
								the sum of the squares of the residuals =	36.35697743		

B vs (2) 11/25/2015

Sampling layer/depth

	x			x'		C	C(x)	Residuals			
	Central Depth	dry weight of samples/ sampling area (450 cm^2)	dry weight /unit area (m^2)	dry mass depth		Cs-137 Conc.	Cs-137 conc. estimated by exponential equation	Difference between actual and predicted values	Squares of the residuals		
	cm	g	kg/m2	kg/m2		kBq/kg	kBq/kg				
Litter Layer		161.9	3.597777778	3.597777778		100	153.0695052	-53.06950517742672	2816.372379	β	6.13
0-0.5		20.93	0.465111111	4.062888889		190	141.8883604	48.1116396382397	2314.729869	C(0)	2.75E+02
0.5-1.0		25.97	0.577111111	4.64		130	129.1434435	0.856556500630177	0.733689039		
1.0-1.5		28.68	0.637333333	5.277333333		140	116.3945544	23.6054455863984	557.2170613		
1.5-2.0		45.81	1.018	6.295333333		94	98.58978206	-4.58978205582144	21.06609932		
2.0-3.0		120.9	2.686666667	8.982		48	63.61306923	-15.61306922279974	243.7679307		
3.0-5.0		298.8	6.64	15.622		16	21.54083052	-5.54083052052399	30.70080286		
5.0-7.0		384.8	8.551111111	24.17311111		5.8	5.340997726	0.459002273556213	0.210683087		
7.0-10.0		692.1	15.38	39.55311111		3.5	0.434830714	3.06516928608731	9.395262752		
								the sum of the squares of the residuals =	5994.193777		

B vs (2) 11/29/2016

Sampling layer/depth

	x			x'		C	C(x)	Residuals			
	Central Depth	dry weight of samples/ sampling area (450 cm^2)	dry weight /unit area (m^2)	dry mass depth		Cs-137 Conc.	Cs-137 conc. estimated by exponential equation	Difference between actual and predicted values	Squares of the residuals		
	cm	g	kg/m2	kg/m2		kBq/kg	kBq/kg				
Litter Layer 1		18.62	0.413777778	0.413777778		10	123.2760813	-113.27608133323	12831.4706		
Litter Layer 2		33.52	0.744888889	1.158666667		97	116.8151768	-19.8151768070918	392.6412319	β	13.84
0-0.5		75.52	1.678222222	2.836888889		250	103.4726412	146.527358768512	21470.26687	C(0)	1.27E+02
0.5-1.0		27.67	0.614888889	3.451777778		170	98.97516775	71.024832248322	5044.526796		
1.0-1.5		66.43	1.476222222	4.928		83	88.9595566	-5.95955659782639	35.51631484		
1.5-2.0		86.27	1.917111111	6.845111111		50	77.44991712	-27.4499171217237	753.49795		
2.0-3.0		133.4	2.964444444	9.809555556		23	62.51396482	-39.5139648168969	1561.353416		
3.0-5.0		493.3	10.96222222	20.77177778		3.6	28.30804381	-24.7080438123993	610.487429		
5.0-7.0		567	12.6	33.37177778		3.8	11.38776125	-7.58776124642863	57.57412073		
7.0-10.0		1006	22.35555556	55.72733333		2.2	2.263460185	-0.0634601854547929	0.004027195		
								the sum of the squares of the residuals =	42757.33876		

B vs (2) 12/11/2017

Sampling layer/depth

	χ			χ'	C	C(χ)	Residuals			
	Central Depth	dry weight of samples/ sampling area (450 cm^2)	dry weight /unit area (m^2)	dry mass depth	Cs-137 Conc.	Cs-137 conc. estimated by exponential equation	Difference between actual and predicted values	Squares of the residuals		
	cm	g	kg/m2	kg/m2	kBq/kg	kBq/kg				
Litter Layer 1		28.76	0.639111111	0.639111111	12	56.56789448	-44.5678944789161	1986.297218		
Litter Layer 2		162.38	3.608444444	4.247555556	81	48.26640382	32.7335961800909	1071.488319	β	22.74
0-0.5		108.48	2.410666667	6.658222222	67	43.41088917	23.5891108343987	556.44615	C(0)	58.18
0.5-1.0		54.57	1.212666667	7.870888889	58	41.15621968	16.843780321295	283.7129355		
1.0-1.5		68.3	1.517777778	9.388666667	41	38.49854621	2.50145379259235	6.257271076		
1.5-2.0		87.03	1.934	11.32266667	32	35.3592384	-3.35923840328154	11.28448265		
2.0-3.0		191.36	4.252444444	15.57511111	18	29.32761558	-11.3276155821101	128.3148748		
3.0-5.0		366.05	8.134444444	23.70955556	7.5	20.50691531	-13.0069153128656	169.179846		
5.0-7.0		413.76	9.194666667	32.90422222	3.7	13.68587487	-9.98587486627631	99.71769684		
7.0-10.0		866.84	19.26311111	52.16733333	2.8	5.86579589	-3.06579589021313	9.39910444		
							the sum of the squares of the residuals =	4322.097898		

B vs (2) 11/13/2018

Sampling layer/depth

	χ			χ'	C	C(χ)	Residuals			
	Central Depth	dry weight of samples/ sampling area (450 cm^2)	dry weight /unit area (m^2)	dry mass depth	Cs-137 Conc.	Cs-137 conc. estimated by exponential equation	Difference between actual and predicted values	Squares of the residuals		
	cm	g	kg/m2	kg/m2	kBq/kg	kBq/kg				
Litter Layer 1		10.5	0.233333333	0.233333333	5.6	94.29179824	-88.6917982449091	7866.235076		
Litter Layer 2		102.45	2.276666667	2.51	110	82.80937121	27.1906287917071	739.3302941	β	17.53265
0-0.5		30.71	0.682444444	3.192444444	140	79.64800808	60.3519919162817	3642.362928	C(0)	95.55507
0.5-1.0		40.12	0.891555556	4.084	110	75.69906938	34.3009306237819	1176.553842		
1.0-1.5		54.57	1.212666667	5.296666667	82	70.64021989	11.35978010812	129.0446041		
1.5-2.0		71.7	1.593333333	6.89	62	64.5036362	-2.50363620392683	6.268194242		
2.0-3.0		169.96	3.776888889	10.66688889	34	52.00299306	-18.0029930626264	324.1077592		
3.0-5.0		375.39	8.342	19.00888889	11	32.31408612	-21.3140861150076	454.2902669		
5.0-7.0		452.09	10.04644444	29.05533333	4	18.21945074	-14.2194507354723	202.1927792		
7.0-10.0		691.98	15.37733333	44.43266667	1.1	7.579303377	-6.47930337745603	41.98137226		
							the sum of the squares of the residuals =	14582.36712		

B vs (2) 11/28/2019

Sampling layer/depth

	χ			χ'	C	C(χ)	Residuals			
	Central Depth	dry weight of samples/ sampling area (450 cm^2)	dry weight /unit area (m^2)	dry mass depth	Cs-137 Conc.	Cs-137 conc. estimated by exponential equation	Difference between actual and predicted values	Squares of the residuals		
	cm	g	kg/m2	kg/m2	kBq/kg	kBq/kg				
Litter Layer 1		17.77	0.394888889	0.394888889	3.9	37.48294907	-33.5829490734607	1127.814468		
Litter Layer 2		633.43	14.07622222	14.47111111	92	27.42967877	64.5703212283792	4169.326384	β	45.07845
0-0.5		85.31	1.895777778	16.36688889	44	26.30004151	17.6999584856716	313.2885304	C(0)	37.81274
0.5-1.0		75.07	1.668222222	18.03511111	28	25.34454275	2.65545724862659	7.051453199		
1.0-1.5		85.86	1.908	19.94311111	19	24.29418988	-5.29418988000607	28.02844649		
1.5-2.0		104.66	2.325777778	22.26888889	12	23.07254126	-11.0725412588635	122.6011699		
2.0-3.0		245	5.444444444	27.71333333	7.5	20.44761252	-12.9476125200598	167.64067		
3.0-5.0		497.6	11.05777778	38.77111111	3.7	15.99962669	-12.2996266886941	151.2808167		
5.0-7.0		444.25	9.872222222	48.64333333	2.4	12.8528359	-10.4528358987725	109.2617783		
7.0-10.0		717.37	15.94155556	64.58488889	1.8	9.024329653	-7.22432965276539	52.19093893		
							the sum of the squares of the residuals =	6248.484656		

Equation Fit for β Values in Saito et al. Model

Cs137 Coeff.			Cs134 Coeff.	
	Dose Conversion Coefficient [(μSv/h) / (Bq/m^2)]	β (g/cm^2)	Dose Conversion Coefficient [(μSv/h) / (Bq/m^2)]	β (g/cm^2)
	3.15E-06	0	8.50E-06	0
	2.83E-06	0.1	7.64E-06	0.1
	2.65E-06	0.2	7.17E-06	0.2
	2.52E-06	0.3	6.83E-06	0.3
	2.32E-06	0.5	6.32E-06	0.5
	2.04E-06	1	5.54E-06	1
	1.71E-06	2	4.66E-06	2
	1.51E-06	3	4.12E-06	3
	1.25E-06	5	3.41E-06	5
	9.09E-07	10	2.48E-06	10
	6.03E-07	20	1.65E-06	20
	4.50E-07	30	1.23E-06	30
	3.04E-07	50	8.35E-07	50
	1.69E-07	100	4.64E-07	100

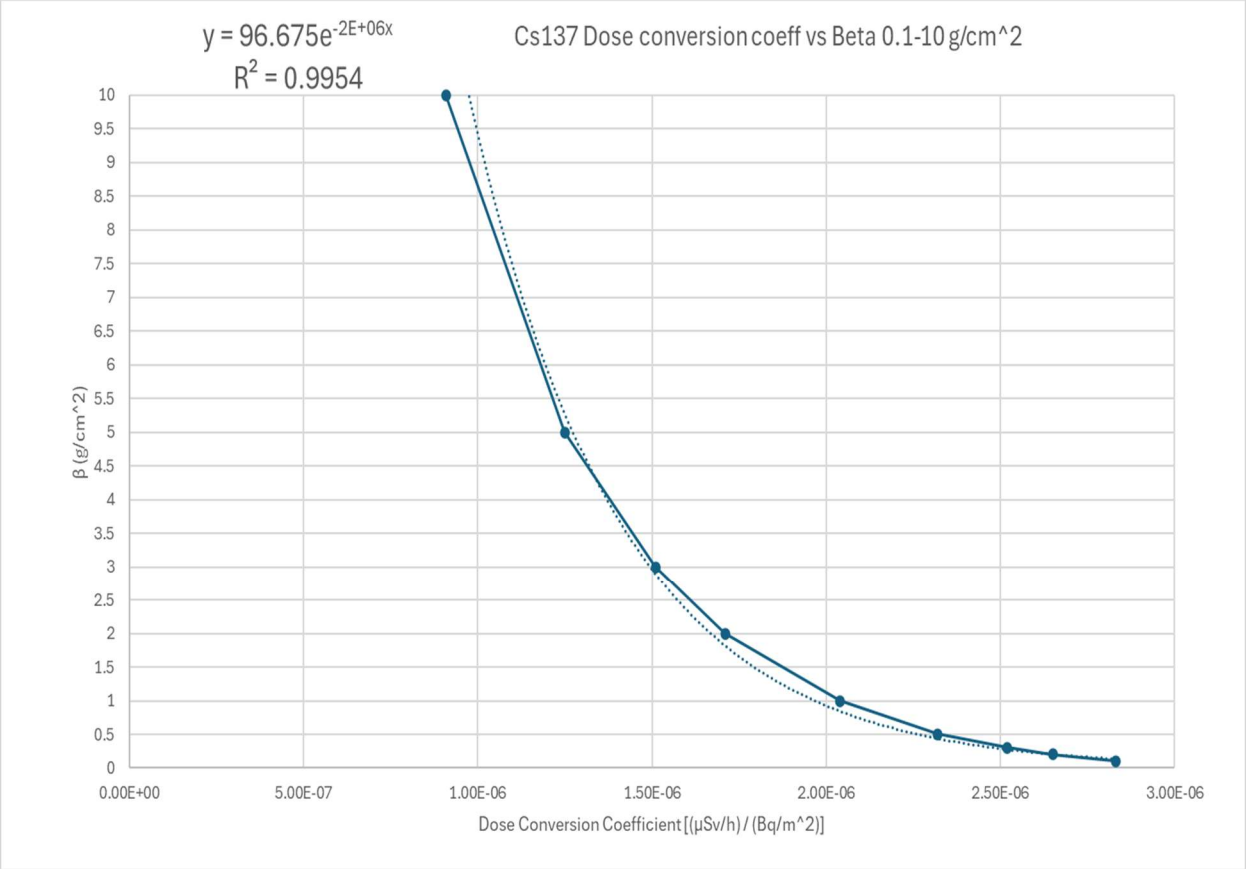

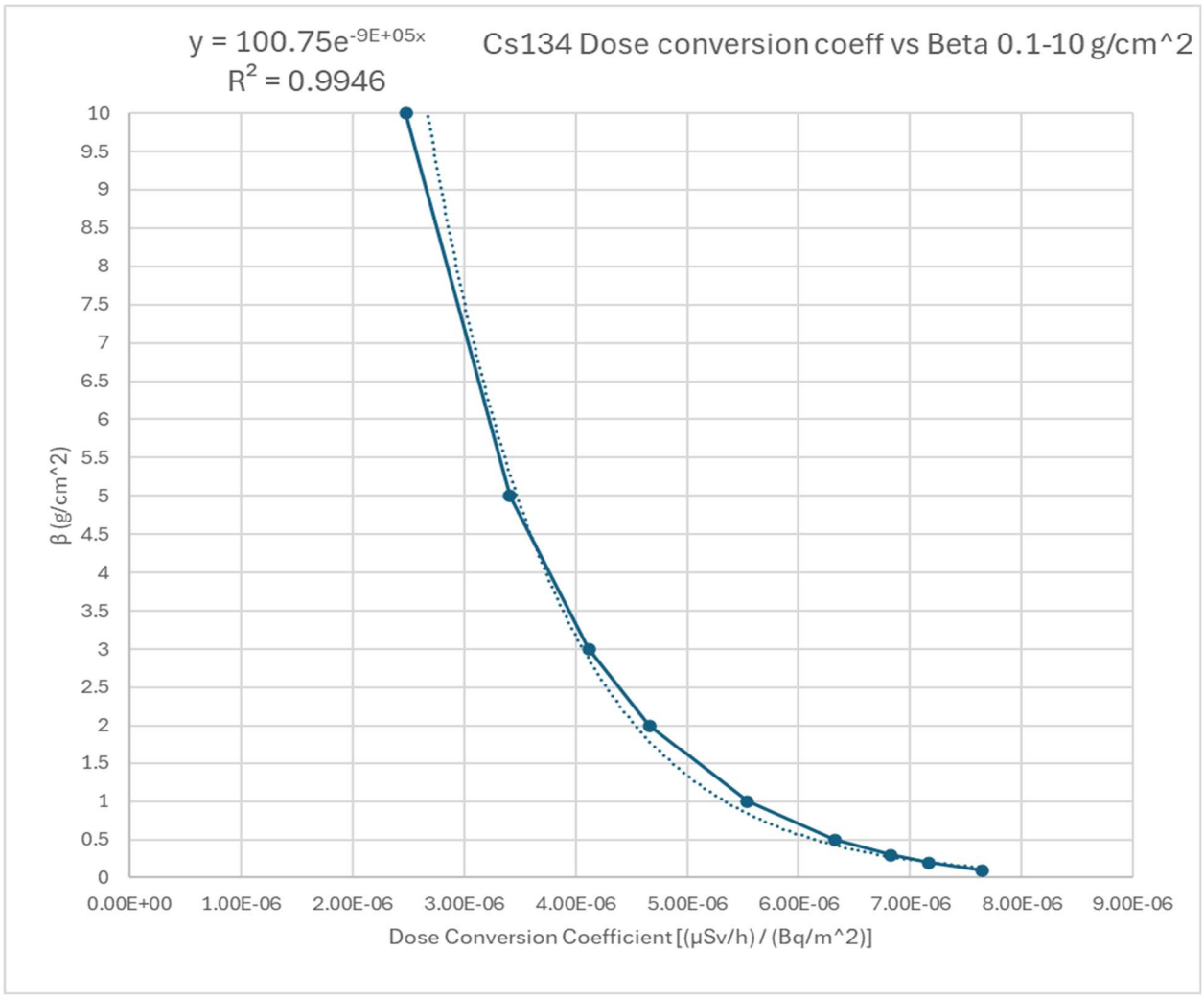
y = 100.75e-9E+05x
R2 = 0.9946
Cs134 Dose conversion coeff vs Beta 0.1-10 g/cm^2
β (g/cm^2)
10
9.5
9
8.5
8
7.5
7
6.5
6
5.5
5
4.5
4
3.5
3
2.5
2
1.5
1
0.5
0
0.00E+00
1.00E-06
2.00E-06
3.00E-06
4.00E-06
5.00E-06
6.00E-06
7.00E-06
8.00E-06
9.00E-06
Dose Conversion Coefficient [(μSv/h) / (Bq/m^2)]

Equation Fit from WebPlotDigitizer for Malins et al. Model

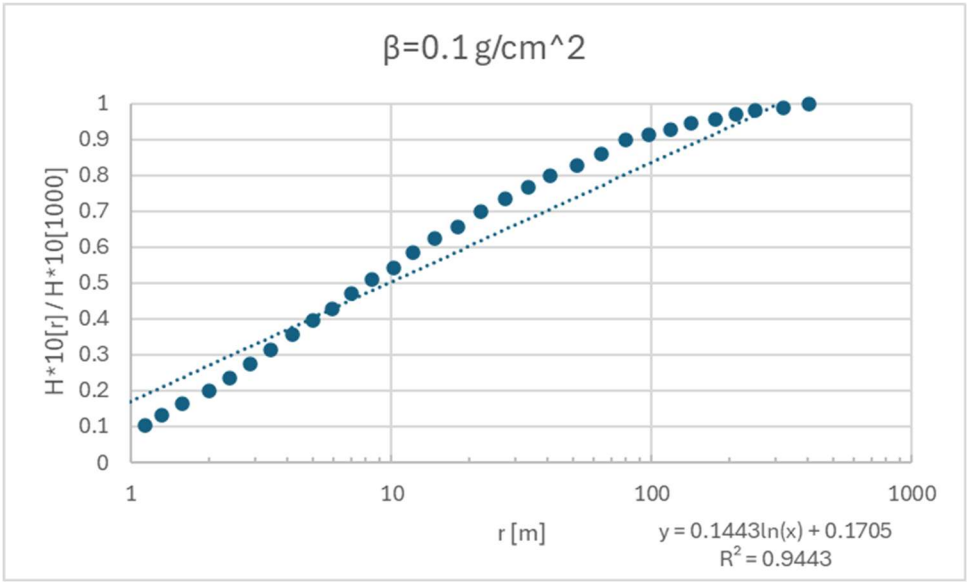

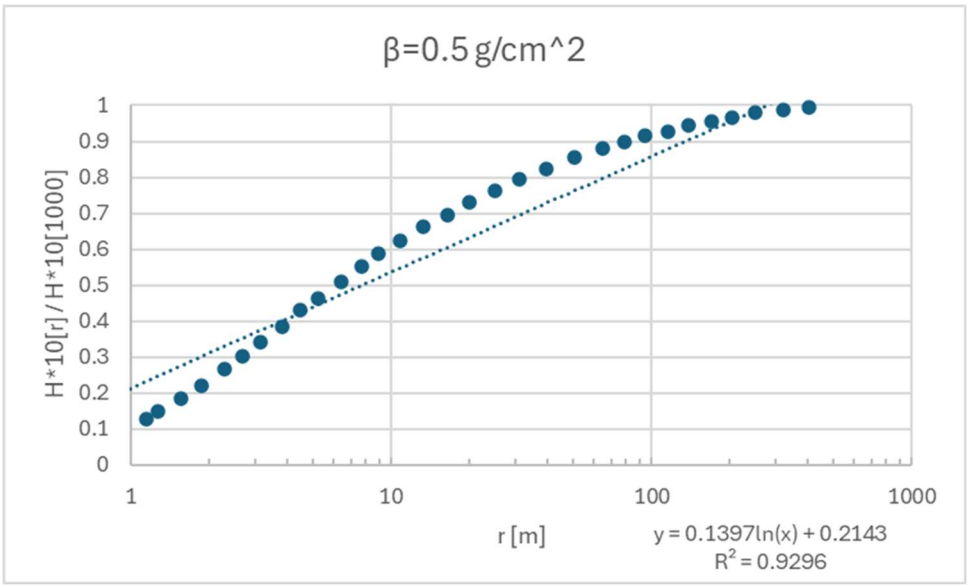

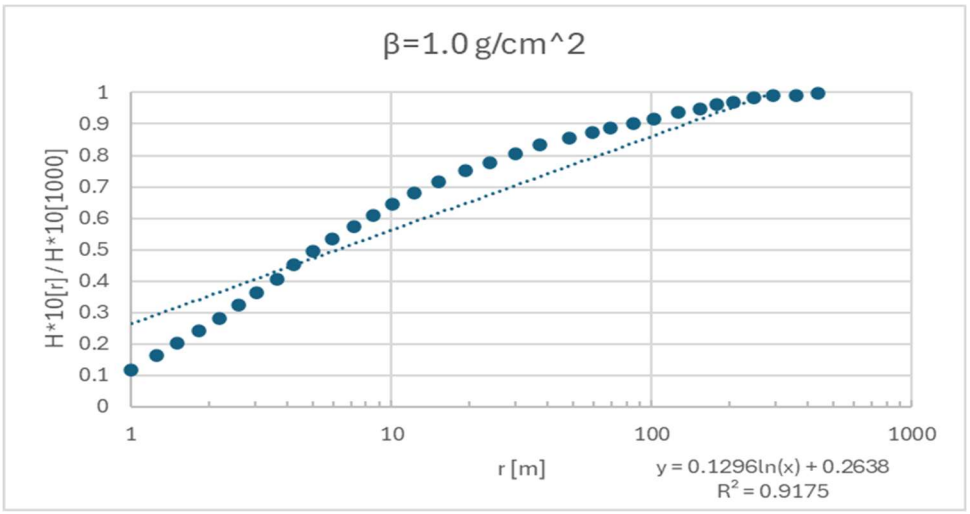
β=1.0 g/cm^2
H*10[r] / H*10[1000]
1
0.9
0.8
0.7
0.6
0.5
0.4
0.3
0.2
0.1
0
1
10
100
1000
r [m]
y = 0.1296ln(x) + 0.2638
R² = 0.9175

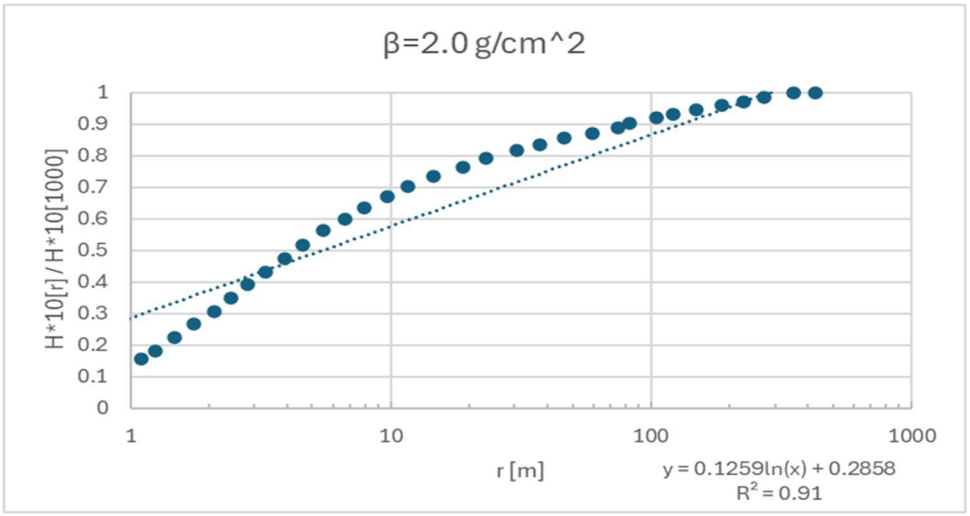
β=2.0 g/cm^2
H*10[r] / H*10[1000]
1
0.9
0.8
0.7
0.6
0.5
0.4
0.3
0.2
0.1
0
1
10
100
1000
r [m]
y = 0.1259ln(x) + 0.2858
R² = 0.91

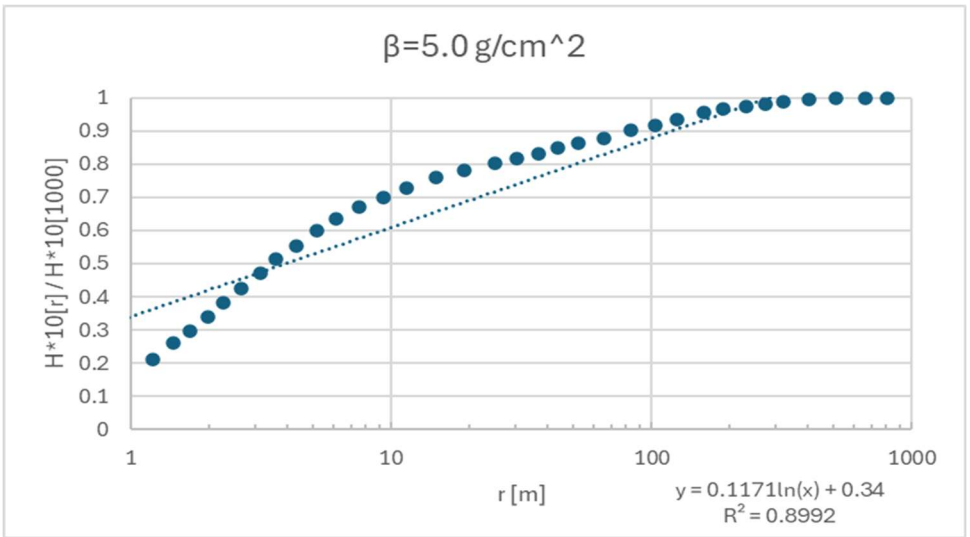
β=5.0 g/cm^2
H*10[r] / H*10[1000]
1
0.9
0.8
0.7
0.6
0.5
0.4
0.3
0.2
0.1
0
1
10
100
1000
r [m]
y = 0.1171ln(x) + 0.34
R² = 0.8992

Email Correspondence from Author of Saito et al. Model

** Caution: EXTERNAL Sender **

Dear Dr. Grabowski,

Thank you for e-mail and using the dose conversion coefficients in my publication.
I am answering your question.

In conclusion, your current method is appropriate.
You can treat the litter layer and the soil as one piece to determine the relaxation depth provided the depth is expressed in g/cm2.

The elemental components and density of litter layer are apparently different from soil.
However, it has been confirmed that the difference makes no significant effects to the evaluated results as long as the depth is treated as a function of g/cm2.

Attenuation of 0.662 MeV gamma rays from Cs-137 depends mostly on the mass of materials but not the elemental compositions because Compton scattering is the dominant reaction in this energy range.
When the gamma ray energy is below 0.1 MeV, in some cases, you have to consider elemental compositions; but there is no need for Cs-137 gamma rays.

Therefore, you can apply the dose coefficients to the combination of litter layer and soil.

Did I answer your question properly?
If you have any further questions, do not hesitate to ask, please.

Best regards,

Kimiaki Saito

----- Original Message -----
>> From: Grabowski,Christian <[redacted]>
>> To: "[redacted]
>> Cc: Yuichi_ONDA <[redacted]
>> Date: 2025-01-11 04:07:56
>> Subject: Question for Application of Conversion Coefficients for
>> radiocesium
>>
>> Hello Dr. Saito,
>>
>> My name is Christian Grabowski, master's student at Colorado State University. I am currently conducting a research study in collaboration with Dr. Onda at the University of Tsukuba. We are investigating radiocesium distribution data from the Kawauchi Test Site and I am applying the conversion coefficients from your 2014 study Ambient dose equivalent conversion coefficients for radionuclides

exponentially distributed in the ground. I am reaching out to you because I have a question on how I should accurately apply the conversion coefficients when there is a litter layer of forestry debris covering the soil.
>>
>> I currently calculated relaxation depth (β) of cesium 137 for my soil data. However, I calculated β considering the litter layer and the soil as one piece, rather than determining β excluding the litter layer. I originally used this approach to make using your conversion coefficients simple to apply. However, I am worried this is incorrect for me to do. So, my question is, how can I use your conversion coefficients to estimate ambient dose equivalent (H*(10)) from the litter layer, where there is no β? This way I can combine H*(10) contribution from the litter layer separate from the contribution of the soil and then sum them together.
>>
>> I hope my question is clearly worded for you to understand. Thank you very much in advance for your attention to this matter. I hope to hear from you soon.
>>
>> Very respectfully,
>>
>> Christian Grabowski
>> Colorado State University
>> Health Physics Graduate Student
>> [redacted]